Integrated Climate Change Impact Assessment and Extreme Event Forecasting in the Lake Victoria Basin (LVB)

（ビクトリア湖流域における統合的な気候変動影響評価と極端事象の予測）

MUTUA FELIX NZIVE

ﾑﾄｳｱ ﾌｪﾘｯｸｽ ﾝｼﾞｨﾍﾞ

The university of Tokyo

Integrated Climate Change Impact Assessment and Extreme Event Forecasting in the Lake Victoria Basin (LVB)

Felix Nzive Mutua

Doctor of Philosophy

Department of Civil Engineering

The Graduate School of Engineering, University of Tokyo

Tokyo, Japan

March, 2013

A thesis submitted to the University of Tokyo in partial fulfillment Of the requirement for Doctor of Philosophy in Civil Engineering

Doctoral Committee :

Professor Toshio Koike, Chair.

Professor Taikan Oki

Professor Shinji Sato

Professor Hiroaki Furumai

Professor Fujio Kimura

Professor Kei Yoshimura

Integrated Climate Change Impact Assessment and Extreme Event Forecasting in the Lake Victoria Basin (LVB)

Felix Nzive Mutua

Student ID : 37 - 107006

River and Environmental Engineering Laboratory

Department of Civil Engineering

Approved as to style and content by:-

Professor Toshio Koike	Professor Taikan Oki
Professor Shinji Sato	Professor Hiroaki Furumai
Professor Fujio Kimura	Professor Kei Yoshimura

Peer Reviewed Papers

1. Mutua, F., Wang, L., Yamamoto, A., Nemoto, T., Kitsuregawa, M., and Koike, T. (2012b). Regional Climate Change And Its Impacts On Future Discharges And Flow Characteristics Of The Nyando Basin, Kenya. *Annual Journal of Hydraulic Engineering, JSCE*, 56

2. Mutua, F., Mohamed, R., and Koike, T. (2013a). Improving Extreme Rainfall Event Prediction Using Microwave Satellite Data Assimilation. *Annual Journal of Hydraulic Engineering, JSCE*, 57:1–6

3. Mutua, F., Nyunt, C., and Koike, T. (2013c). Multi-scale climate change impact assessment on extreme events in the Lake Victoria Basin (LVB). *WATER RESOURCES RESEARCH*, (in prep.)

4. Mutua, F., Rasmy, M., Kuria, D., and Koike, T. (2013d). Sensitivity analysis of the CALDAS system : Surface temperature estimation and Significance of rain-water assimilation. *IEEE Transactions on Geoscience and Remote Sensing*, 50(1):(in prep.)

5. Mutua, F. and Koike, T. (2013). Adaptation to extreme climate : Improving weather prediction in the Lake Victoria Basin. *Climatic Dynamics*, page (in prep.)

Conferences

1. Mutua, F., Mohamed, R., and Koike, T. (2012a). Improving extreme rainfall event prediction using microwave satellite data assimilation and bogus wind modification. *AGU Fall Meeting Abstracts*, 57:1–6

2. Mutua, F., Mohamed, R., and Koike, T. (2013b). Projections of extreme weather events in the Lake Victoria basin under climate change. *EGU General Assembly Conference Abstracts*, 15:(submittted)

Abstract

Extreme weather events have been the leading cause of disasters and damage all over the world. Recent events have led to mass displacement, loss of income, and hampered access to clean water and health to many. The primary ingredient to these disasters especially floods is rainfall which over the years, despite advances in modeling, computing power and use of new data and technologies, has proven to be difficult to predict. Numerical weather prediction (NWP) and climate models using global forecasts and emission scenarios as initial and boundary conditions have provided short to midterm forecasts and climate projections in many parts of the world. The Lake Victoria Basin (LVB) in East Africa supports over three million livelihoods and hosts the world record for elaboration of vertebrate species diversity, species extinctions, and exotic species invasions. The second largest freshwater lake in the world is a valuable resource to five East African countries as a source of water and means of transport. However, with a Mesoscale climate regime driven by land and lake dynamics, extreme Mesoscale events have been prevalent and the region has been on the receiving end during anomalously wet years in the region. This has resulted in loss of lives, displacements, and food insecurity. As an essential aspect of early warning there is a need to strengthen adaptation through improved prediction of rainfall and floods.

It is now more evident than ever that climate change will have adverse impacts on the global population in coming years. Since the release of Intergovernmental Panel on Climate Change (IPCC) Fourth Assessment Report: Climate Change 2007 (AR4) in 2007, it has been shown that impacts of climate change are already being felt, with increases in sea level rise, retreating glaciers and more frequent weather extremes. In the LVB, the effects of climate change are increasingly being recognized as a significant contributor to poverty, by its linkage to agriculture, food security and water resources. One aspect that is investigated widely with respect to climate change is the impacts it will have on extreme weather events. There is a general consensus that changes in frequency and intensity of extreme weather and climate events will have adverse effects on both humanity and nature.

Adaptation to climate change needs an understanding of climate change impacts

at local scales. There is a need to connect the global scale projections with impacts it may have on people through downscaling and other means. The LVB is a regional basin with multiple land uses and water resource needs. In addition, it is one of the basins that have been heavily affected by extreme weather, especially storm-induced floods. Of particular importance are the likely impacts of climate change in frequency and intensity of extreme events. To tackle this aspect, this study adopted an integrated regional, mesoscale and basin scale approach to climate change assessment. The study investigated the projected changes in mean climate over East Africa, diagnosed the signals of climate change in the atmosphere, and transferred this understanding to mesoscale and basin scale. Changes in rainfall were analyzed and similar to the IPCC AR4 report, the selected three General Circulation Models (GCMs) project a wetter East Africa with intermittent dry periods in June-August.

The highest projected changes are in the October-December season whose variability is closely linked to inter-annual variability of sea surface temperature anomalies in the Indian Ocean. Weakening of the Walker circulation, anomalous monsoons, and moisture advection into East Africa in the two seasons are some of the phenomena associated with increased rainfall. Investigation on the Niño3 sea surface temperature (SST) anomaly index reveals an increasing trend with the selected target period of study projected to experience increased frequency of El–Niño/La–Niña events. GCMs projections for the past (1981-2000) and future (2045-2065) were bias corrected and projected changes at a river basin scale investigated. In the Nyando river basin, a perennial flood basin, the selected three GCMs project a wetter future with extreme events occurring almost two times the magnitude of the past climate. The trend by the three GCMs is the same; increased flood probability in the future and about 10-20% increase in mean discharge.

In addition to climate change assessment; the study also focused on short-term weather forecasting as a step towards adapting to a changing climate. This involved dynamic downscaling of global weather forecasts to high resolution with a special focus on extreme events. The skill of operational weather forecasts has increased over the last five decades. This improvement has taken place gradually and relatively steadily; driven by advances in scientific understanding of physical processes and rapidly increasing

computational resource developments. The last decade has seen remarkable progress in exploring satellite observations especially microwave measurements and the launching of new platforms. Numerical weather prediction and assimilation satellite data in the microwave band has been shown to improve predictability. In this tropical inland lake basin with a sizeable water body and locally controlled Mesoscale weather system; an improved prediction would be greatly useful for flood early warning and water resources management.

By utilizing complex model dynamics, the system was able to reproduce the Mesoscale dynamics well, simulated the land/lake breeze and diurnal pattern but was inadequate in some aspects. The quantitative prediction of rainfall was inaccurate with overestimation and misplacement but with reasonable occurrence. This was a remarkable improvement compared to the coarse resolution of 100km which had not factored in local scale dynamics induced by the land-lake interaction and low-high altitude contrast in this region. To address these shortcomings this thesis investigated the value added by assimilating Advanced Microwave Scanning Radiometer (AMSR-E) brightness temperature during the event. By assimilating 23GHz (sensitive to water) and 89GHz (sensitive to cloud) frequency brightness temperature; the predictability of an extreme rain weather event was investigated. The assimilation of AMSR-E brightness temperature through a Cloud Microphysics Data Assimilation (CMDAS) into the weather prediction model considerably improved the spatial distribution of this event.

Data assimilation improved the simulation of the rain event by more than 50% with the spatial location of maxima at 00hrs and 03hrs after assimilation matching Tropical Rainfall Measuring Mission (TRMM). In addition, overestimation of rainfall predicted by the NWP (without data assimilation) was reduced considerably. The assimilation of brightness temperature is implemented through a Radiative transfer model (RTM). The RTM involves the calculation of the surface emissions, scattering and absorption of passive microwave energy on soil, land surface and the atmosphere. A key component of this determination is the computation of surface emissivity which is derived from surface temperature. Results in this region showed that the NWP had a tendency to overestimate surface temperature which in turn affected the assimilated brightness

temperature. This had the negative impact of reduced water vapor in the system and the model could not keep the induced model state for long. Sensitivity experiments conducted by subtracting 2-10K from the surface temperature at the assimilation time showed that changes in the amount of water vapor corresponded to the magnitude of temperature change. This highlighted the uncertainty in water vapor assimilation due to model errors in estimation of surface temperature. This study identified this challenge and proposes a major validation / improvement of the RTM.

The downscaled/predicted quantitative rainfall was then assessed for its suitability as an input to a decision making process with respect to floods. Hydrological modeling using the QPF from the NWP showed promising flood simulation results even though there was a tendency to overestimate flow. Nonetheless, it shows a potential for future application as an input to an early warning system.

Contents

List of Figures

List of Tables

Acknowledgements

First and foremost, I would like to express my sincere gratitude to my advisor Prof. Toshio KOIKE first for accepting me to be part of this wonderful family and research group. Secondly, for the continuous support during my Ph.D. study and research, for his patience, motivation, enthusiasm, and immense knowledge. Thirdly, for his continuous faith and believe in me even when hope seemed to be lost. His guidance helped me in all the time of research and writing of this thesis. I could not have imagined having a better advisor and mentor for my Ph.D study. I will forever be grateful for this opportunity and the support beyond research activities. Besides my advisor, I would like to thank the rest of my thesis committee: Prof. Taikan OKI, Prof. Shinji SATO, Prof. Hiroaki FURUMAI and Prof. Kei YOSHIMURA for their encouragement, insightful comments, and hard questions.

My sincere thanks go to Dr. Rasmy MOHAMED, for his help in mixed programing, troubleshooting and understanding of atmospheric modeling. Special thanks to Dr. Patricia SANCHEZ, Dr. Kumiko TSUJIMOTO, Dr. Toru TAMURA and Dr. Ahmad Shakil, for offering me guidance in their respective expertise in my hour of need. I thank Tetsu OHTA, Katsunori TAMAKAWA for their valued help in programming and data processing. I would also like to appreciate the DIAS members of staff Akiko GODA, Tomoko FUJITA, Yumiko IKEYA and Yoshie ISHII for their support while I was studying here. Special regards to my host family Dr. ISHII Yumio and his family for their support. I would like to appreciate Hiroki YAMAMOTO for his selfless support and tutoring on my first days in Japan. I thank my fellow labmates in REEL Group: Cho Thanda NYUNT, Sixto DURAN-BALLEN, Yohei SAWADA, Rie SETO and all the students in the stimulating discussions and for all the fun we have had in the last three years. Also, I thank my colleagues in Jomo Kenyatta University: Dr. Ndegwa, Dr. Kuria, Dr. Waithaka and members of the GEGIS department for the support and the opportunity to study and enlightening me the first glance of research.

Last but not the least, I would like to thank my family: my wife Catherine; for the unending love, faith, support and encouragement; my daughter, for the silent support and encouragement; my mother Rose, for her unending love and prayers for my well-

being, my brother Peter and his wife, sisters Carol and Ronah and their children for best wishes and support during this time. I express special acknowledgement to my late father Samuel; for instilling the value of education in me, supporting and guiding me throughout my life.

Dedication

I dedicate this dissertation to my wonderful family, particularly to my understanding and patient wife, Catherine, who has put up with these many years of research, and to our precious daughter Shantelle, who is the joy of our lives. Through hardships, absence and the challenges; I found in you the strongest source of inspiration and strength to soldier on. Finally, to my late father, who believed in diligence, science, and the pursuit of academic excellence .

Chapter 1

Introduction

1.1 Background and overview

Extreme weather and climate events interacting with exposed and vulnerable human and natural systems can lead to disasters (Field et al., 2012). Some types of extreme weather and climate events have increased in frequency or magnitude, but populations and assets at risk have also increased, with consequences for disaster risk. According to recent studies (Easterling and Evans, 2000; Rahmstorf and Coumou, 2011; Coumou and Rahmstorf, 2012), it has been shown that extreme weather events have increased in the past century. There have been statistically significant trends in the number of heavy precipitation events in some regions and it is likely that more of these regions have experienced increases than decreases, although there are strong regional and sub-regional variations in these trends. Regional and global analyses of temperature extremes on land show recent changes consistent with a warming climate at the global scale(Treut et al., 2007). While some of these changes can be attributed to natural climate variability; a bulk of them tends to be associated with global warming caused by anthropogenic emissions. A changing climate leads to changes in the frequency, intensity, spatial extent, duration, and timing of extreme weather and climate events(Field et al., 2012).

The climate system is a complex, interactive system consisting of the atmosphere, land

surface, snow and ice, oceans and other bodies of water, and living things. According to the Intergovernmental panel on climate change (IPCC) climate change refers to a change in the state of the climate that can be identified (e.g., using statistical tests) by changes in the mean and/or the variability of its properties, and that persists for an extended period, typically decades or longer (Treut et al., 2007). These changes may be caused by internal processes as well as external forcing. Some of these are natural e.g. solar radiation and volcanic activity whilst others (like changes in the atmospheric composition that started during the industrial revolution), are as a result of human activities. Changes in the radiation balance can be achieved by changing incoming solar radiation, changing the earth's albedo or by altering the longwave radiation from Earth back towards space (e.g., by changing greenhouse gas concentrations). Climate, in turn, responds directly to such changes, as well as indirectly, through a variety of feedback mechanisms.

One aspect that has been investigated widely with respect to climate change is the impacts of extreme weather events. There is a general consensus that changes in frequency and intensity of extreme weather and climate events will have adverse effects on both humanity and nature. A major concern with climate change is that future extreme events will increase(Easterling et al., 2000). Recent extreme events all over the world have caused untold suffering to many people and caused major damages to economies. Extreme rainfall and associated floods have been the leading disasters globally with more than six million lives lost between 1900-2012 (Table 1.1). According to the International Disaster Database (EM-DAT), on average USD 65B dollars of global GDP is lost annually due to floods/storms related to extreme weather.

While some of these flood events can be attributed to man-made disasters; majority of global natural disasters is due to extreme weather. For example, the 2010 Thailand floods are estimated to have led to massive loss of jobs and damage of about USD 3B of Thailand's national income. The 2010 floods in China are reported to affect over 135m people, left over 3000 people dead, and led to over USD 51B damages. In 2010, extreme floods in Pakistan displaced many households with damages totaling about USD 41B. The Pakistan floods were

linked to the Russian heat wave and blocking in the extra tropics (Houze et al., 2011; Reale et al., 2012).

Table 1.1: Hydrological disasters from 1900 to 2012.

Continent	*# Events*	*# Deaths*	*Damage (000 US$)*
Africa	799	24,134	6,437,949
Americas	944	103,635	95,407,840
Asia	1,645	6,792,031	337,594,378
Europe	499	8,867	105,983,664
Oceania	125	500	13,826,875

Precipitation is a critical component of the global hydrologic cycle. Rainfall is essential for providing fresh water that sustains life; hence the water cycle and future availability of fresh water resources are big concerns globally. In developing countries, accurate forecasts of rainfall are critical as they can make or break these fragile economies, as by nature most of them are agricultural, relying heavily on rain-fed farming.

1.2 Problem statement

Mean changes in climate usually have catastrophic effects on our environment and ultimately human life. According to the IPCC, the temperature rise will likely lead to a sea level rise, changed rainfall patterns as well as extreme weather induced disasters. To address this, research has been conducted on how best to adapt (Smith and Lenhart, 1996; Lobell et al., 2008; Nordhaus, 2007; IPCC, 2007) and even how to reverse greenhouse gas emissions (e.g. (Trexler and Kosloff, 1998; Oberthür and Ott, 1999; Palm et al., 2004; Schils et al., 2005; DeFries et al., 2006)). While these attempts have been noble, well-coordinated and timely, some of the approaches have been thematic, science-driven and specific to regions. Few

attempts have been done to unify short term and long term climate studies as well as basin scale and regional or synoptic scales.

1.2.1 Extreme weather events

Extreme rainfall events usually have devastating effects on communities especially those living in developing countries. Floods, infrastructure damage, loss of lives and destruction of crops are some of the adverse effects associated with extreme rainfall. To mitigate, prevent, or even anticipate these natural disasters, it is important to have a reliable weather prediction system that provides timely and life/property saving early warnings. Numerical weather prediction models, regional and global weather forecasting systems are some of the integrated systems used to provide timely early warning systems. In Africa as well as other developing regions; the utilization of these tools and knowledge are still limited. Faced with a changing climate coupled with recurrent floods, there has been a continuous loss of property and lives.

The primary ingredient to these disasters (especially floods) is rainfall, which over the years, despite advances in modeling, computing power and use of new data and technologies, has proven to be difficult to predict. Numerical weather prediction (NWP) models using global forecasts as initial and boundary conditions have been used to provide short to mid-term forecasts globally. The prediction of landfall for cyclones, hurricanes, and typhoons has benefited greatly from the advanced regional and global forecast models. In addition, satellite data have provided immense improvement in prediction of extreme events. Through data assimilation of visible and microwave satellite data, the prediction of frequency and intensity of rainfall events has seen great improvement. Assimilation of weather variable retrievals (Andersson et al., 1994; Reichle, 2004; Phalippou, 1996) from satellite data as well as the raw radiances (Eyre et al., 1993; Rossow and Garder, 1993; Saunders et al., 1999; Dee and Uppala, 2009; Aravéquia et al., 2011) has produced improvements.

Despite this, Quantitative precipitation forecast (QPF) remains the most challenging tasks of weather prediction (Kuligowski and Barros, 1998; Bousquet et al., 2006; Lu et al., 2010) which has not yet been satisfactorily resolved in the numerical weather prediction

(NWP) models. Global weather forecasts have been used widely in many applications like hydrological flood modeling, crop monitoring, and disaster management. One challenge that has been hindering advancement in this field is the inability of the global and regional weather prediction models to represent local short term weather patterns in an accurate way. Global forecasts are coarse in nature, cannot represent local weather patterns well, and thus limits their application to global scales. However, since the development of the weather satellite technology, important improvements have been achieved. Using regional scale models, global forecasts can be downscaled to basin scales. In addition, through data assimilation, the prediction of extreme weather events has improved. Such improvements have been useful in regions that usually experience extreme weather; mostly in developed countries. The most vulnerable and usually agriculture-driven economies have been at a loss when these events occur. This is because the utilization of such advanced technologies is limited and the technical know-how is still at low levels. This study seeks to develop a framework through which extreme rainfall event forecasting in the LVB can be improved.

1.2.2 Climate change

There is a general lack of integrated climate change studies with more regional and basin scale studies having a weak link between the temporal, spatial and thematic dimensions. Few multi-dimensional holistic studies exist and these provide useful guidelines for application (Black et al., 2011; Jarvis et al., 2011; Arndt et al., 2010; Vuuren et al., 2009). Africa has been identified as one of the most vulnerable continents to climate change and climate variability, a situation aggravated by the interaction of "multiple stresses", occurring at various levels, and low adaptive capacity (Boko M et al., 2007). East Africa has been classified as one of the regions likely to experience adverse climate changes. Being a predominantly agricultural region, the economic and social impacts in this region will negatively affect the rapidly increasing population. For example, whilst some farmers have developed several adaptation options to cope with current climate variability, such adaptations may not be sufficient for future changes of climate. Thus, it is important to understand the likely variability of extreme

climate events (e.g. floods) which destroy households, infrastructure, and leads to loss of life/crops. GCM projections based on several climate change scenarios have been useful inputs for these kinds of studies. However, their spatial resolutions have been a limiting factor to local scale investigations. To achieve this, there is a need to downscale these into higher spatial and temporal resolutions.

The LVB is classified as one of the regions likely to experience adverse climate changes (IPCC, 2007; LVBC, 2011). It is one of the basins that have been heavily affected by extreme weather and especially storm-induced floods; and an understanding of the likely impacts of climate change in frequency and intensity of extreme events is important. Waako et al. (2009); Beyene et al. (2009) recently investigated the potential effect of climate change in the Nile basin and suggested increasing mean runoff and extreme peak flows. Taye et al. (2011) focused on impacts of extremes on floods in Nyando catchment (within LVB) for the 2050s, but the associated mechanisms for these extremes were not clarified. Sang (2005) evaluated the impact of changes in land cover, climate, and reservoir storage on flooding in the Nyando river basin using synthetic climate change and suggested afforestation and dam structures as some of the possible adaptation mechanisms. Regionally, Shongwe et al. (2011) investigated changes in mean and extreme precipitation in EA under global warming and suggested a change in the structure of the eastern hemisphere Walker circulation as being consistent with an increase in EA precipitation. Williams and Funk (2011) focused on regional dynamics of projected changes in climate in the EA region using long term observations and suggested a westward extension of the Walker circulation as causing the drying up in EA.

These previous studies can be grouped into two broad categories: regional and local (river scale) analysis. The linkage between global/regional dynamics and local impacts on smaller scales in this region is lacking. In addition, the use of synthetic climate change, randomly selected GCMs and basic statistical downscaling approaches add to the already established uncertainties associated with GCM projections.

Numerical modeling using GCMs is one of the most used approaches to study and project future climate change based on various emission scenarios. Some of the challenges associated

with use of climate projections for local scale impact analysis are 1) coarse resolution; 2) inability to represent local phenomena due to lack of parameterization; and 3) their general biases. That notwithstanding, with appropriate statistical and/or dynamic downscaling, reasonable impact studies can be carried out as a guide or as a framework for policy and integrated resource management systems. For example, Githui et al. (2009) used the "delta-method" of statistical downscaling in this region while Elshamy et al. (2009) applied the cumulative distribution function (CDF) matching approach downscaling proposed by Ines and Hansen (2006) to investigate impacts on the Blue Nile. However, one weakness in these approaches is the generalization of the precipitation field. Without bias correction of extreme rainfall independently; the outcome from these bias corrections can provide conflicting results. In this thesis for local scale analysis, we use an improved approach proposed by Nyunt et al. (2013) where rainfall is divided into three components and bias-corrected independently to preserve seasonality, frequency and intensity of extreme events. This bias-corrected rainfall is then used to force a hydrological model to investigate the likely changes in floods under climate change. We extended our study to Meso and regional scales to investigate the related regional scale disturbances in EA as a whole. This includes changes in regional mean climate, circulation patterns, and extremes by use of indices.

1.3 Research framework

Climate change and impact studies are usually geared towards enhancing adaptability, reducing vulnerability, and harnessing these changes in positive ways. The likely increase in floods, prolonged droughts, and changed rainfall patterns will lead to food insecurity, displacements, and loss of livelihoods. To prepare and counter these changes, there is a need for an integrated approach to study climate change. It is beneficial to factor in the competing and conflicting dimensions of climate change as well as balancing benefits and losses in designing adaptation policies. This can only be achieved through an integrated approach, combining the various aspects of weather forecasting and climate projection.

In the past, climate change studies have been fragmented and focused on specific interests. For example: hydrologists might be interested on climate change impacts on water resources and flood management; Ecologists might be interested in the impacts of climate change on species characteristics health; scientists and global development agencies might be interested in the future prevalence of diseases as well as human development indices; climate scientists and meteorologists are interested in regional changes in circulations and synoptic scale phenomenon like ENSO, IOD and monsoons. While each of these aspects is important and critical, their integration and interdependence has not been investigated fully. The respective studies vary with respect to scales (10 to 1000 of km), scope and interest, as well as technological (thematic vs. circulation models). To be able to utilize the available resources efficiently and draw conclusive decisions, there is a need to integrate by creating a common reference point with shared knowledge, skill and tools.

This study provides a holistic approach to climate change assessment with different dimensions. Specifically this thesis answers three questions: 1) What are the projected local changes in extreme rainfall and floods in the Nyando river basin? 2) What are the projected changes in Meso and regional scale changes and how does it link with these local scale changes? 3) What are the physical and dynamic characteristics of these extreme events? We use a systematic approach by selecting " the best (least biased)" GCMs for this region, perform a statistical downscaling, and analyze the regional dynamics associated with these changes. We demonstrate an integrated modeling framework that helps us translate regional climate projections into river basin scales. Finally, we explore numerical weather prediction coupled with land data assimilation as one of the options for adapting to adverse climate change.

Because climate change involves a wide range of interlinked problems; solutions must be pursued in an interdisciplinary manner. This study focuses on a few selected dimensions significant in the LVB East Africa. Figure 1.1 summarizes the various components and dimensions; temporal and spatial dependence, data and tools integration as well as short to long term investigation. The objectives and plans for each of these components are as

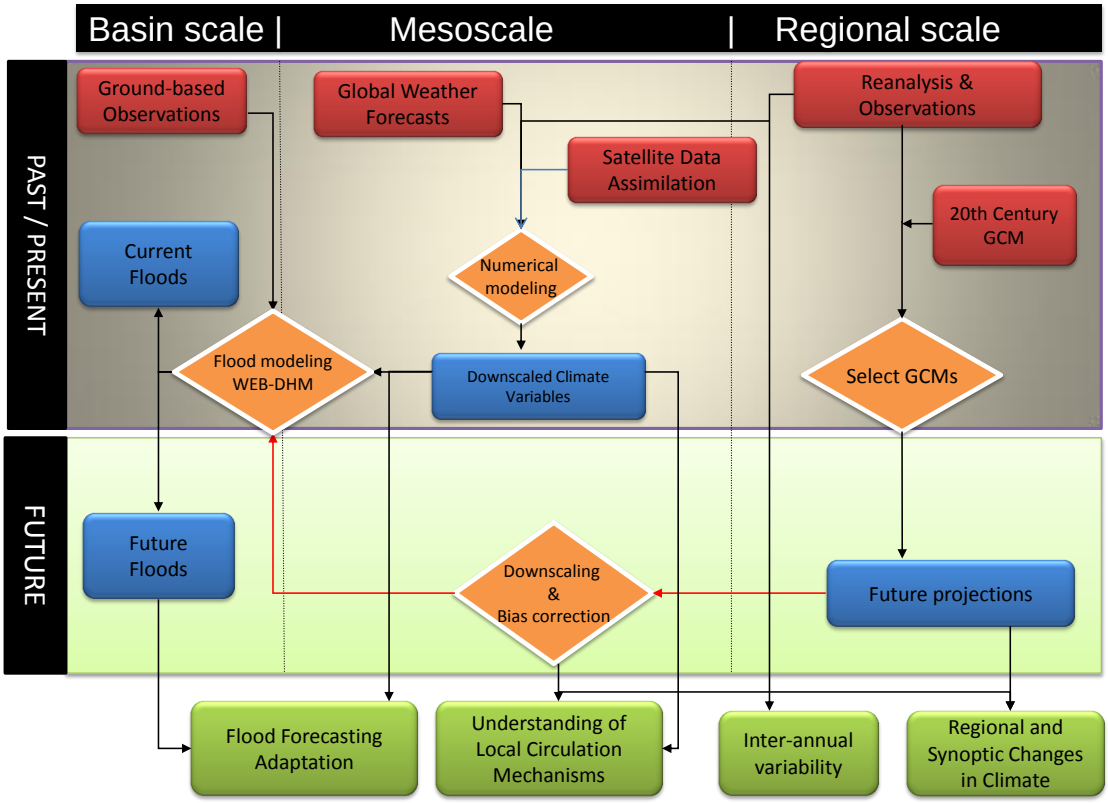

Figure 1.1: Research framework.

discussed in the succeeding sections.

1.3.1 Spatial and temporal dimensions

Different studies have focused on temporal and spatial scales relevant to their interests. Climate studies mainly focus on regional scales (1000 km) while hydrological models focus on higher resolutions (10 km). Temporally, this also differs from hundreds of years for climate studies to hours/days in cases of flash floods. This study seeks to bridge these gaps by:

- investigating regional changes of mean and extreme weather events using GCM projections
- investigating projected changes in mean and extreme precipitation and flow regimes

at a basin scale through statistical downscaling. The transfer of knowledge and understanding from the regional scale is key to interpreting projected changes at the basin scale.

At the mesoscale and regional scales, climatic changes in Mesoscale dynamics especially locally induced phenomena like terrain based convection rainfall, land and lake breezes is desirable. This can be adequately addressed through dynamic downscaling using regional climate models.

1.3.2 Time-scale interdependence

Weather refers to short timescales with events lasting from hours to several days. Climate on the other hand is the long-term mean weather conditions over a region. Knowledge and understanding of the short-term mesoscale dynamics are always valuable to understanding long term climatic conditions and ultimately climate change. For example, improved knowledge of extreme storms in the short-term is useful as a baseline for investigating the likelihood of the same type of events in the future. To add value to this dimension, this study attempts to improve the understanding of storm events in the LVB region through downscaling of the Global Forecast System (GFS) model forecasts, a similar approach to dynamic downscaling of climate projections. The study also seeks to investigate the usability of downscaled variables as forcing for hydrological models with a view of improving flash floods predictability. Gaps and areas needing improvement in numerical modeling are also identified.

1.3.3 Data, tools and analytical integration

Integrated modeling is a novel approach to couple knowledge and models from different disciplines and research fields and to use their potential in the strategic planning of water management at the river basin scale(Gaiser et al., 2008). Numerical models have found central significance in modern day science. Climatologists and climate change scientists use GCMs to understand and project future climates while hydrologists use hydrological

models to investigate water resources, flow regimes, flood recurrence, and as inputs to early warning systems. Coupling of models has previously been conducted but with respect to comprehensive integrated basin scale, mesoscale, and regional, application case studies are few. We demonstrated a comprehensive approach in which value from GCMs and global forecasts is translated to small scale using regional and basin scale models through an offline approach. Specifically, this study also seeks to:

- Downscale GCM projections for basin scale investigation of future floods
- Downscale GFS forecasts using a regional mesoscale model for flood prediction

In addition, satellite data is used to investigate value added to downscaling/forecasting of an extreme weather event in the LVB. In this approach we integrate statistical and numerical methods, local regional and global models as well as ground-based observations with global satellite data.

1.3.4 Key objectives

In summary, the study seeks to provide a holistic approach to weather and climate integration, giving a comprehensive view on the key aspects as a step towards disaster management. In principle, the study focuses on *climate change assessment* at multiple spatial and temporal scales as well as *first steps towards adaptation* to extreme events under the current climate. Specifically, the objectives of this study are:

- To investigate projected changes in rainfall at river basin scale through downscaling of Coupled Model Inter-comparison Project Phase (CMIP3) GCMs projections
- To investigate projected changes in flow regimes in the Nyando river basin (within LVB) under climate change

- To investigate projected regional climatic changes using CMIP3 GCM and the mechanisms of extreme events

With respect to *extreme weather adaptation* under the current climate, the study seeks to:

- dynamically downscale global weather forecasts and improve extreme rainfall event prediction in the LVB through data assimilation
- investigate the applicability of downscaled forecasts as forcing for hydrological flood simulation

1.4 Research strategy

Being a multi-dimensional study, this study attempts to investigate to reasonable depths the interaction and significance of each of the aforementioned themes. Several tools and datasets at disposal have been used to achieve this. At the regional scale, global data sets i.e. reanalysis, climatologies, and climate projections have been used to analyze East African climate: past climatology, future projections as well as projected changes. In addition, projected changes in the synoptic scale phenomenon and known climate drivers like the Indian Ocean SST anomalies have been investigated. To retain some objectivity and reduce uncertainty in the GCMs, screening of the available GCMs was carried out and only the least biased three were used. In the future, considerations to use higher spatial and temporal resolutions from the Coupled Model Inter-comparison Project Phase 5 (CMIP5) will be looked at.

At the mesoscale dimension, our focus was on how to improve short term weather forecasts through dynamic downscaling. This was achieved by using the Advanced Regional Prediction (ARPS), a mesoscale storm model that has been used widely to study storms, extreme weather events and downscaling of forecasts. To add value to downscaling and address some of the challenges associated with downscaling, a Coupled atmosphere land data assimilation

system (CALDAS) was used to improve prediction of extreme events with a focus on the LVB. The AMSR-E passive microwave data which is sensitive to water vapor and cloud water was used for this purpose. Improvements in QPF and the value added by the introduction of satellite observations are investigated and key issues needing further development identified.

It is expected that mesoscale models are able to represent mesoscale/local weather dynamics, which are the key drivers of activities and interactions at the basin scale. With this in mind, the downscaled meteorological variables from the regional model are used to drive the Water and Energy Budget-Based Distributed Hydrological Model (WEB-DHM) and study suitability as inputs for an early warning system for floods in the Nyando river basin, located in the greater LVB.

1.5 Justification of the study

Lake Victoria and its catchment support millions of people in agriculture, transport, and fishing. It provides food (fish), hydropower, transport and communication, tourism, water for domestic agricultural and industrial use, wastewater disposal, and recreation. In addition, this basin is the main source of the Nile river . Extreme weather-induced disasters like droughts and floods have been prevalent and this has affected farming widely, the main subsistence economic activity in the basin. Perennial floods have led to loss of lives, property and incomes and so it is important to understand the likely changes in climate dynamics (especially rainfall) since this will have major impacts in the region. Improving predictability of short term extreme rainfall is also important as this can form the backbone of early warning systems in the flood zone areas.

According to the Lake Victoria Basin Commission(LVBC), Lake Victoria is one of the most dangerous waterways in the world (LVBC, 2012). Each year 4,000-5,000 people die in the lake due to drowning, pirate attacks, and accidents . Most of the victims are fishermen who leave behind an average of 8 dependents and hence the hazard affects over 30,000 people annually. It is not clear what portion is caused by human error or weather, but the

likelihood of an extreme event would only exacerbate the situation. In addition, areas bordering Lake Victoria also experience the highest number of thunderstorms (more than 200 a year) associated with nocturnal convection over the Lake (Fraedrich, 1972; Anyah et al., 2006). Land-breeze convergence over the lake during the night releases latent instability of the moist lower layers of air over the lake which participate in the land breeze circulation, resulting in the development of cumulonimbus clouds and thunderstorms over the lake most nights of the year (Lumb, 1970). An understanding of the likelihood of increases or decreases in these events would be helpful in supporting early flood warning systems, extreme weather monitoring for maritime safety systems such as LVBC (2012) and general safety and sustainability in the lake basin.

In a feasibility study Semazzi et al. (2011) commissioned by the LVBC, several aspects associated with extreme climate were reviewed through interviews, modeling, desk reviews and consultations with stakeholders in the LVB. They identified extreme weather as a big challenge to transportation in the LVB. The study included assessment of atmospheric and marine, monitoring and modeling requirements from which a Plan for a Navigation Early Warning System (NEWS) (CTOR1, CTOR3, and CTOR4) was one of the proposed interventions. This is in addition to a plan for a Hotspots Atlas (CTOR2), Marine and Atmospheric Observational Network and Water/Air Quality (CTOR3) and a plan for the Consultant's Proposal for a Centre for Meteorological Services (CMS) for the LVB (CTOR5).

One key finding from this study was that there was a general lack of reliable and useful weather forecasts: *"The final daily forecast in each country is largely based on the analysis of output from a handful of regional mesoscale models run daily in Nairobi and Dar es Salaam. These numerical weather prediction systems are initialized using the analyzed output from global models such as the Global Forecast System (GFS) or the European Centre for Medium-Range Weather Forecasts (ECMWF). Numerical models can provide useful guidance for forecasters concerned with severe storms, but their usefulness is conditioned on their ability to interpret the current weather scenarios and integrate the patterns forward in time. In the future, mesoscale models for the LVB region would be well served to utilize the surface*

data being collected to improve the initial conditions in the model. Additionally, any future radar or buoy data collected could be assimilated into the models to improve their predictive capabilities. "

Even though our study is not part of this project; this is one aspect we seek to provide an input into improving weather prediction in the LVBC.

1.6 Dissertation outline

Chapter one of this thesis addresses the problem statement, the issue of climate change, and current challenges of numerical weather prediction toward extreme events. Chapter 2 discusses the concept of holistic approach to climate change for flood monitoring with a focus on extreme events. The results of climate change assessment of the Nyando river basin scale are presented. Chapter three builds on Chapter 2's findings; the associated changes in regional and synoptic systems are discussed. In addition, the possible mechanisms of extreme events under CMIP3 are discussed.

Chapter four presents an overview of numerical weather prediction of extreme events. The concepts of dynamic downscaling and data assimilation are briefly discussed. The results of numerical weather prediction and dynamic downscaling of global weather forecast experiments at the LVB are presented. The assessment of performance of ARPS in representing a selected extreme event is analyzed and strengths and deficiencies identified. The value added by assimilation is discussed as well as the performance of the system. Extra sensitivity experiments on aspects that need improvement are presented and key issues identified. Finally, chapter five presents the key findings, conclusions and recommendations for future improvement.

Chapter 2

Climate change: Expected changes in rainfall and flow Regimes in Nyando river basin

2.1 Climate change overview

The importance of climate change has been highlighted in many studies. In developing early warning systems in relationship to health (Patz et al., 2005) emphasized on the need for factoring climate change. In developing a framework for community interactions under climate change, Gilman et al. (2010) showed that species interactions can dramatically alter species responses to climate change. In their study, Fankhauser and S.J. Tol (2005) drew attention to the fact that the direct impact of climate change on the economy is not the only way in which global warming affects the future welfare but also the prospect of future damages (or benefits) also affects capital accumulation and people's propensity to save, and hence the rate of economic growth.

Water is the key to life and its availability, quantity, and quality is important for humanity. It has been suggested that "if there is going to be a World War III, it will be fought over water". It is therefore of greater importance to consider the water issue both for sustain-

ability. The impacts of climate change (both natural and anthropogenic) on water resources have been investigated widely and there is an almost consensual agreement on the need for sustainable management of the available water resources and strategic planning for future generations, both nationally and globally (Bates et al., 2008; Piao et al., 2010; Delpla et al., 2009; Whitehead et al., 2009). Sustainable use of the available water resources as well as sound future planning based on the most likely scenarios of future climate is very important both at the regional and local planning levels. In designing policies and strategic management plans, it is imperative and almost a requirement to consider climate change impact possibilities.

One of the adverse effects of climate change as identified in the AR4 report is the likelihood of a global increase in extreme weather events. These events, whose recurrence cannot be wholly attributed to climate change, tend to have more negative impacts. It is thus essential and important to understand the probabilities of such events in the future not only at global and regional scales but also at smaller scales (e.g. river basin scale). This chapter presents the results of such an investigation at Nyando river basin (NRB) a part of LVB characterized by perennial floods occasioned by extreme rainfall. The CMIP3 GCM output is analyzed with 1981-2000 chosen as the base period and 2045-2065 as the future. Through bias correction and downscaling, precipitation from the coarse GCMs was transferred to the basin scale and changes between the past and future investigated. The impact of changes in mean and extreme rainfall in flood simulation was done using WEB-DHM. The mechanisms of changes in extreme events are discussed in chapter 3.

2.1.1 History of climate change

The climate system is a complex, interactive system consisting of the atmosphere, land surface, snow and ice, oceans and other bodies of water, and living things. Weather and climate are an essential aspect of the climate system. They are part of the daily experience of human beings, and are essential for health, food production and well-being. If one wishes to understand, detect and eventually predict the human influence on climate, one needs, to

understand the system that determines the climate of the Earth and of the processes that lead to climate change (Baede et al., 2001). "Weather", as we experience it, is the fluctuating state of the atmosphere around us, characterized by temperature, wind, precipitation, clouds and other weather elements. Weather is the result of rapidly developing and decaying systems (such as mid-latitude low and high pressure systems) with their associated frontal zones, showers, and tropical cyclones.

Weather has limited predictability with mesoscale convective activity lasting only a few hours while synoptic scale cyclones may be predictable over a period of several days to a week. Beyond a week or two individual weather systems are unpredictable. Climate, on the other hand climate refers to the average weather, the mean and variability over a certain time-span and a certain area. Classical climatology provides a classification and description of the various climate regimes found on the Earth. The climate varies from place to place, depending on latitude, distance to the sea, vegetation, the presence or absence of mountains or other geographical factors. Climate varies also in time, from season to season, year to year, decade to decade or on much longer time-scales, such as the Ice Ages.

The study of climate change study can be traced back to the 19^{th} century where in 1890's and 1900's Samuel Pierpoint Langley, Arvid Hgbom and Svante Arrhenius working independently tried to quantify the amount of carbon dioxide in the atmosphere as well as its sources. It was possible during these early stages of climate change science to hypothesize that an increase in carbon dioxide would lead to eventual warming of the climates. However, with only rudimentary observations and low emission rates those times, it was impossible to quantify the trends and many thought any reasonable warming would take thousands of years and even be beneficial to humanity (Weart, 2003).

2.1.2 The IPCC

The advent of computers and advancement in the understanding of the atmospheric dynamics led scientists and meteorologists to give Svante Arrhenius arguments more weight and several studies were conducted. Better understanding of ocean chemistry led to a realization that

the ocean surface layer had limited ability to absorb carbon dioxide. By the late 1950s, more scientists were arguing that carbon dioxide emissions could be a problem, with some projecting in 1959 that CO_2 would rise 25% by the year 2000, with potentially "radical" effects on climate (Weart, 2003). By 1970's global warming studies had taken center stage and many scientists were involved in modeling of current and historical climate.

The Intergovernmental Panel on Climate Change (IPCC) was created in 1988. It was set up by the World Meteorological Organization (WMO) and the United Nations Environment Program (UNEP) as an effort by the United Nations to provide the governments of the world with a clear scientific view of what is happening to the climate. The initial task for the IPCC as outlined in the UN General Assembly Resolution 43/53 in December, 1988 was to prepare a comprehensive review and recommendations with respect to the state of knowledge of the science of climate change, social and economic impact of climate change, possible response strategies and elements for inclusion in a possible future international convention on climate.

Today this also aims

"...to assess on a comprehensive, objective, open and transparent basis the scientific, technical and socioeconomic information relevant to understanding the scientific basis of risk of human-induced climate change, its potential impacts and options for adaptation and mitigation. IPCC reports should be neutral with respect to policy, although they may need to deal objectively with scientific, technical and socioeconomic factors relevant to the application of particular policies."

Released in 1990, the first IPCC Report concluded that the world had indeed been warming.

"...Global mean surface air temperature has increased by 0.3 to 0.6^{0}C over the last 100 years, with the five global-average warmest years being in the 1980's. Over the same period, global sea-level increased by 10 to 20 cm. These increases were not smooth in time, or uniform over the globe..."(IPCC, 1990)

The report further predicted an average rate of increase of global mean temperature

during the next century of about 0.3^0C per decade (with an uncertainty range of 0.2–0.5^0C per decade) assuming the IPCC Scenario A (Business-as-Usual) emissions of greenhouse gases. The IPCC Second Assessment Report (1995) provided key input for the adoption of the Kyoto Protocol in 1997. The Third Assessment Report came out in 2001 and the Fourth in the course of 2007. *"Climate Change 2007"*, clearly brought to the attention of the world the scientific understanding of the present changes in our climate and led the organization to be honored with the Nobel Peace Prize at the end of that same year (IPCC, 2007). A fifth assessment report is scheduled to be released in 2013/2014. The reports have given scientists and policymakers, a platform not only for information on climate change but also for debate, and a main reference point for evaluation of climate change.

2.2 Modeling of climate change

Concern about potential human impacts on the climate system has generated interest in predicting future climate and focused public attention on climate models-the tools used to make such predictions (Keefe and Kueter, 2004). Scientific models, which are mathematical descriptions of behaviors of natural systems including climate, allow scientists to study the cause-effect relationships between the phenomena and systems. Climate models are based on well-established physical principles and have been demonstrated to reproduce observed features of recent climate and past climate changes (Randall et al., 2007). There is considerable confidence that Atmosphere-Ocean General Circulation Models (AOGCMs) provide credible quantitative estimates of future climate change, particularly at continental and larger scales. Confidence in these estimates is higher for some climate variables (e.g. Temperature) than for others (e.g., precipitation).

However, there remains a big challenge in addressing the uncertainties between the different models, the trends and future projections which on many occasions have been conflicting. The term "projections" is commonly used in climate modeling partly due to uncertainty in drawing strong conclusions from model outputs. According to the IPCC AR3 report:

..Climate projection is the response of the climate system to emission or concentration scenarios of greenhouse gases and aerosols, or radiative forcing scenarios, often based upon simulations by climate models. Climate projections are distinguished from climate predictions to emphasize that climate projections depend upon the emission/concentration/ radiative forcing scenario used, which are based on assumptions, concerning, (e.g., future socioeconomic and technological developments), that may or may not be realized, and are therefore subject to substantial uncertainty..(Baede et al., 2001).

As noted in Randall et al. (2007), there has been significant improvements in climate modeling notably: 1) coordinated international efforts and scrutiny of climate models, 2) The ability of AOGCMs to simulate extreme events, especially hot and cold spells, has improved and 3) the possibility that metrics based on observations might be used to constrain models projections of climate change has been explored for the first time, through the analysis of ensembles of model simulations. This has been achieved through coordinated modeling efforts.

2.2.1 CMIP3 - Coupled Model Inter-comparison Project Phase 3

Climate change modeling was first characterized in the 1980s by a number of distinct groups developing, running, and analyzing model output from their own models with little opportunity for anyone outside of those groups to have access to the model data (Meehl et al., 2007). In the mid 1990's the World Climate Research Program (WCRP) committee organized the first global coupled climate model inter-comparison (CMIP) exercise whereby modeling groups performed control runs and idealized 1% CO_2 increase experiments and made the data available to researchers outside the modeling group. This was later followed by CMIP2 and CMIP3 with more variables and scenarios. This model data was collected and archived at the Program for Climate Model Diagnosis and Inter-comparison (PCMDI) and is currently available to the public through a registered download (WRCP CMIP3 Multi-Model Data).

The data were meant to serve IPCC's Working Group 1, which focused on the physical climate system – the atmosphere, land surface, ocean and sea ice – and the choice of variables

archived at the PCMDI reflects this focus. Currently, a total of 17 modeling groups from 12 countries participate with 24 models. Considerable resources (human and computing) were devoted to this project (Meehl et al., 2007). Data from the CMIP3 archive has been used widely in climate change studies all over the world as listed on the PCMDI website.

2.2.2 CMIP5 - Coupled Model Inter-comparison Project Phase 5

After the success of CMIP3, a group of 20 climate modeling groups from around the world, the WCRP's Working Group on Coupled Modeling (WGCM), with input from the International Geosphere-Biosphere Programme's (IGBP) Analysis, Integration and Modeling of the Earth System (AIMES) project agreed to promote a new set of coordinated climate model experiments. These experiments comprise the fifth phase of the Coupled Model Inter-comparison Project (CMIP5) (Taylor et al., 2012).

CMIP5 will provide a multi-model context for 1) assessing the mechanisms responsible for model differences in poorly understood feedbacks associated with the carbon cycle and with clouds, 2) examining climate "predictability" and exploring the ability of models to predict climate on decadal time scales, and, more generally, 3) determining why similarly forced models produce a range of responses. The CMIP5 project is expected to address some of the questions that arose from the Fourth Assessment Report (AR4) and provide a valuable input into the Fifth Assessment Report (AR5), scheduled for publication in late 2013.

2.3 Extreme weather

An extreme (weather or climate) event is generally defined as the occurrence of a value of a weather or climate variable above (or below) a threshold value near the upper (or lower) ends ('tails') of the range of observed values of the variable. Some climate extremes (e.g., droughts, floods) may be the result of an accumulation of weather or climate events that are, individually, not extreme themselves (though their accumulation is extreme)(Field et al., 2012). Extreme weather events include spells of very high temperature, torrential

rains, and droughts. Under an enhanced greenhouse effect, changes can occur in both mean climate parameters and the frequency of extreme meteorological events. Small changes in mean temperature can result in disproportionately large changes in the frequency of extreme events(Rosenzweig et al., 2001). Many weather and climate extremes are due to climate's natural variability including synoptic phenomena such as El–Niño/La–Niña .

A changing climate leads to changes in the frequency, intensity, spatial extent, duration, and timing of weather and climate extremes, and can result in unprecedented extremes. Conversely, not all extremes necessarily lead to serious impacts (Seneviratne et al., 2012). In Field et al. (2012) and references therein, observations since 1950, observations suggest statistically significant increases in the number of heavy precipitation events (e.g., 95th percentile) in more regions than there have been statistically significant decreases, but there are strong regional and sub-regional variations in the trends. There is medium confidence that since the 1950's some regions have experienced a trend of more intense and longer droughts, in particular in southern Europe and West Africa, but in some regions droughts have become less frequent, less intense, or shorter, for example, in central North America and northwestern Australia. Some of these extremes have been attributed to anthropogenic influences, including increases in atmospheric concentrations of greenhouse gases. Subsequently, most models project substantial warming in temperature extremes of the 21st century and that it is likely that the frequency of heavy precipitation or the proportion of total rainfall from heavy rainfalls will increase in the 21st century over many areas of the globe. This implies that the likelihood of extreme floods in many parts of the globe remains high. However, uncertainties in projections of large-scale patterns of natural variability remain large.

2.3.1 Extreme weather indices

Extreme indices have been widely used in the study of extreme weather events with respect to climate change. Typical indices include the number, percentage, or fraction of days with maximum temperature (Tmax) or minimum temperature (Tmin), below the 1st, 5th, or 10th percentile, or above the 90th, 95th, or 99th percentile, generally defined for a reference time

period. Extreme Value Theory is also an approach used for the estimation of extreme values (e.g.(Coles and Davison, 2008)) to derive a complete probability distribution for such low-probability events, which can also help analyze the probability of occurrence of events that are outside of the observed data range.

Tebaldi et al. (2006) analyzed historical and future simulations of 10 such indicators as derived from an ensemble of 9 GCMs contributing to the IPCC-AR4 report. Under a range of emissions scenarios, he showed an agreement in greater temperature extremes consistent with a warmer climate. Peterson (2002) demonstrated that extreme precipitation showed an increasing trend since the 1950's in the Caribbean while the measure of dry conditions, the maximum number of consecutive dry days, showed a decreasing trend. At regional scales, these indices provide a first step analysis of the likely patterns of extremes at local scales.

2.3.2 Extreme weather impacts

Increasing exposure of people and economic assets is the major cause of long-term increases in economic losses from weather- and climate-related disasters (Handmer et al., 2012). Transport infrastructure is vulnerable to extremes in temperature, precipitation/river floods, and storm surges, which can lead to damage in road, rail, airports, and ports, and electricity transmission infrastructure is also vulnerable to extreme storm events. The tourism sector is sensitive to climate since the climate is the principal driver of global seasonality in tourism demand. Most economies in the developing world are dependent on agriculture. Droughts in Africa, especially since the end of the 1960's, have impacted agriculture, resulting to substantial famine. In many regions, the main drivers of future increases in economic losses due to some climate extremes will be socioeconomic in nature. Developing countries are more likely to suffer from future disasters than developed countries, especially in relation to extreme impacts.

2.4 Study area: Nyando river basin

Knowledge in hydrological response to climate change in a particular basin is important not only for operational purposes like dam control and irrigation but also for policy planning of disaster management, early warning, and preparedness. Thus investigation of likely impacts of climate change on a basin scale is important, though there are limitations attributed to the spatial resolution and uncertainties in the use of GCM projections. These uncertainties still remain to be a limiting factor as well as the multiple future water uses not accounted for in future projections. Downscaling is one way in which GCM projections are used to investigate climate change at the basin scale. Two downscaling approaches are typically available; statistical downscaling and dynamical downscaling. Dynamic downscaling involves the use of finer resolution numerical weather prediction models with GCM output as initial and boundary conditions. Statistical downscaling involves the use of statistical relationships to convert the large-scale projections from a GCM to finer spatial resolutions. The statistical downscaling approach was used.

Nyando river basin (Figure 2.1) is on the western parts of Kenya and is within the greater LVB. It is geographically located along the equator bounded by latitudes 0^o 7' N and 0^o 24'S; longitudes 34^o 25' E and 35^o43'E . It covers an area of about 3500 km^2 and experiences some of the most severe problems of agricultural stagnation, environmental degradation, and deepening poverty found anywhere in Kenya (Githui, 2008). The Nyando River drains into the Winam Gulf of Lake Victoria and is a major contributor of sediment and phosphorus to Lake Victoria. Annual flooding resulting to loss of lives, crops, and housing is one of the major challenges in this basin. About 750,000 persons reside within the Nyando basin, most of whom live in Nyando District in Nyanza Province, Nandi and Kericho districts in Rift Valley Province (LVBC, 2007).

Rainfall in this region is mainly influenced by the migration of the Intertropical Convergence zone (ITCZ) and exhibits a bi-modal pattern with peaks in March-April-May (MAM) and October-November-December (OND) known as long rains and short rains respectively.

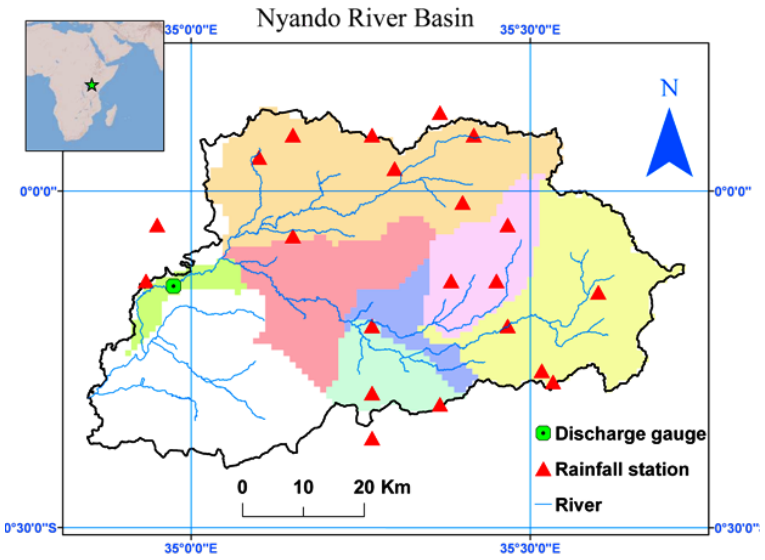

Figure 2.1: Nyando river basin.

In addition to the observed bimodal pattern, a replica of the regional seasonal march, this region has an additional peak in August. The mean annual rainfall ranges from 800 mm in the lowlands to about 1600 mm in the highlands. Regional and synoptic scale phenomena like the Indian Ocean Dipole have been shown to influence the East African climate as whole (Nicholson, 1996; McHugh, 2006; Black, 2005; Hastenrath, 2007; Latif and Dommenget, 1999; Indeje et al., 2000). Floods on the lower Kano plains occur frequently and this has affected the livelihoods of about 1.1 million people (Sang, 2005; Swallow et al., 2009; Mutua et al., 2012b).

2.5 GCM projections

Testing models' ability to simulate "present climate" (including variability and extremes) is an important part of model evaluation (Solomon et al., 2007). However, there is no universal methodology in selecting GCMs for climate projections (Overland et al., 2011). One of the criteria that is often used is the ability of the GCM to simulate present day climate (IPCC, 2007). This is based on the assumption that GCMs that present climate

well are likely to simulate more plausible future climates. While this assumption may be insufficient in some aspects, combining the approach with how well the GCM represents the interannual variability can reduce the uncertainty. We therefore select the GCMs based on their representation of the East African climatology for 1981-2000 under the 20^{th} Century experiment. We focus on the spatial pattern and bias as compared to Global Precipitation Climatology Project (GPCP) for precipitation, reanalysis data for humidity, zonal wind, and Geopotential height.

We used JRA-25 reanalysis as "proxy" observations since long term reliable meteorological observations in this region are usually unavailable. Even though the reanalysis has a weak representation of trends in observations caused by different sources of satellite data for JRA25 and large temperature bias in the stratosphere, its advantages outweigh the disadvantages. For example, the performance of the long time series of the global precipitation is the best among the other reanalysis. JRA-25 is also the first reanalysis to assimilate wind profiles, and also low-level cloud along the subtropical western coast of continents is well simulated (Onogi et al., 2007).

Table 2.1: Selected GCMs used in this study.

Institute	**GCM**	**Acronym**
Max Planck Institute for Meteorology, Germany	ingv_echam4	ingv
Max Planck Institute for Meteorology, Germany	mpi_echam5	mpi
Meteorological Research Institute, Japan	mri_cgcm2_3_2a	mri

2.6 Projected changes in the Nyando river basin

Climate change and its variability will continue to exert additional pressure on the already strained water resources in the East African region. Previous analysis of climate change (Arnell, 2004; Thieme et al., 2010; Arnell, 1999) and its effect on water resources in Africa

shows a likely increase in the number of people experiencing water scarcity by 2055. In their investigation of climate change in this basin, Gathenya et al. (2011) showed that temperature change had a relatively minor effect on streamflow and sediment yield compared to change in rainfall and land surface condition. They suggested that improvements in the land surface condition that result to higher infiltration are an effective adaptation strategy to minimize the effects of climate change on supply of watershed services.

2.6.1 Methods

Figure 2.2 summarizes the framework used at the basin scale investigation on the impact of climate change on floods in the Nyando river basin. This comprises of: GCM selection (based on seasonality and bias), bias correction and downscaling of GCM outputs, flood simulation for the past, and likely flood scenario in the future.

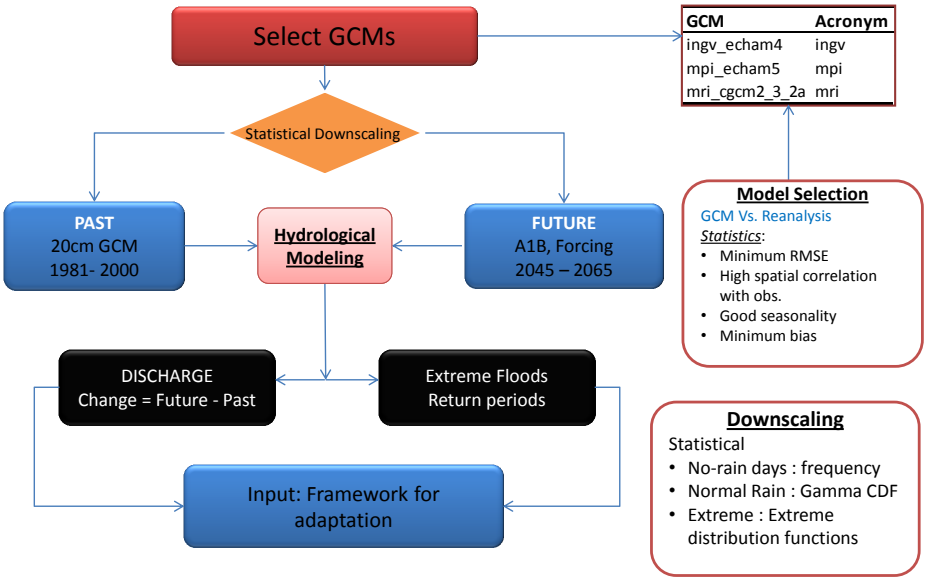

Figure 2.2: Framework: Basin scale flood simulation under climate change.

2.6.1.1 Downscaling and bias correction

At the basin scale, the statistical downscaling approach developed by Nyunt et al. (2013) was used in this thesis for its simplicity, computation cost and applicability to other regions. This was carried out for each station to capture heterogeneities that may be inherent in in-situ observations due to localized mechanisms. The rainfall bias correction was split into three separate parts: 1)no-rain days, 2)extreme rainfall, and 3)normal rainfall. A common characteristic of all GCMs is unrealistically high number of wet days. Most of this is represented as drizzle and it can be attributed to coarse resolution and lack of parameterization in GCMs. GCM data were extracted for all grids matching the stations within and around Nyando basin. The general procedure is detailed below:

1. Both GCMs and observations were ranked
2. A threshold of 0.1mm/day was considered for no-rain day in the observations. The equivalent rank of this threshold in the GCM was then used to define the amount below which it was considered no-rain
3. The same threshold in the past was used in the future since the assumption is that systematic bias in the GCMs remains same

Most of the GCMs have a tendency to underestimate extreme rainfall compared to observations. The General Parreto Distribution (GPD) was used for extreme rainfall bias correction. Annual maximum rainfall was selected for each year in the observed dataset (1981-2000) and the lowest value of the annual maxima selected as the threshold for extreme events. The same numbers of extremes were then set for the past GCMs and the GPD parameters (shape, scale, and location) determined using the Methods of Moments (MOM). GCM extremes for future projections were extracted and a transfer function of the past GCM extremes correction was applied.

For all values greater than a threshold u, the distribution of excess x is defined by

$$F_u(y) = [X - u \leq x | X \geq u] = \frac{F(x) - F(u)}{1 - F(u)} \tag{2.1}$$

With the Generalized Pareto Distribution given by :

$$G(x; K, \alpha, u) = \begin{cases} 1 - [1 - K\frac{x-u}{\alpha}]^{\frac{1}{\xi}} & \text{if } \xi \neq 0 \\ 1 - e^{\frac{-(x-u)}{\delta}} & \text{if } \xi = 0 \end{cases} \tag{2.2}$$

Where $K = 0$ is the exponential distribution, $K < 0$ is the Pareto distribution and $K > 0$ is the Pareto II type distribution and

$$\alpha = \frac{1}{2}u[\frac{u^2}{\delta^2} + 1] \tag{2.3}$$

$$K = \frac{1}{2}u[\frac{u^2}{\delta^2} - 1] \tag{2.4}$$

with u sample mean and δ^2 variance.

Normal rainfall was defined as the range between zero rainfall and the extreme rainfall. Correction in this band is based on the gamma distribution function. The assumption is that both GCM and observed rainfall fit a gamma distribution function. Both past and future GCM cumulative distribution functions (CDF) were mapped onto the observed CDF and a transfer function used for future correction. The gamma function is defined by-:

$$F(x) = \frac{\lambda^\beta x^{\beta-1} e^{-\lambda x}}{\Gamma(\beta)} \tag{2.5}$$

$$\lambda = \frac{\bar{x}}{s_x^2} \tag{2.6}$$

$$\beta = \frac{\bar{x}^2}{s_x^2} \tag{2.7}$$

Where $\bar{x}$ is the mean of the sample, s_x^2 is the variance of the sample and $\Gamma()$ the gamma function. The inverse of the gamma distribution of past observed rainfall is used to correct

for past GCM rainfall. This is then used as a transfer function for the future normal rainfall correction.

$$x'_{gcm\_fut} = F^{-1}_{obs}(F_{gcm\_past}(x_{gcm\_fut})) \tag{2.8}$$

Where x'_{gcm_fut} is the future bias corrected rainfall, F^{-1} is the gamma inverse function, and x_{gcm_fut} raw future GCM CDF.

2.6.1.2 Temporal downscaling of temperature

Since no temperature observations were available, an empirical temporal downscaling approach developed by Cesaraccio et al. (2001) was used. This uses the daily minimum and maximum to regenerate the diurnal pattern which is necessary for hydrological modeling.

2.6.2 Changes in precipitation at basin scale

To facilitate downscaling, daily GCM data were downloaded for the three selected GCMs from the DIAS system, University of Tokyo, for the periods 1981-2000 and 2045-2065 corresponding to the past and future respectively. Extraction of daily data was based on spatial location of the 21 gauge stations within and around the basin. Downscaling and bias correction was then carried out on a station by station basis. Figures 2.3(a) and (b) shows the raw GCM rainfall for the base and future periods. The performance of the GCMs in representing this basin's climatology was very similar in the past and future. The models are heavily biased for the months of June to September, which coincides with the drier periods in this basin. The GCMs show peaks in March-May and October-December which correspond to the long and short rain seasons in this region but fail to replicate the third weak season in August partly because of the coarse resolution and parameterization weakness in the GCMs.

2.6.2.1 Changes in mean rainfall

Figures 2.3(c) and (d) show the bias corrected rainfall for the past and future respectively and seasonality is introduced after bias correction for both the past and future. The bias correction method reproduces a good match between the observed and the downscale precipitation. Table 2.2 summarizes the projected basin average changes. There is a projected increase in both seasons with all the three models agreeing to an increase in February, March, September, October, November and a decrease in July and August. The three selected models project a 7% increase (2046-2065) in annual precipitation over the basin with the largest annual increase of 9% represented by the *ingv* model. The other two models project a 6.8% increase.

The three models agree on seasonal increase but differ in magnitudes. The *ingv* GCM projects an increase of about 11% in MAM and about 21% in OND, the *mri*, and *mpi* GCMs project less than 5% increase in MAM and about 15% in OND. At the monthly scale, the three models agree to a decrease in the months of July and August, an increase in February, March, September and November. The magnitude of change in all months varies widely. For example, in May, *ingv* projects a 15% increase and *mri* a 17% decrease. But this is just part of GCMs uncertainties inherent in the use of GCM data.

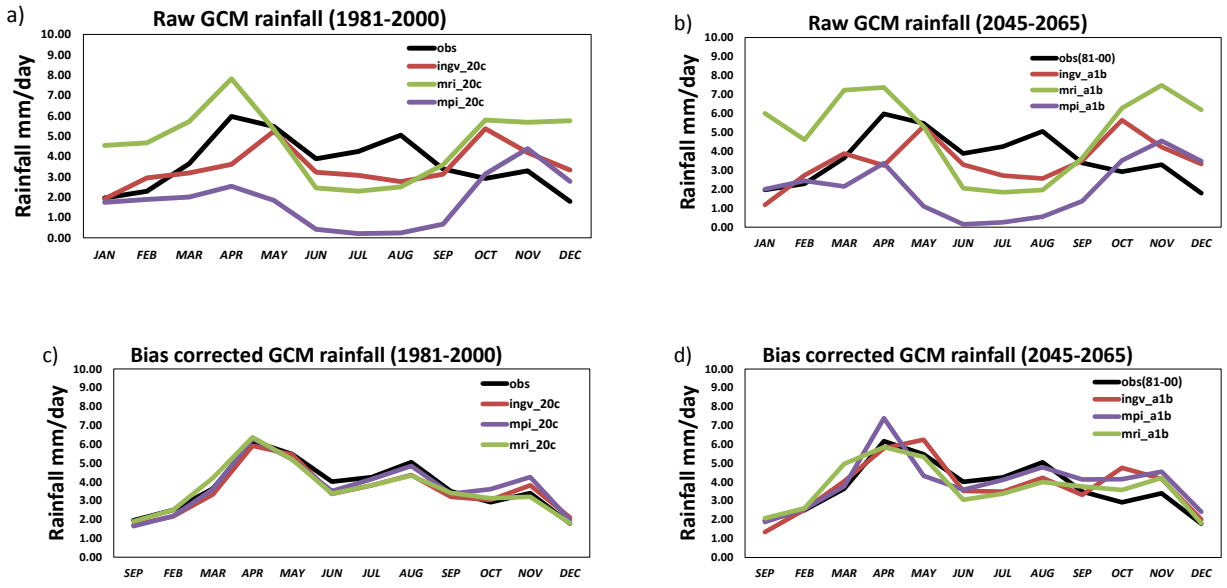

Figure 2.3: Raw GCM data (a, b) and bias corrected/downscaled rainfall GCM rainfall (c, d) for 1981-2000 and 2045-2065 respectively.

Table 2.2: Projected change in rainfall and discharge, Nyando river basin (%).

GCM	**Season**	**Rainfall**	**Discharge**
ingv	MAM	11.3	66.0
	OND	20.5	89.0
mri	MAM	4.0	-25.0
	OND	15.5	37.0
mpi	MAM	1.7	-4.0
	OND	17.0	18.0
Annual		**7.0**	**15.5**
MAM	*Mar- May*		
OND	*Oct - Dec*		

2.6.2.2 Changes in extreme rainfall

As highlighted in the previous section, the assessment of extreme events and future likelihood of floods is important. Most extreme floods in this basin is as a result of individual extreme mesoscale rainfall events related to synoptic changes in atmospheric conditions as well as locally induced convection. According to the IPCC AR4 report; the global projection of extreme weather events in East Africa is likely to increase. This study investigated the likely changes of extremes at a basin scale which can be used for informing decision makers in designing policies and adaptation mechanisms for strengthening the resilience of Nyando's population towards climate change.

A two-pronged analytical approach was used to cater for GCM bias in extreme event representation.

- Statistical downscaling using the generalized Pareto distribution (GPD) by Nyunt et al. (2013) for the past (1981-2000) and future (2045-2065) at basin scale
- Regionally, the signal identified at the basin scale was investigated by analyzing the statistical and dynamic characteristics of 30 extreme events as projected by the three selected GCMs. This is discussed more in chapter 3.

Figure 2.4 shows the top 20 extreme events in three selected rain gauges in the basin for observed rainfall and past/future GCM rainfall after bias correction. The pattern of the past GCM closely follows that of the observation with the exception of a few stations. The three GCMs show an increasing trend in future extremes with some stations having more than 50% increase in intensity. This is an indicator that this basin is very likely to suffer more floods as a result of extreme rainfall.

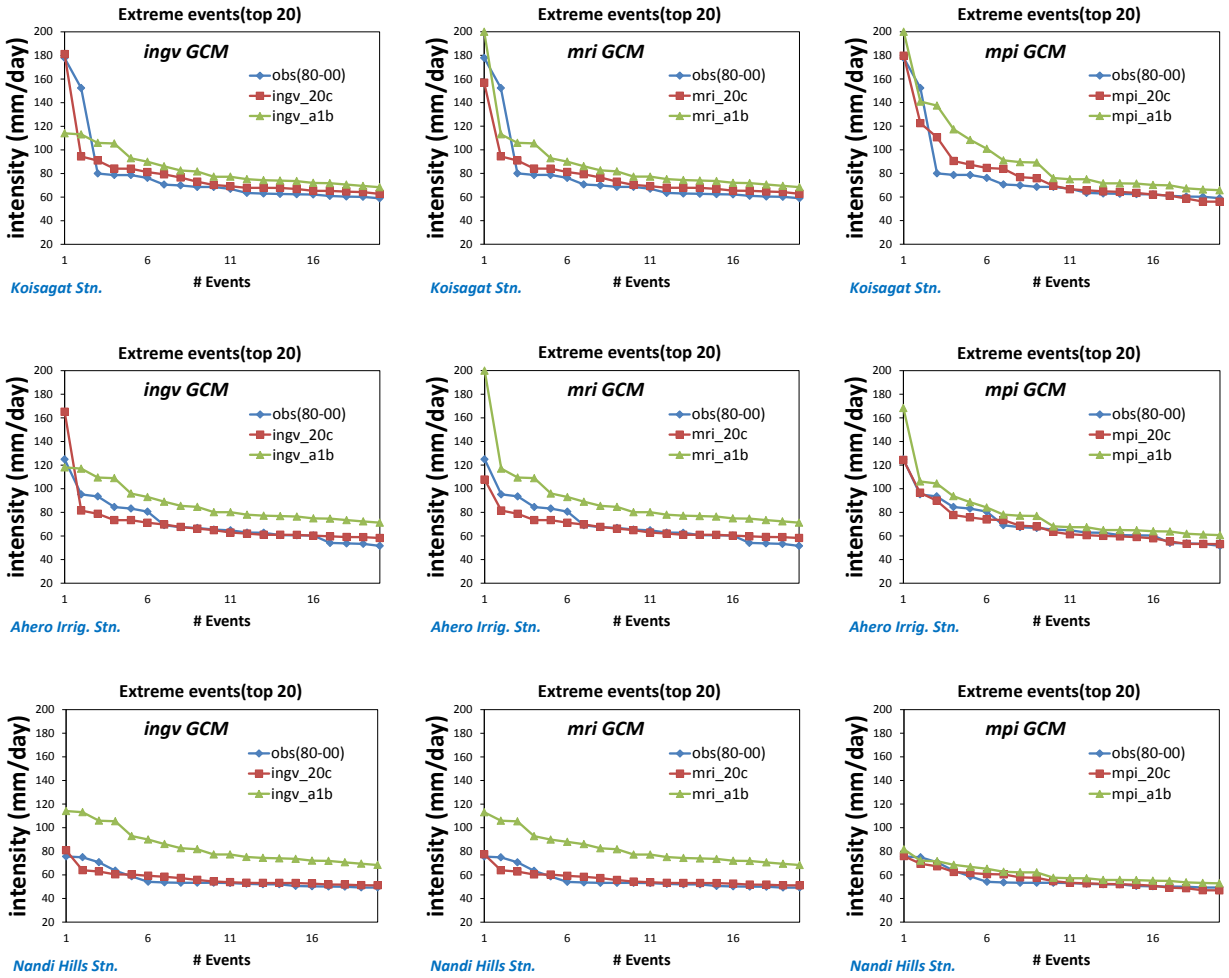

Figure 2.4: Extreme rainfall bias correction for top 20 extreme events (selected stations)

2.6.3 Changes in flow regimes

This section presents the methodology and results on climate change impacts on mean flow and flood extremes in the Nyando river basin.

2.6.3.1 Hydrological model

Watershed models are powerful tools for water resources planning and management. Models are used to predict how conditions are expected to change over time, to understand the nature and scope of a problem or to evaluate alternative management options. The Water and

Energy Budget-Based Distributed Hydrological Model (WEB-DHM)(Wang et al., 2009) is a distributed biosphere hydrological model developed by coupling the Simple Biosphere Model 2(SiB2)(Sellers et al., 1996) with a geomorphology-based hydrological model(GBHM)(Yang et al., 1998). The model is capable of providing at a basin scale, the spatial description of water, energy and CO_2 fluxes. The structure and framework are as shown in figure 2.5. More details on WEB-DHM can be found in Wang et al. (2009).

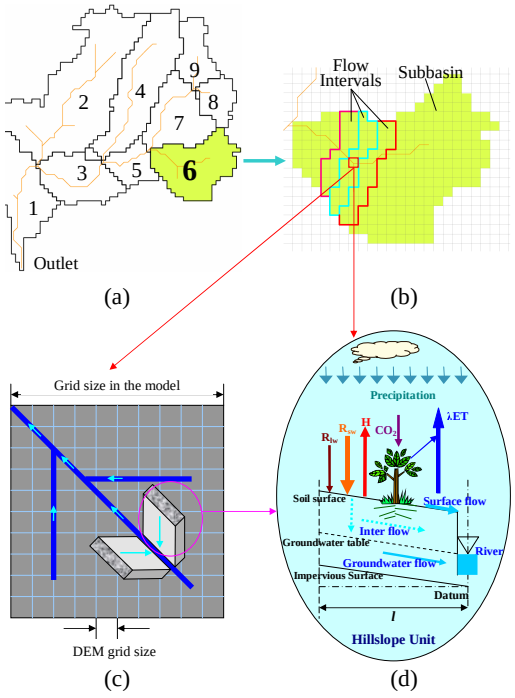

Figure 2.5: The WEB-DHM.

2.6.3.2 Model forcing data

To investigate the likely changes in flow regimes in this basin, the hydrological model was forced with rainfall, temperature, wind and other meteorological variables from the respective GCMs. Rainfall data were acquired from the Kenya Meteorological department and the JICA Kisumu field office. River discharge was acquired from the Water Resource Management Authority (WRMA). Since most of the rainfall data had missing values (approximately 25%) geostatistical approximation proposed by Mutua (2012) in the Nyando basin was used. In

addition, since some meteorological variables (e.g. Air temperature, wind and pressure) were not available in in-situ observations, the JRA25 reanalysis datasets were used and it was demonstrated to be a good proxy (Mutua et al., 2012b).

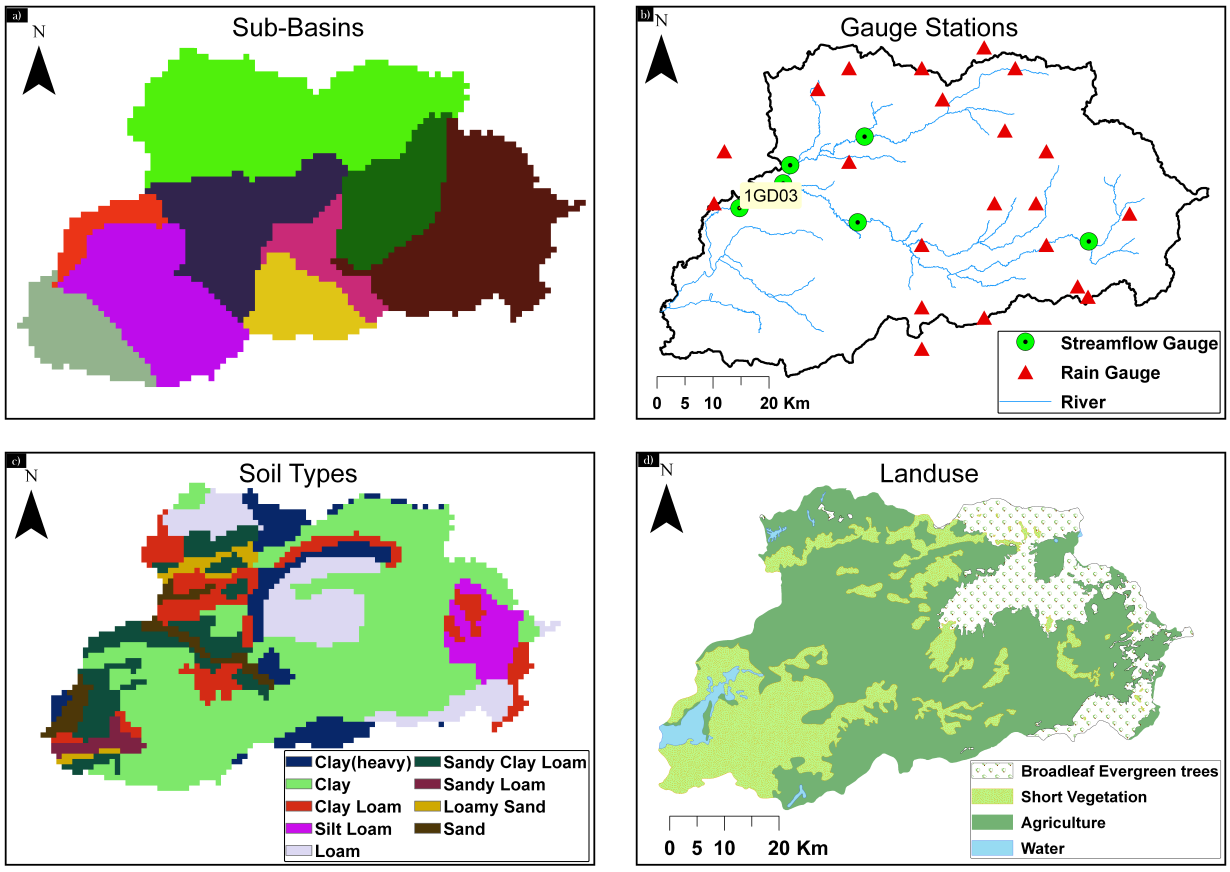

Figure 2.6: Nyando River basin, Kenya. a) Sub basins, b) Rain-gauge stations, c) Soil types, and d) Land use.

Figure 2.6 shows the locations of the river gauges with the most downstream gauge (1GD03) used for calibration, validation, and assessment of floods because it had the most complete data. Also included in this figure is the distribution of the rain gauges, with most of the stations located upstream. This basin is predominantly agricultural with most of the domain having loamy sandy soils.

2.6.3.3 Changes in mean discharge

The WEB-DHM was calibrated for the year 1988 and validated for 1989-1990. Saturated hydraulic conductivity for the soil surface (KS), anisotropy ratio (Anik), and hydraulic conductivity decay factor (f), as well as the maximum surface water detention parameters were calibrated by matching simulated and observed discharges. Visual interpretation, percentage bias (PBIAS) and Nash coefficient (Nash and Sutcliffe, 1970) were used in adjusting these parameters. The results presented here are for the upstream of the discharge gauge 1GD03. Figure 2.7 shows the daily hydrograph for both the calibration and validation periods. Though calibration produced higher values of the Nash coefficient (0.7), the validation period produced a weaker measure (0.30) attributable to rainfall data gaps.

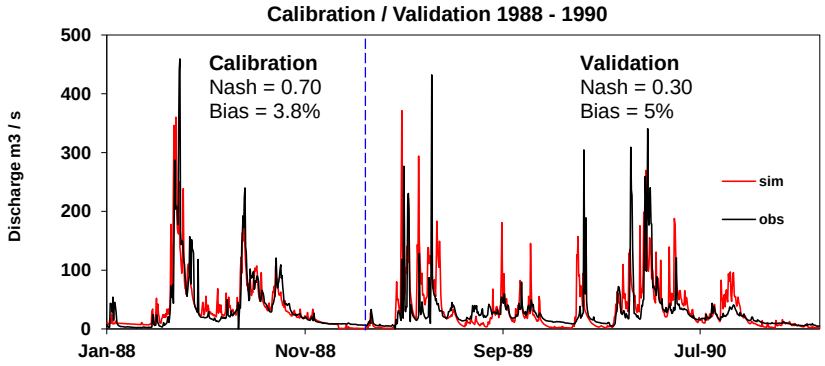

Figure 2.7: Calibration and validation, WEB-DHM.

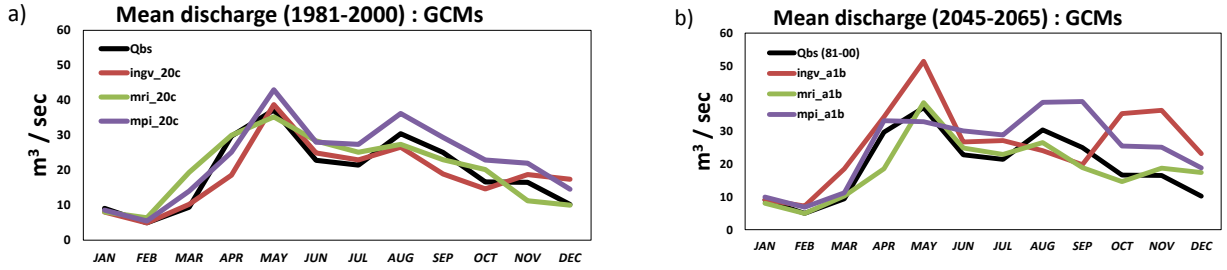

Figure 2.8: Discharge for 1981-2000 (a) and 2045-2065 (b).

Evaluation for discharge is based on baseline simulated discharge using bias corrected GCM rainfall for 1981-2000 to eliminate any systematic model bias. A simple future minus past calculation was used to calculate changes in the mean flow and averaged over 12 months. In addition, a flood exceedance probability was done to investigate flood recurrence in the future. The selected models project an annual increase of 46%(*ingv*) and 15%(*mpi*) respectively with the *mri* model predicting a decrease of 2%. On the seasonal scale the GCM mean projects an increase of 13% in the MAM season and 49% in the OND season. November and December are projected to experience the largest increase of about 58% and 45% respectively while August is projected to decrease by 2%. This follows the rainfall pattern with the OND season projected to experience more rainfall.

2.6.3.4 Probability of flood

The study also investigated the flood extreme probabilities and figure 2.9 shows the simulated future and past discharge extremes based on GCM simulations. The probability of 10 and 100-year flood is very likely for all the GCMs even though the *ingv* projects higher rate of increase compared to the others.

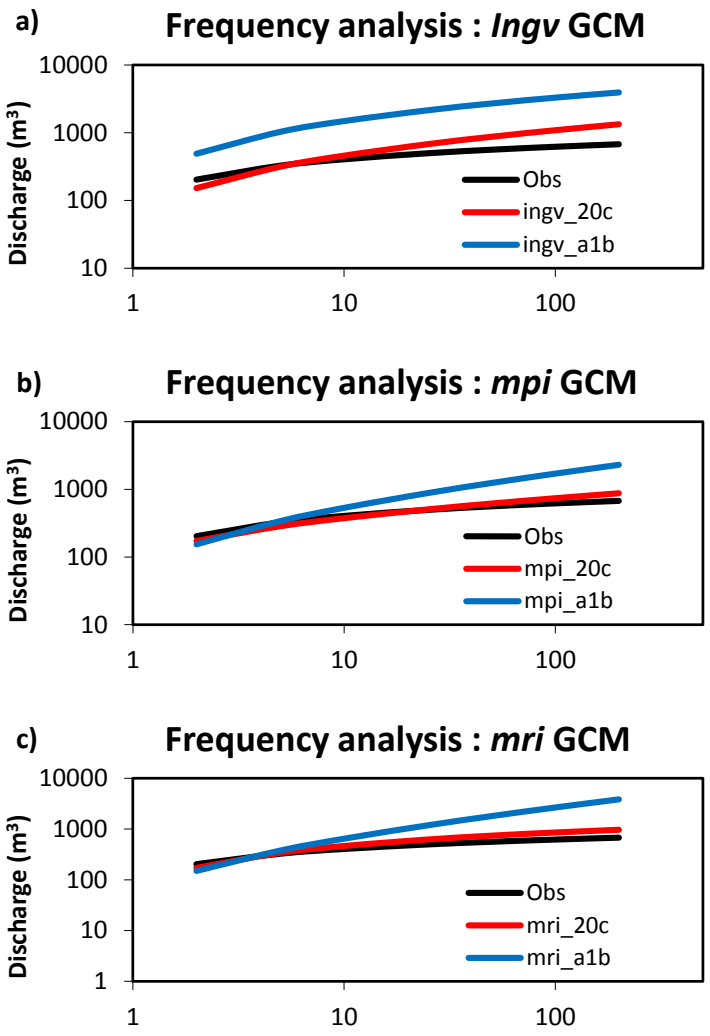

Figure 2.9: Flood exceedance frequency analysis of (a) ingv, (b) mpi and (c) mri.

2.7 Summary

This chapter introduced the concept of climate change, IPCC projections on extreme events, and the necessity to factor in climate change in development. Preliminary climate change assessment study in the Nyando river basin was carried out. Frequency and intensity of extreme rainfall were bias corrected and downscaled to the basin scale. The three selected GCMs project a water basin in the future, which is in line with the regional projected increase

in mean rainfall in East Africa by the IPCC AR4 report. Of particular importance is the projected increase in the intensity of extreme events with an almost consensual agreement of more than 50% increase by the three GCMs. Through hydrological modeling, the three selected GCMs project a wetter basin with a likelihood of increase in mean discharge with all GCMs projecting an increase in the peak floods, almost two times historical floods. A statistical and dynamic analysis of these extreme events as projected by the GCMs is discussed in detail in chapter three.

Chapter 3

Climate change: Projected changes in climate in the LVB, East Africa

3.1 Introduction

In Chapter two, we focused on basin scale analysis of climate change through downscaling and flood projections based on CMIP3 SRESA1B. The three selected models project an increase in both mean rainfall and intensity of extremes. This chapter builds on these findings and investigates projections at the regional scale. Statistical analysis of these events is done and preliminary dynamics of the highest 30 extremes in April and November are analyzed. In addition, East Africa's mean climatology is introduced together with a review of established synoptic mechanisms.

3.2 East Africa climate characteristics

The East African region meteorologically is one of the most complex sectors of the African continent (Nicholson, 1996). Major convergence zones, superimposed regional factors with lakes, topography, and maritime influence are some of the complex tropical influences. Seasonality changes dramatically in the region, sometimes in the order of tens of kilometers.

Some regions have one, or multiple seasonal maxima. There is usually a stark contrast with the transition from deserts with rainfall less than 200mm a year to tropical rainforests exceeding 2000mm a year, and usually over short distances.

Nevertheless, the climate in this region is more regionally controlled and generalities can be drawn. The wind and circulations governing this region include three major streams and three convergence zones. These are: the Congo air mass (westerly and south westerly), the northeast monsoons, and the southeast monsoons. Both monsoons are relatively dry while the Congo air mass is humid, convergent and thermally unstable. The two monsoons are separated by the inter-tropical convergence zone (ITCZ). Several aspects of the climate in this region are still poorly understood especially the cause of the dry air and the shallow moist air streams.

Localized systems have been suggested to play a critical role. Nicholson (1996) suggesting that the highlands act to block the moist westerly Congo flow from reaching the coastal areas and some parts of Ethiopia and Somalia. Kinuthia (1992) suggested a low-level Turkana jet which produces a pattern of descending air that enhances aridity over the northeastern sides of the region. The Somali jet (Krishnamurti et al., 1976), a part of the South East monsoon flows parallel to the coast inducing subsidence and divergent flows also enhancing aridity. The true cause of rainfall is not yet fully clarified but in general the incursion of humid westerly Congo air mass brings rainfall in the region. Further it has been shown that the rainfall pattern also closely follows the migration of the ITCZ (Ogallo, 1988; Mutai and Ward, 2000; Nicholson, 2009; Suzuki, 2010).

3.2.1 Climatology

Figure 3.1 shows the mean annual rainfall for the period 1981-2000 from the Global Precipitation Climatology Project (GPCP). Regions receiving the highest amounts of rainfall are also the same that have longer seasons and highest relief (e.g. Mt. Kenya, Mt. Kilimanjaro, northwest of Lake Victoria, and the Ethiopian highlands). The driest areas are to the northeast of the region with northeastern districts of Kenya, Somalia and south, south-

west of Ethiopia is the driest, receiving about 400 mm a year. Most of the region receives a bimodal rainfall pattern with maxima occurring during the transitions between the two monsoons (Nicholson, 1996; Ogallo, 1988; Mutai and Ward, 2000; Nicholson, 2009). In Kenya and other regions there is a third maximum in July-august especially over the Lake Victoria region. In the northern and southern parts of the region, rainfall is mainly unimodal with maxima occurring during the peak of the ITCZ.

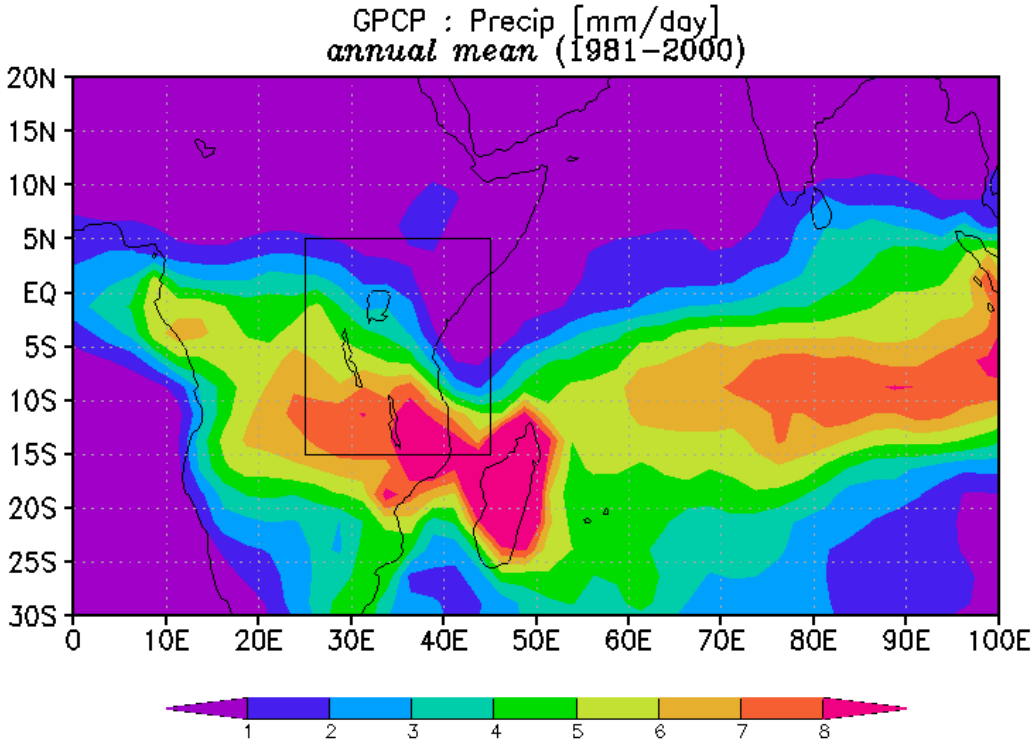

Figure 3.1: Rainfall climatology (1981-2000).

Figure 3.2 shows the latitudinal migration of rainfall maxima in the region for (Lat:10S-5N and Lon: 30E-40E) as defined in Indeje et al. (2000). The dominant pattern is the South-North-South migration as a main consequence of the ITCZ. High amounts of rainfall in the southern hemisphere occur from December to April while in the north the maximum occurs during March-May and again in October-December. Between June and September, most

of the region is dry except for some areas northwest of Lake Victoria. This region receives rainfall nearly all year round. The March-April-May (MAM) season is usually referred to as the long rains season while the October-November-December (OND) is referred to as the short rains season. The long rains are more economic importance to the region and also associated with floods and related disasters.

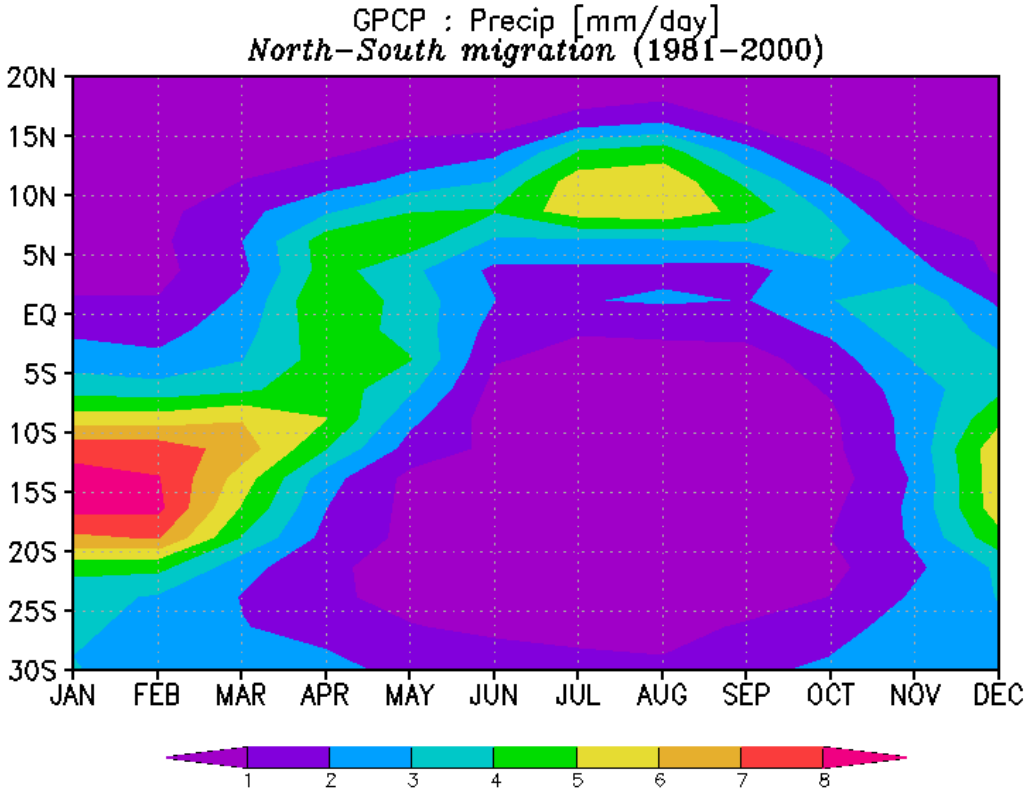

Figure 3.2: The North-South rainfall climatology (1979-2000).

3.2.2 Variability

Despite the inhomogeneity of the regional mean rainfall conditions, the variability in the region is quite coherent. This implies that the primary factors that govern variability are large scale and affect the region the same way (Nicholson, 1996). The short rains tend to have stronger Inter-annual variability, stronger spatial coherence of rainfall anomalies across

a large part of the region, and a substantial association with El-Niño Southern Oscillation (ENSO)(Mutai and Ward, 2000).

3.2.3 Rainfall, ENSO, and IOD

The ENSO is a quasi-global climatic fluctuation related to an asymmetric east-west tropical circulation limited to the subtropical highs (Nicholson, 1996). It is marked by a weakening of the global Walker circulation (Bjerknes, 1969). ENSO is monitored using the Southern Oscillation Index, defined by pressure differences in Tahiti and Darwin. The ENSO period is characterized by above average rainfall (El–Niño) in most of the regions and drought during the next year (La–Niña).

The Indian Ocean Dipole Mode (IOD) (Saji et al., 1999), an irregular oscillation of sea-surface temperatures in which the western Indian Ocean becomes alternately warmer and then colder than the eastern part of the ocean, the ENSO cycle and SST anomalies have been shown to influence the inter-annual variability in this region. Black (2005) used observations to investigate the relationship between ENSO, IOD, and East African short rains. She concluded that heavy rainfall is strongly associated with strong warming in the pacific and the western Indian Ocean and cooling in the East Indian Ocean. Recent studies (Indeje et al., 2000; Mutai and Ward, 2000; Nicholson, 1996) analyzed this variability and demonstrated some interesting associations with the atmosphere and ocean phenomena. Indeje et al. (2000) suggested a strong relationship between the ENSO and East African rainfall but the SST anomalies even have strong associations with SST in both Atlantic and Indian oceans (Latif and Dommenget, 1999).

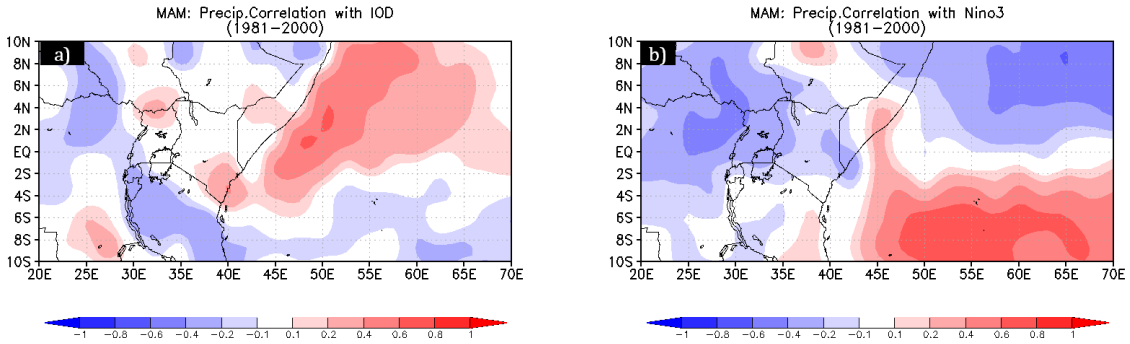

Figure 3.3: MAM seasonal rainfall correlation with (a) IOD and (b) Niño3.

Figure 3.3 shows the spatial correlation between the long rains (MAM), IOD, and Niño3(ENSO). As it can be seen the MAM rainfall is weakly related to the IOD mode which is a direct reflection of the SST anomalies in the Indian Ocean. Consequently, the relationship between MAM rains and ENSO is also weak and has been a subject of intense research without conclusive explanation of the mechanisms of inter-annual variability.

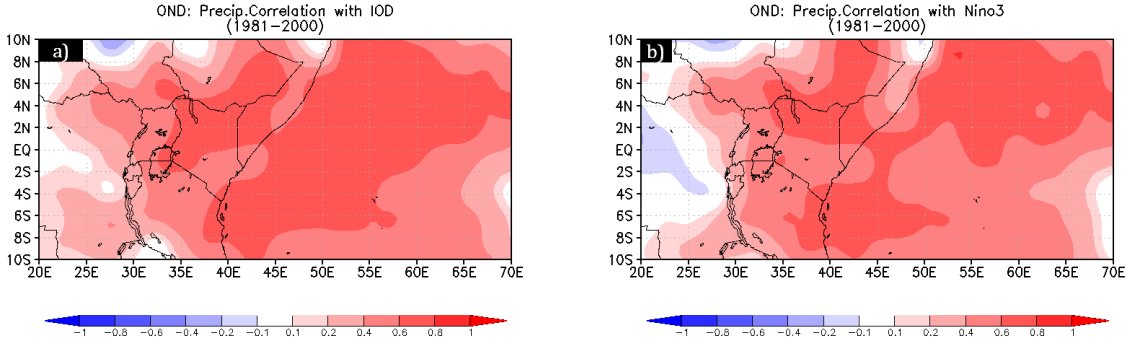

Figure 3.4: OND seasonal rainfall correlation with (a) IOD and (b) Niño3.

Figure 3.4 shows the spatial correlation between the short rains (OND), IOD, and Niño3(ENSO). As it can be seen the OND rainfall is strongly correlated to the IOD mode which is a direct reflection of the SST anomalies in the Indian Ocean. Consequently, the relationship between

OND rains and ENSO is also strong. Mutai and Ward (2000) evaluated the atmospheric teleconnections giving rise to the SST correlations, the circulation anomalies associated with East African rainfall using National Centers for Environmental Prediction National Center for Atmospheric Research(NCEP-NCAR) reanalysis data and, as a proxy for large-scale tropical convection anomalies, outgoing longwave radiation (OLR). They concluded that in the seasonal OND mean, a sequence of three horseshoe structures is evident in the OLR anomalies, with an anomaly sign in phase over the central Pacific and East Africa, and out of phase over the Maritime Continent. This gives rise to the positive ENSO association with East African rainfall. The horseshoe structures in the Indian Ocean are absent in September and through much of the long rains in March-May, though weakly evident again in May. It is suggested that the presence or absence of this teleconnections structure is related to the state of the background annual cycle. Generally, warm (cold) ENSO events are associated with enhanced (suppressed) rainfall in this region.

The response of these Mesoscale systems with respect to climate change is important for it will have a direct impact on rainfall in this region. In their study Conway et al. (2007), used GCM simulations to study the simulated ENSO and IOD systems and concluded that, using the available GCMS, it is not possible to clarify the likely changes in the future. It is on the basis of this basic understanding that this study attempts to investigate at a preliminary stage, the projected changes in rainfall and these teleconnections.

3.3 Data and methodology

Global datasets were used to investigate projected climatic changes in this region in the future due to lack of ground based observations. The base period was chosen to coincide with the basin scale data available for the river basin. Figure 3.5 summarizes the regional analysis framework for climate change in the LVB. The same GCMs selected in chapter 2 were used in this section. Changes in regional extreme rainfall (without bias correction) and analysis of the extreme event characteristics and mechanisms are the key focus for this chapter.

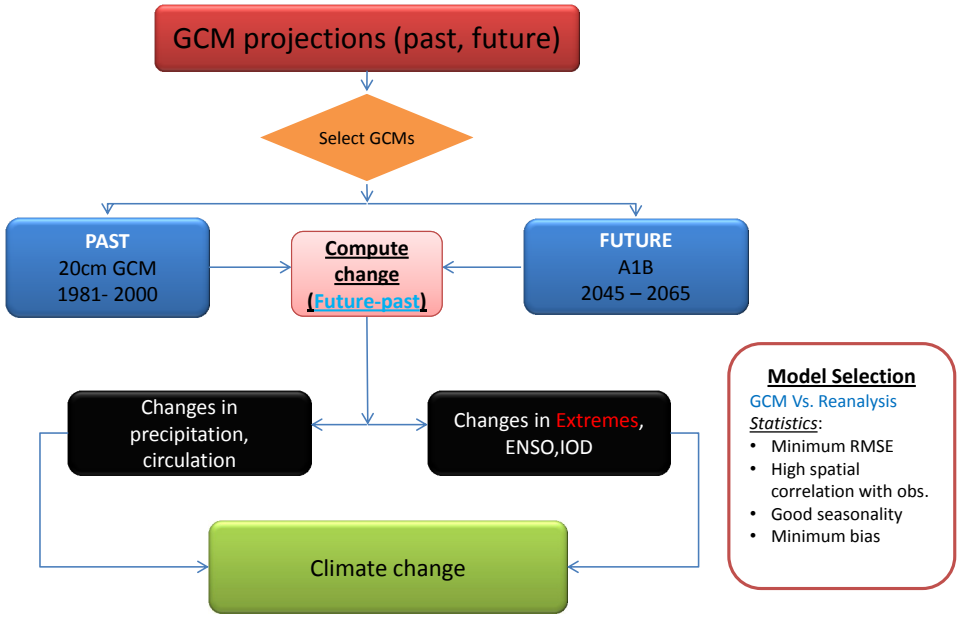

Figure 3.5: Framework : Regional analysis of scale climate change.

3.3.1 Rainfall

At the regional scale, the GPCP climatology (Adler et al., 2003) was selected as the reference for past rainfall. GPCP data, which is a combination of observations and satellite estimates has been used successfully in other studies and has been suggested to be of reasonable quality. The GPCP data has already been found capable of revealing changes in observed precipitation on seasonal to inter-annual time scales and in validating model generated precipitation from reanalysis systems, such as those from NCEP/NCAR and ECMWF (Gruber, 2008).

3.3.2 Other meteorological variables

Air temperature, zonal and meridional wind as well as pressure and other meteorological variables were acquired from the Japanese 25-year Reanalysis (JRA-25) project (Onogi et al., 2007). The JRA-25 model and data assimilation is from the operational system in April 2004. It was the first reanalysis to assimilate wind profiles around tropical cyclones deduced from best-track data, resulting in improved tropical cyclone analysis in a global context. In addition, low-level (stratus) cloud decks along the western subtropical coasts of continents are also better simulated, improving radiation budgets in these regions. A primary goal of JRA-25 is to provide a consistent and high-quality reanalysis dataset for climate research, monitoring, and operational forecasts, especially by improving the coverage and quality of analysis in the Asian region. However, it has also been found useful in hydrological studies of river basins without adequate ground-based observations such as Mutua et al. (2012b); Jaranilla-sanchez et al. (2010).

3.4 Projected regional changes in rainfall

Precipitation and zonal wind (U-850hPa) variables were analyzed from the three selected GCMs. Investigations were done at a regional scale to determine the qualitative projected changes relative to the 1981-2000 baseline. Figure 3.6 shows annual mean precipitation (GPCP), zonal wind (JRA25), and the three GCMs for the period 1981-2000. The correlation factors for the three models are greater than 0.8 with an average Root Mean Square Error (RMSE) less than 2.6. The three selected models represent the regional climatology well though the *mpi* model seems to underestimate precipitation.

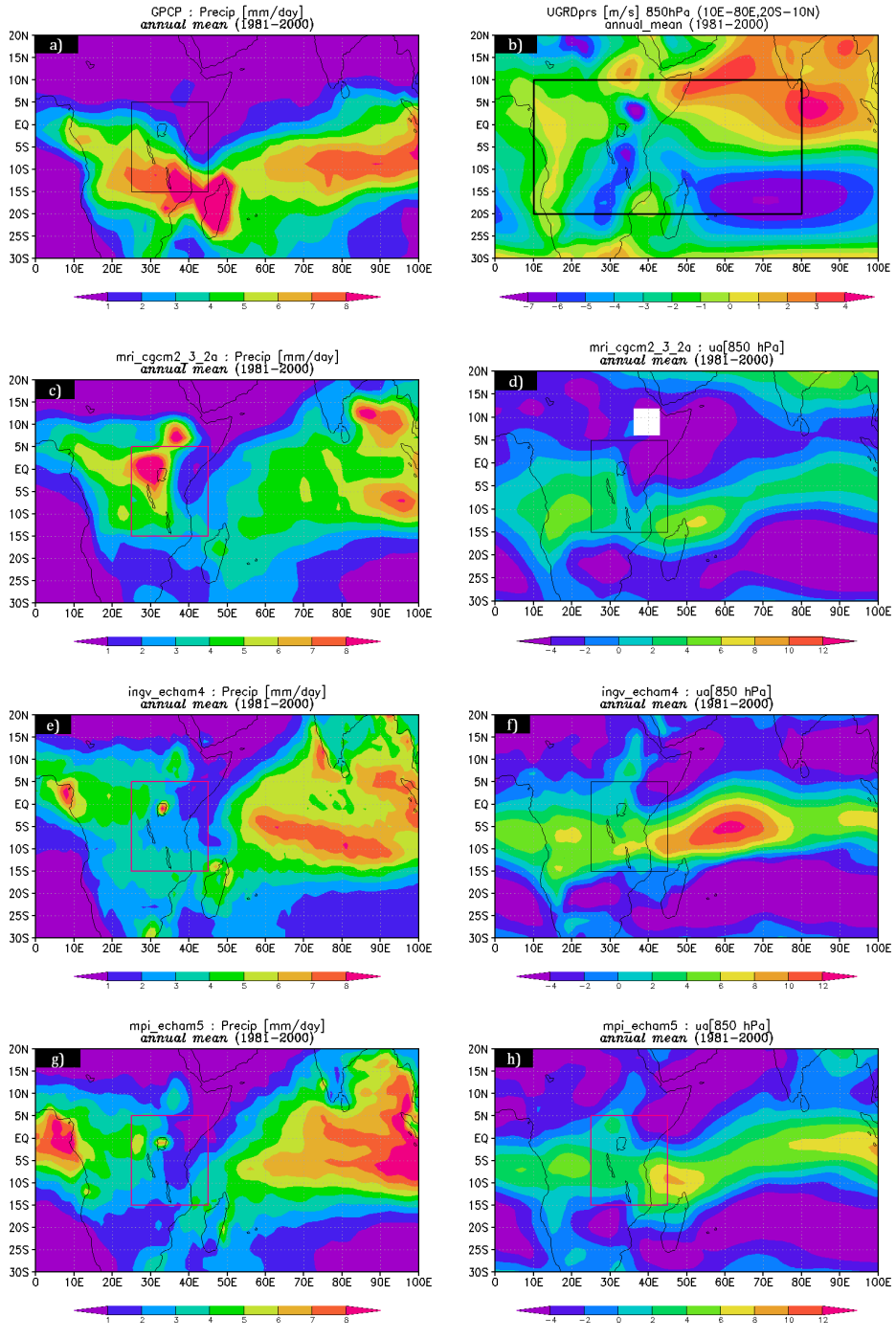

Figure 3.6: Annual mean precipitation (a) GPCP, (c) MRI, (e) INGV, (g) MPI and annual mean zonal wind (b) JRA, (d) MRI, (f) INGV, (h) MPI .

Rainfall maxima is recorded south of the region in the observations but rather biased

in the GCMs. The northern parts are dry in the observations and the GCMs were able to reproduce this pattern. The GCMs seem to have a positive bias over the LVB with observations-GCM difference of about 3mm/day. Figure 3.7 shows the mean annual bias for the three GCMs. There is a tendency of positive bias on the wet regions (e.g the Congo basin and Western Indian Ocean) by the GCMs. The driest regions e.g. Northern Kenya, Southern Ethiopia, and Somalia are negatively biased by the GCMs. The selected GCMs represent this climatology well and thus are suitable for further regional analysis.

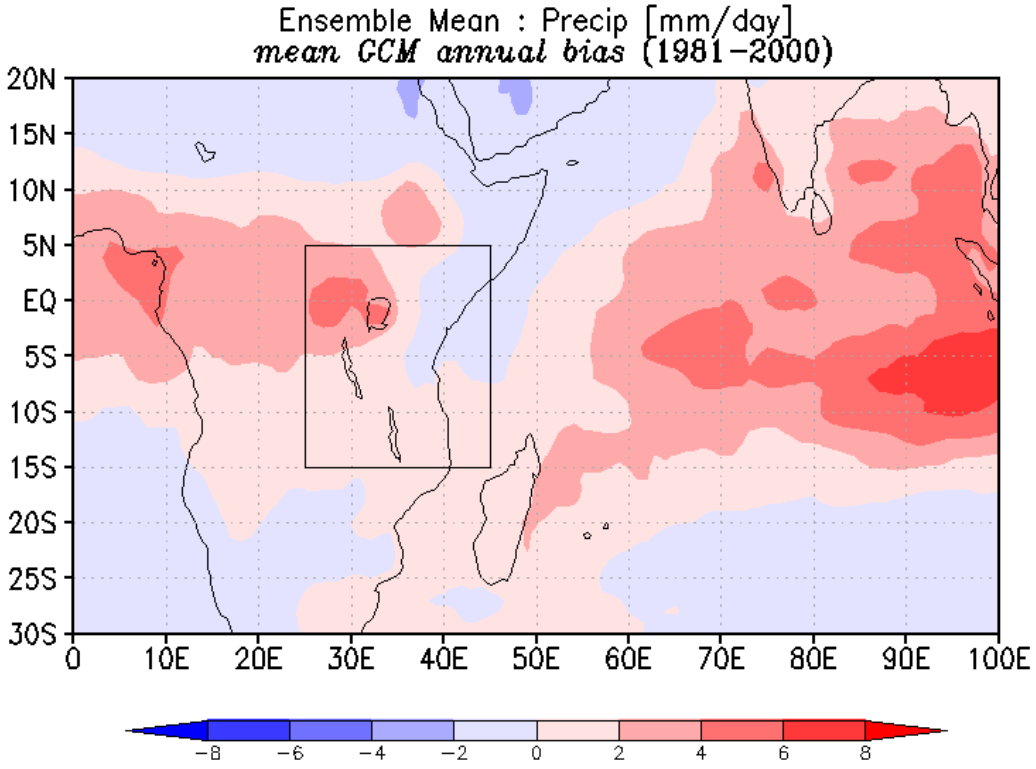

Figure 3.7: Mean GCM annual bias (1981-2000).

Figure 3.8 shows the respective mean MAM and OND GCM bias. The models are more biased towards the MAM season than the OND season. During the MAM season, they are unable to reproduce matching climatology which is strongly related to the presence of the ITCZ and this serves to highlight the challenge of explaining the long season's variability.

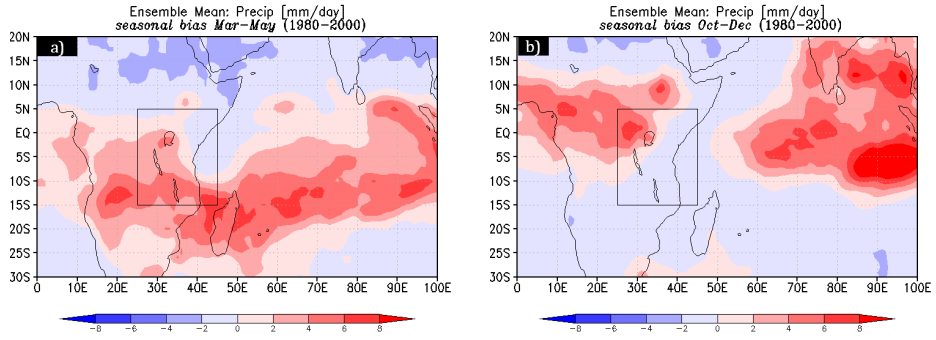

Figure 3.8: Mean GCM seasonal bias (1981-2000) (a) MAM season and (b) OND season.

Figure 3.9 and figure 3.10 show the projected mean seasonal variation of precipitation (a, c, e) and zonal wind (b, d, f), GCM baselines and projected future anomalies (2040-2065) for MAM and OND respectively. There is a general agreement between the three GCMs favoring an increase in precipitation. During the MAM season (Figure 3.9), the GCM ensemble mean projects positive anomalies all over the region with the LVB projected to experience more rainfall with notable increases over the lake area. The northern parts of Kenya, Somalia and northeastern parts of Ethiopia are projected to experience reduced rainfall. Increase in the southern parts of the East African region and decrease in the northern parts highlight that these changes are in line with the S-N-S migration of the ITCZ with regions that are predominantly wet having more rainfall and the drier parts getting drier. This indirectly suggests the strengthening of the ITCZ during this season. Zonal wind anomalies over the central Indian ocean suggest a weakening of the westerlies and this is closely associated with increased rainfall in the central Indian ocean, extending to the East African coast as previously shown by Hastenrath (2007).

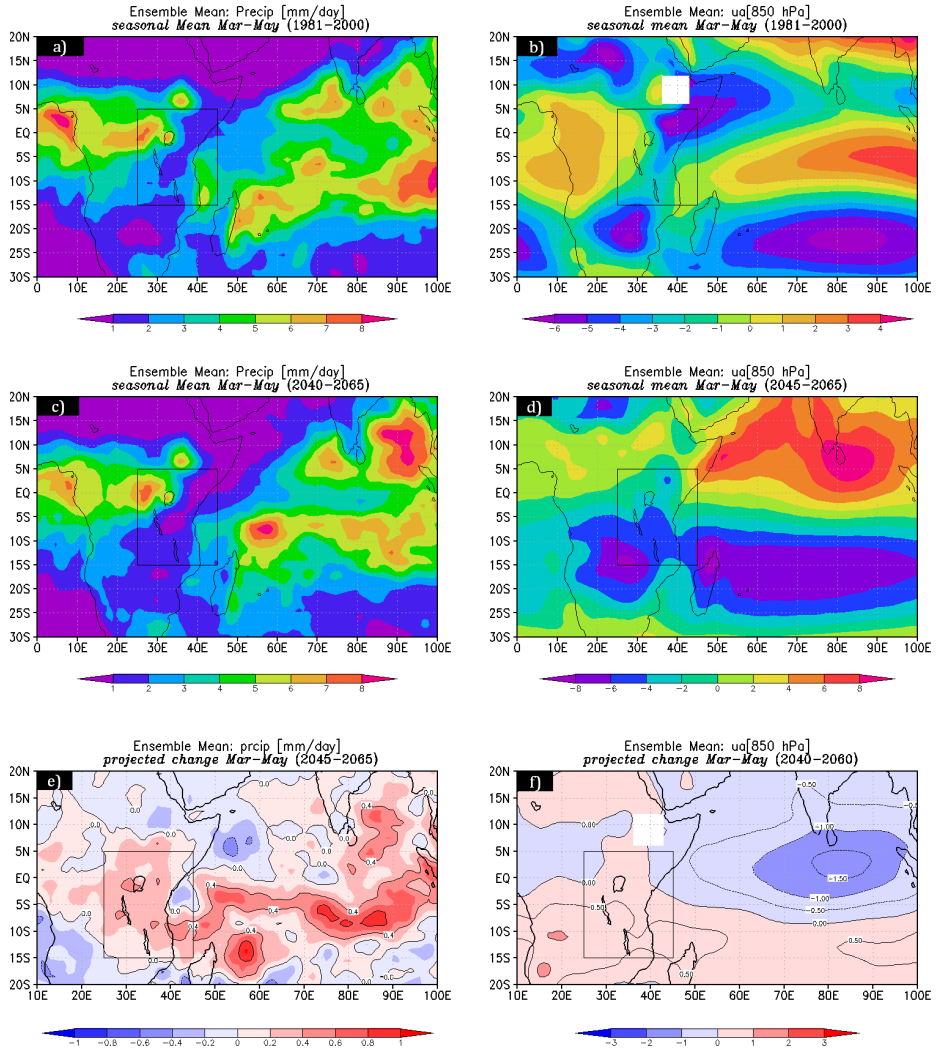

Figure 3.9: Mean seasonal (MAM) precipitation (a) past, (c) future, (e) change, and mean zonal wind (b) past, (d) future and (f) change .

Although a similar trend is observed during the OND season (Figure 3.10), it is more pronounced over the western, northern parts and the coastal areas. The intensity is almost two times the MAM season and this period coincides with the north segment of the ITCZ. The Ethiopian highlands, western Kenya and the LVB basin are projected to have enhanced rainfall in the future. The southern parts of Africa around 15^0S are projected to have reduced rainfall. This season is also associated with weakened westerlies extending all the way to

central Kenya around the equator.

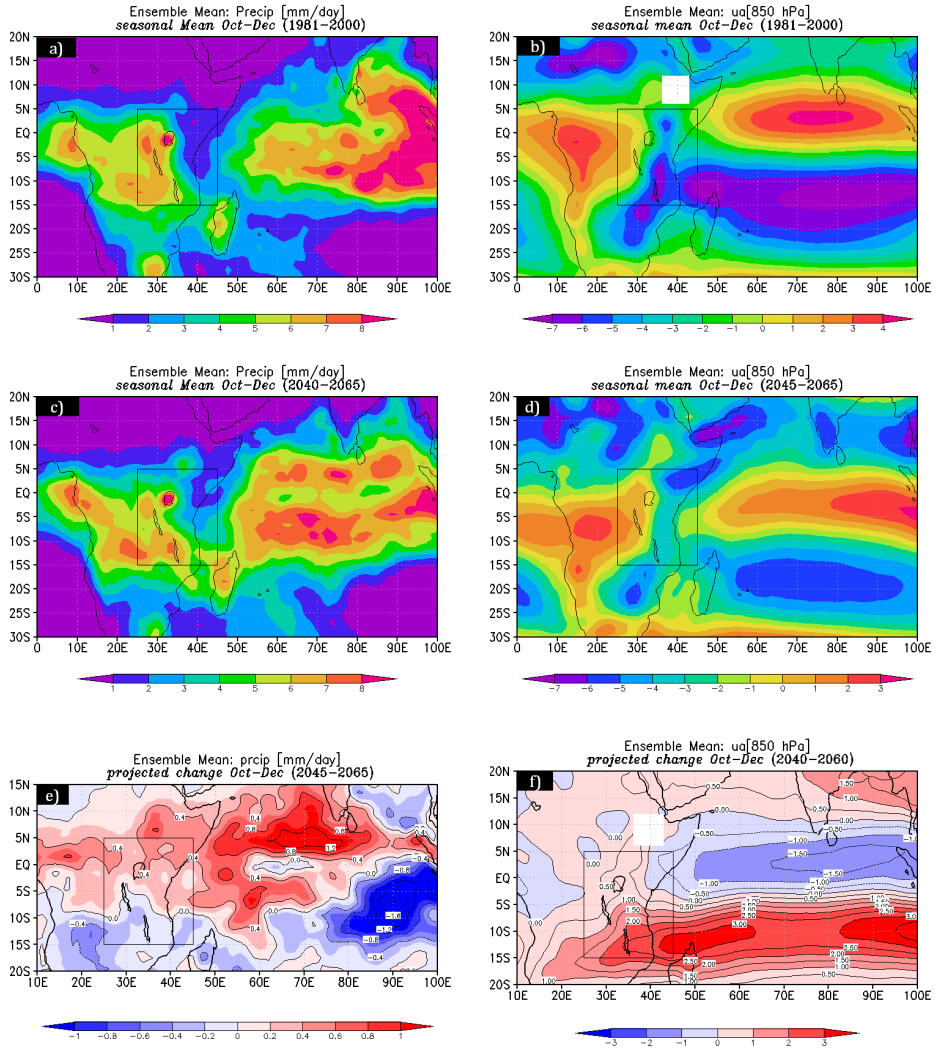

Figure 3.10: Mean seasonal (OND) precipitation (a) past, (c) future, (e) change, and mean zonal wind (b) past, (d) future and (f) change.

3.5 Synoptic scale correlations

We carried out a preliminary check on the correlation signal between the OND seasonal rainfall and West Indian Ocean SST dynamics. Figure 3.11 shows the IOD and ENSO correlations with the east African OND season for 2045-2065. Compared to the past, the

correlation between OND rainfall is suggested to weaken over most of the east African region. The GCM suggests a weaker (0.2) correlation over the Congo basin. A similar trend is observed for OND-ENSO correlations but widely overshadowed by the GCM bias. Based on this, it is not possible to conclusively suggest the likely changes in ENSO and IOD influences in this region. However, diagnostic investigation of the likely pattern of ENSO suggests a more likely El–Niño/La–Niña events in the future (figure 3.12). The period of study is projected to experience more ENSO-like events compared to the period 1981-2000.

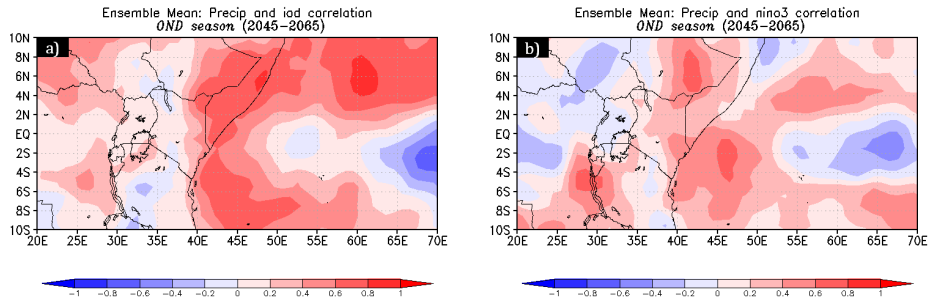

Figure 3.11: OND seasonal rainfall correlation with (a) IOD and (b) ENSO for (2045-2065).

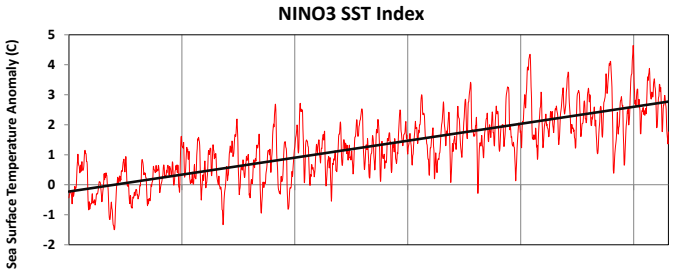

Figure 3.12: Niño3 SST index Anomalies (base period : 1981-2000).

3.6 Changes in Regional Scale Dynamics

Previous studies by Hastenrath (2007) and Lyon and DeWitt (2012) identified a strong correlation between the western Indian Ocean zonal wind anomalies (westerlies) and precipitation over EA. Also, SST anomalies are closely linked to EA precipitation especially during the

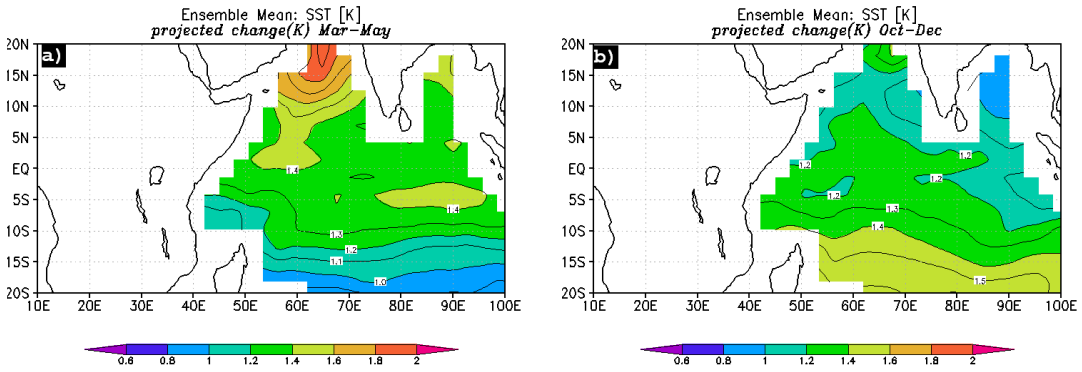

Figure 3.13: Projected seasonal changes in SST (a) MAM season and (b) OND season.

OND season (Nicholson, 1996; Latif and Dommenget, 1999; Black, 2005). We investigated changes in these patterns in addition to changes in precipitation.

3.6.1 Sea Surface Temperature (SST) Anomalies

Shongwe et al. (2011) analyzed SST-rainfall link in the CMIP3 GCMs using an ensemble of 12 models and showed that the models were able to simulate this link well. We extended a similar approach focusing on the selected GCMs (since two were not included in that study) and investigated this pattern. The mean of the three GCMs shows a trend consistent with 1-2 K warming all over the Indian Ocean(Figure 3.13). It is more pronounced on the western than the eastern regions. The warming also depicts a South-North gradient with regions east of the Somalia coast having a 1.4K increase compared to the east of Madagascar (1.7K). This anomalous warming of the western Indian ocean has been shown to be strongly correlated with extreme rainfall over EA (Okoola et al., 2008; Lyon and DeWitt, 2012) and has been previously demonstrated through a coupled modeling framework by Latif and Dommenget (1999).

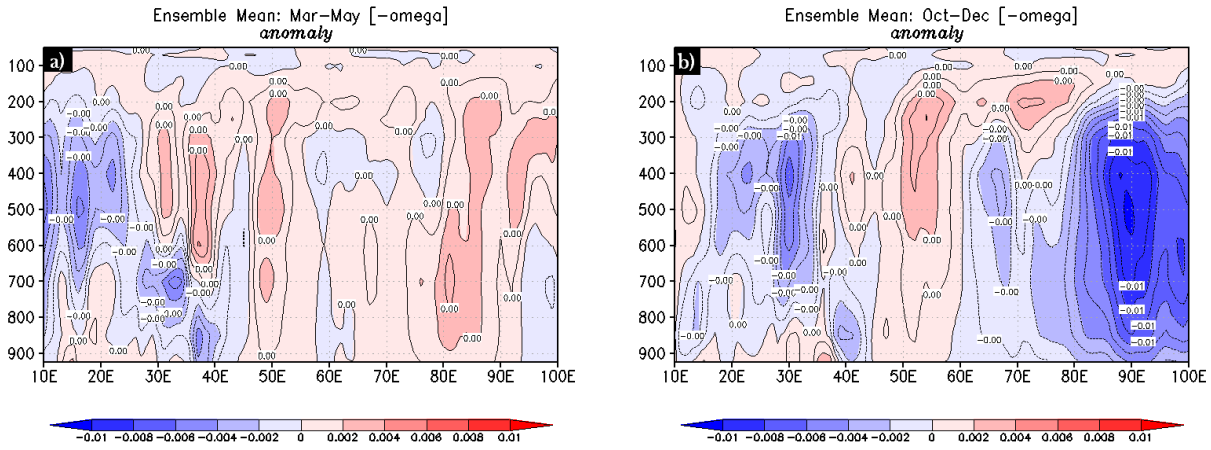

Figure 3.14: Projected seasonal changes in ω averaged over 10S-5N for (a) MAM season and (b) OND season.

3.6.2 Projected regional changes in circulations

Recently, Tierney et al. (2013) showed that in addition to the SST anomaly influence on EA rainfall, the Indian ocean drives the EA variability by altering the Walker circulation and showed that a moist EA coast is associated with cool SSTs over the eastern Indian ocean and an ascending motion over EA further strengthening the role of Indian ocean for multi-decadal scales. Changes in the zonal SST gradient in the Indian Ocean coupled with a reversal of the reversal of the Walker circulation typically cause anomalous convergence and rainfall in the western Indian Ocean extending into easternmost Africa (Tierney et al., 2011). These changes in zonal circulation can be caused by anomalously warm SSTs in the western Indian Ocean.

Our investigations on SST anomalies(Figure 3.13) reveal this warming pattern on western Indian Ocean consistent with increased precipitation. Also the ω anomalies suggest a strengthening of the ascending motions implying a weaker Walker circulation (Figure 3.14b). The GCMs project a weakening of the Congo ascending cell which is consistent with reduced rainfall while on the EA front, the models suggest a strengthening of the ascending cell (40E) and the associated descending motion. The weakening of this descending motion is closely

linked with enhanced precipitation consistent with Shongwe et al. (2011) and Vecchi et al. (2006).

3.7 Projected regional changes in extreme weather events

Projection of changes in climate extremes is critical in assessing the potential impacts of climate change on human and natural systems (Tebaldi et al., 2006). We used an approach first proposed by Peterson (2002) and later used on a global scale by Tebaldi et al. (2006). In this method, climate extreme indices are defined and evaluated based on thresholds and climatology of the past. These include: total number of frost days, growing season length, heat wave duration index, maximum 5-day precipitation total, etc.. In this region, located at the equator, not all indices are relevant and this study focused on rainfall indices only. The following indices were defined as outlined in Tebaldi et al. (2006).

- Number of days with precipitation greater than 40mm (ECAR40MM)
- Simple daily intensity index (ECASDII)
- Fraction of total precipitation due to events exceeding the 90th percentile of the climatological distribution for wet day amounts
- Fraction of total precipitation due to events exceeding the 99th percentile of the climatological distribution for wet day amounts

The threshold of 40mm was selected as extreme since the LVB has a localized Mesoscale climate and tends to be wet almost all year round. Also, rainfall events above this in observations are common. In addition, since most GCMs cannot represent extreme events well, 40mm was identified as a reasonable threshold.

(a) *Fraction of total precipitation due to events exceeding the* 90^{th} *and* 99^{th} *percentile of the climatological distribution for wet day amounts*

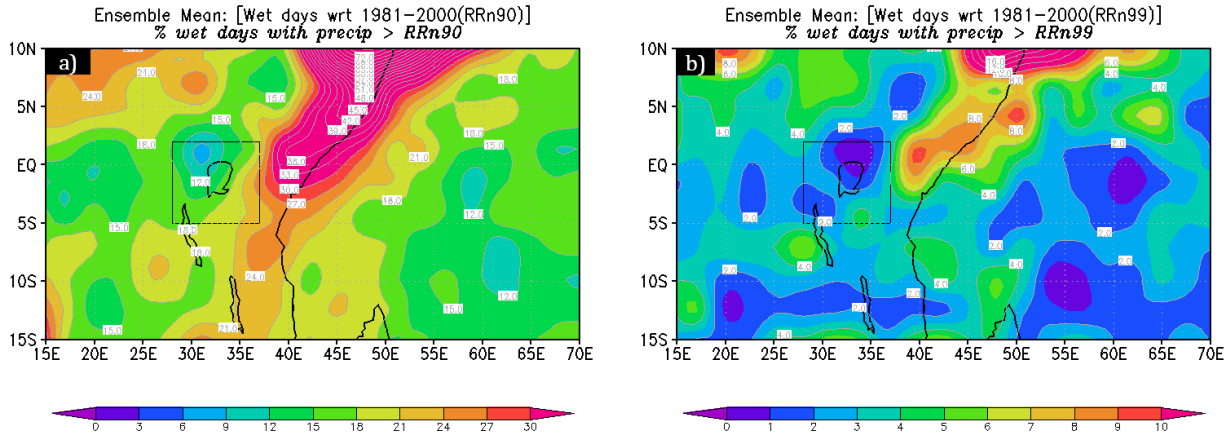

Figure 3.15: Change in fraction of total precipitation due to events exceeding (a) the 90th and (b) the 99th percentile of the climatological distribution for wet day amounts.

Figure 3.15 shows that under SRESA1B scenario, the number of wet days exceeding the 90% threshold of 1981-2000 is likely to increase by 20-30 % in the whole region. An increase of about 5-20% is projected in the LVB and the Congo basin with the highest changes of about more than 30% being projected for the Kenyan-Somali coast. This is also reflected in the number of wet days exceeding the 99% threshold with about 1-8% projected increase.

(b) *Number of days with precipitation greater than 40mm (ECAR40MM)*

Figure 3.16 shows the total number of days exceeding 40mm/day in the LVB for the past and future as well as the projected changes. Regions bordering the Lake to the east are likely to suffer more extremes with the majority of the events centered on the Kenyan highlands. This increasing trend is also projected over central Kenya, Northern Tanzania and parts of Ethiopia and Somalia. However, the largest increase is projected east of Lake Victoria centered over the Nandi Hills.

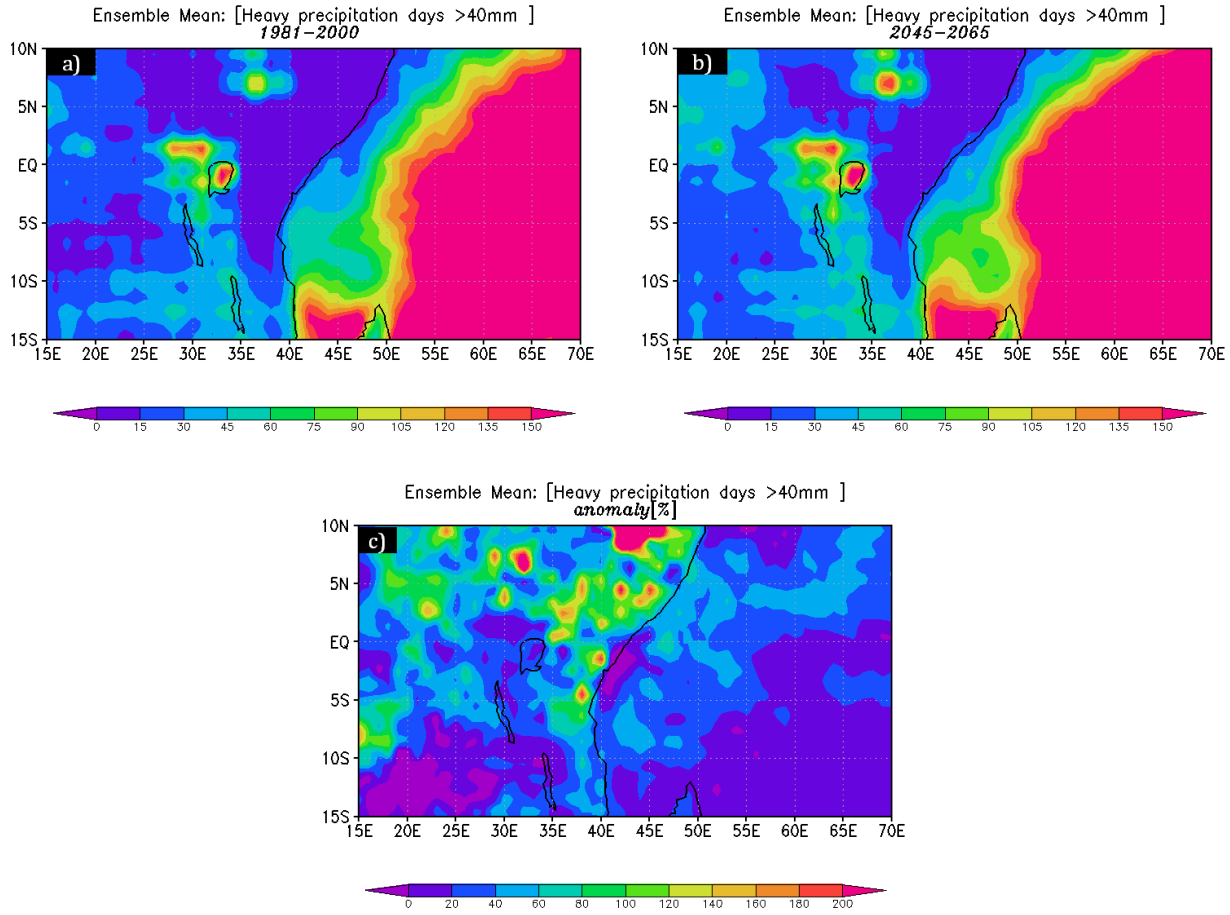

Figure 3.16: Number of days exceeding 40mm/day (a) Past, (b) future and (c) projected change (%)

(c) *The Simple daily precipitation intensity index (ECASDII)*

The Simple precipitation intensity index (ECASDII) describes the mean daily precipitation amount during a time period. Figure 3.17 represents the projected change (in %) of the Simple Daily Intensity Index (ECASDII) by the three GCMs for 2045-2065 compared to 1981-2000. The daily precipitation intensity index increases over East Africa. According to these results, if rainfall occurs in the future its intensity will be higher than in the past. This intensification is about 10% for Central Kenya, however, it is only less than 10% for regions west of Lake Victoria, similar to frequency of extreme days .

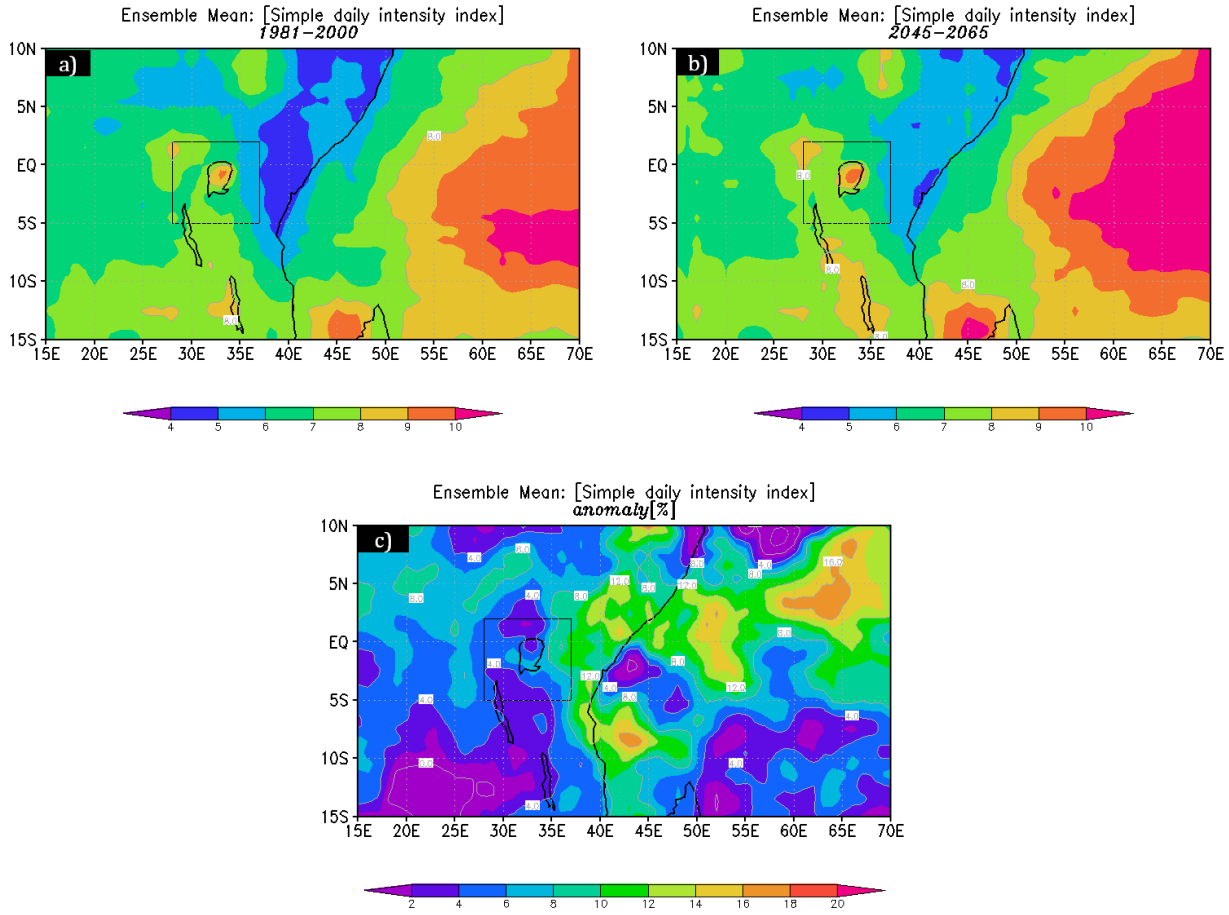

Figure 3.17: Simple precipitation intensity index (ECASDII) (a) Past, (b) future and (c) projected change (%)

3.7.1 Mechanisms of Extreme Events

Precipitation variability in this region is heavily influenced by changes in the Indian Ocean dynamics. For areas receiving precipitation from the Congo Air Boundary (CAB), inter-annual changes in the Atlantic Ocean sea surface temperatures (SSTs) and SST gradients can modulate the strength of the trade winds and the advection of moisture into equatorial Africa (Tierney et al., 2011). We selected the highest 30 events in April and November (2045-2065) over LVB and analyzed the regional dynamic characteristics of surface pressure, circulation patterns as well as moisture advection. Since these two months represent the

peaks of the MAM and OND season respectively, their characteristics can be assumed to be representative of the seasonal trend. April events(Figure 3.18 c-d) are characterized by above normal precipitation south of the equator and stronger anomalies on the southwestern Indian Ocean. Northern parts of the EA are consequently projected to receive less than normal precipitation during these times.

In November (Figure 3.18 f-h), the northwestern parts of the EA are wetter with positive anomalies concentrated over the LVB extending westwards. NW Indian ocean at this time is projected to experience above normal precipitation while the Somali coast is projected to receive less precipitation (but only a weak signal in *mpi and mri*). Southern Africa is projected to experience less precipitation during these events. The *mri* and *mpi* show stronger signals compared to the *ingv*.

3.7.1.1 Mean Sea Level Pressure (SLP) and Wind Anomalies

SLP anomalies were computed as departures from the 1981-2000 base period and this was done for each GCM independently. Investigations suggest anomalous low pressure over the region during April (Figure 3.19 b-d) for the three GCMs. The low pressure system is present all over EA extending from the south-west Indian Ocean to Central Africa. In addition, the easterly flows which transport moisture to EA during this time are projected to be anomalously strong. Over the central Indian Ocean, easterlies develop and these are associated with weakening of the Walker circulation cell associated with anomalous precipitation.

The low pressure system simulated by the GCMs south of EA is associated with weakened trade-winds and this are strongly linked to enhanced convergence along the CAB(Tierney et al., 2011). This enhanced convergence over the CAB is responsible for the increased precipitation on the western branch of the EA rift valley as previously shown through numerical modeling by Tierney et al. (2011).

In November (Figure 3.19 f-h), a high pressure pattern is projected in southern parts of Africa by *ingv* and *mpi* and centered over Madagascar. However, for *mri* this high pressure system is more inland and extends to southern EA covering some parts of the LVB. Concur-

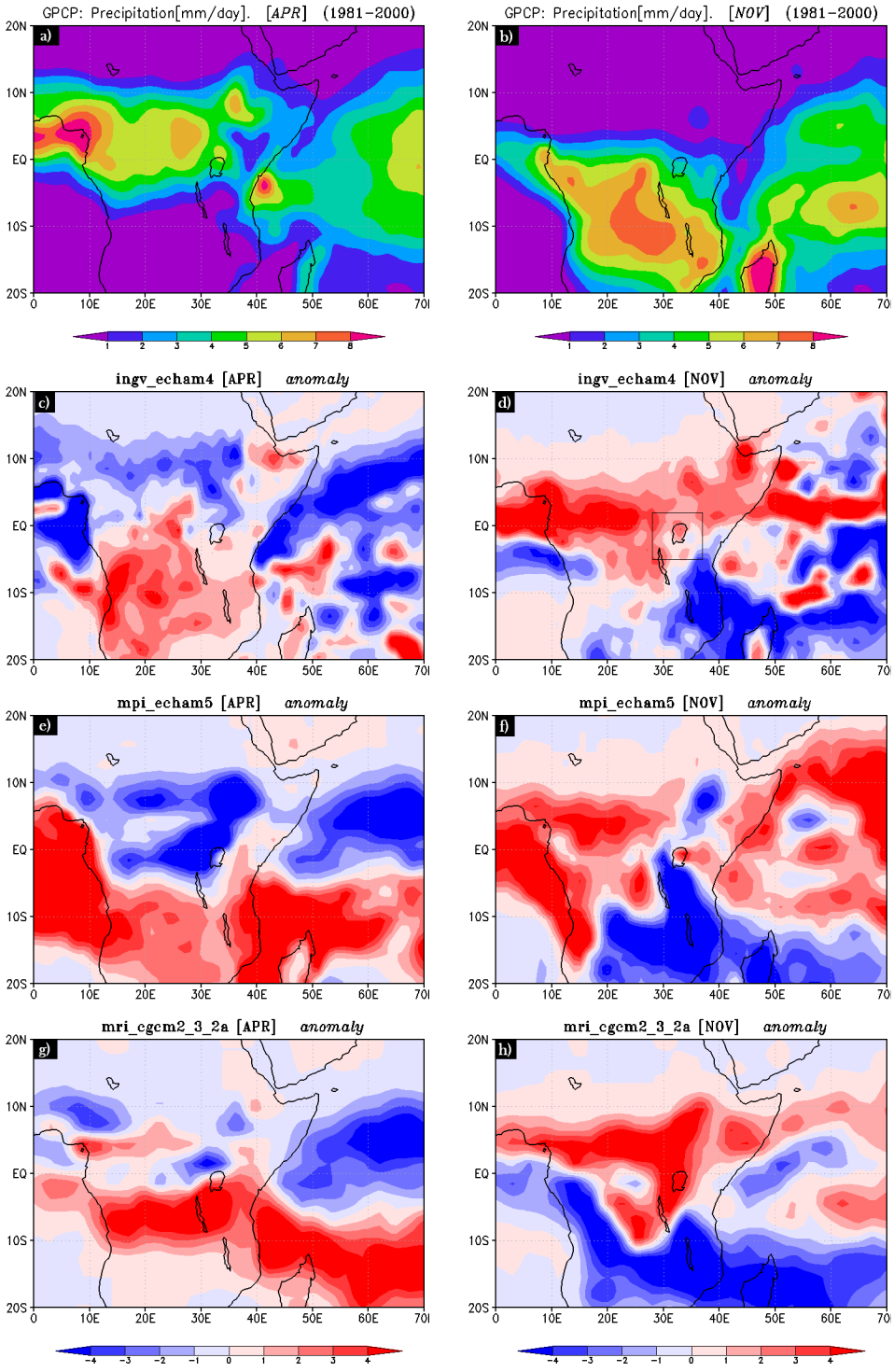

Figure 3.18: a) Mean precipitation climatology for the EA region based on NCEP reanalysis for April and b) November for *ingv*. c) Mean anomaly for the highest 30 events in April and d) November. Similarly e,f) for *mpi* and g,h) for *mri*.

rently, a low pressure system is projected by all the GCMs covering the horn of Africa and parts of Ethiopia. The high pressure zones are associated with reduced precipitation during the OND season (Figure 3.18e) while the low pressure systems show more precipitation. During this time, the surface wind speeds decrease over the western Indian Ocean reducing evaporation and feeding into the development of warm SST anomaly which reduces the SST gradient. This weakens the Walker circulation causing a large increase in convection over the western Indian Ocean extending to EA.

3.7.1.2 Moisture Flux Anomalies

Figure 3.20 shows moisture advection anomalies as projected by *ingv* and *mpi*. In April, the models show positive moisture anomalies over EA, consistent with increased precipitation. Surface wind anomalies suggest advection from the NE Indian ocean and Arabian sea and this is more pronounced for the *ingv* model in April. In November, a similar pattern of positive advection is present all over EA and this is reflected by the heavy precipitation. Anomalously strong SE flows transport more moisture into the EA region evident in both models. The positive advection in the region is projected to intensify with anomalous flow from the western Indian ocean expected to transport more moisture inland and this is closely linked to enhanced precipitation.

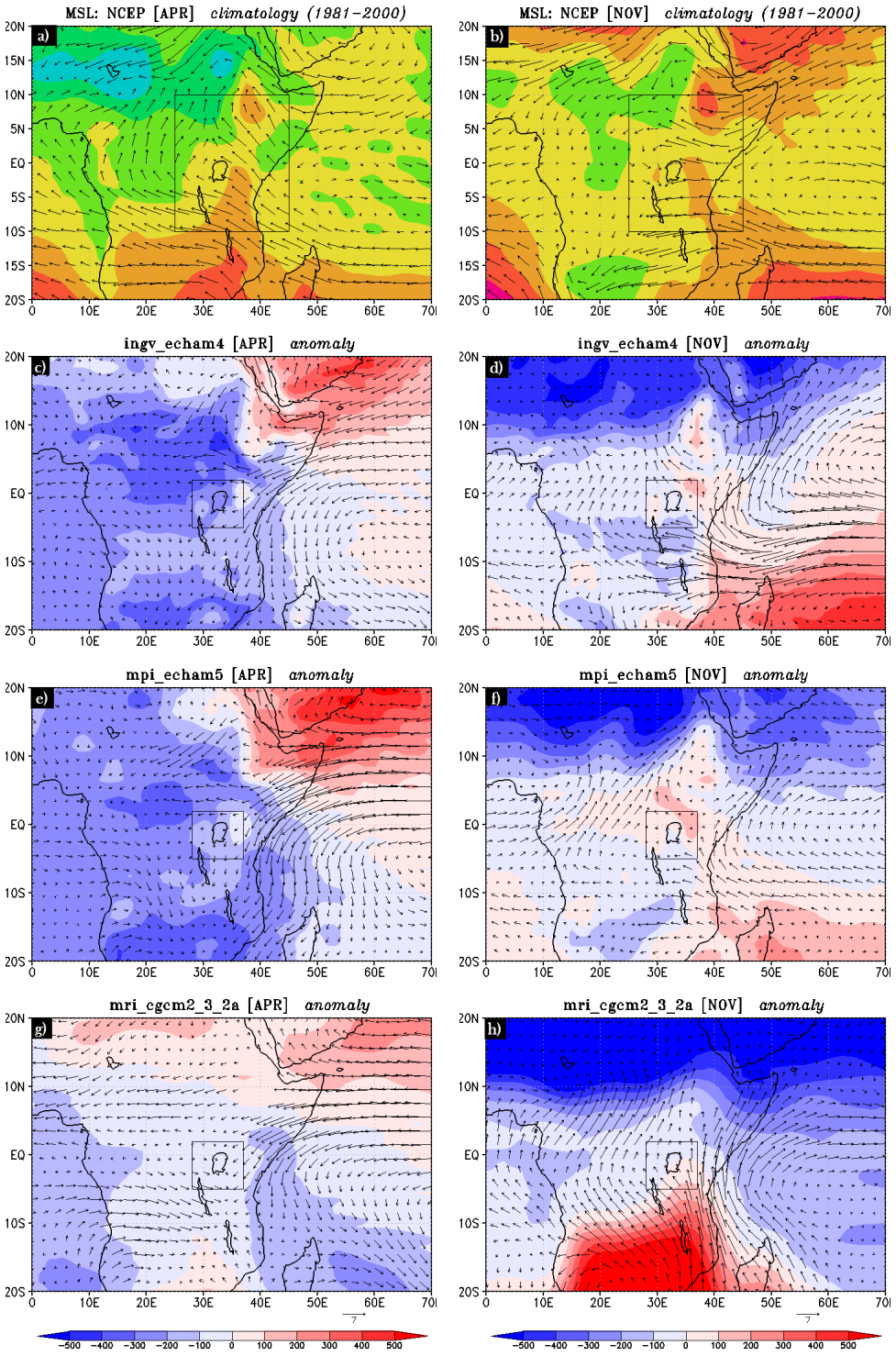

Figure 3.19: a) Mean PSL and surface wind climatology for the EA region based on NCEP reanalysis for April and b) November for *ingv* c) Mean anomaly for top 30 events in April and d) November. Similarly, e, f) for *mpi* and g, h) for *mri*.

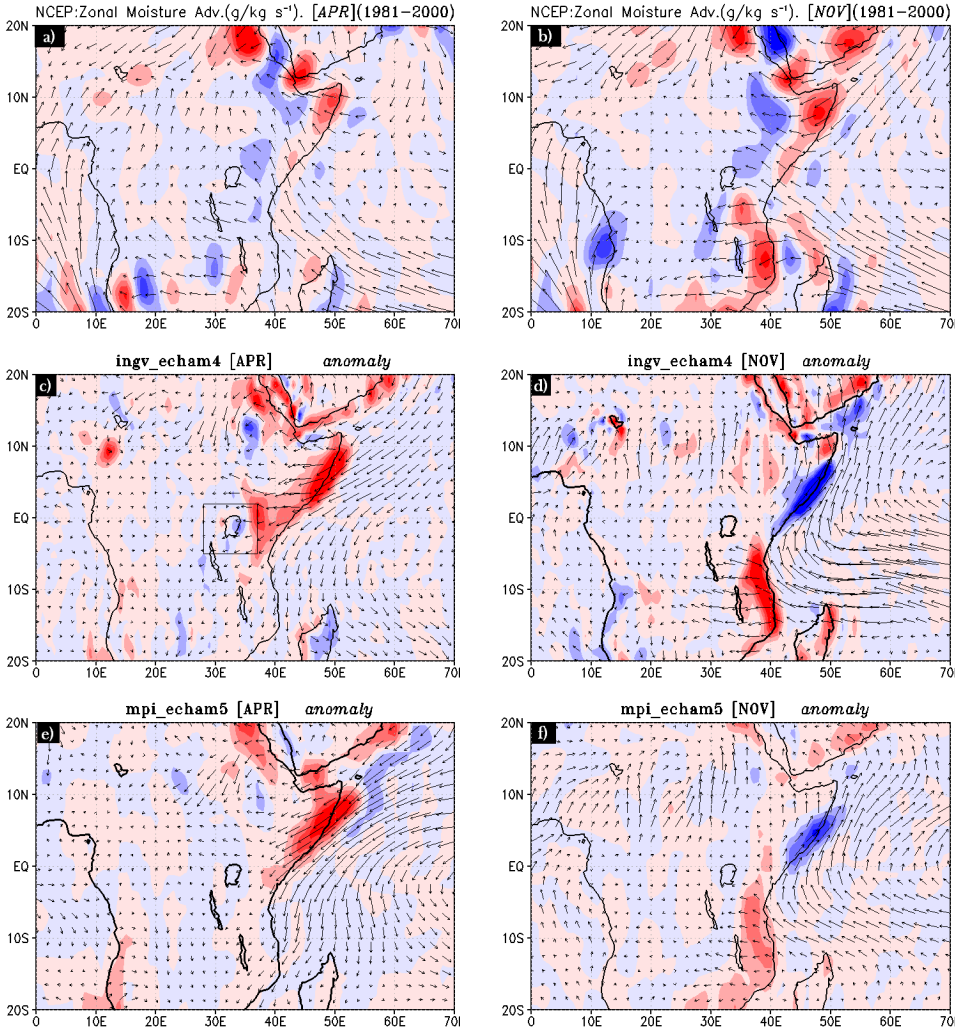

Figure 3.20: a) Moisture advection climatology for the EA region based on NCEP reanalysis for April and b) November. c) Mean anomaly for top 30 events in April and d) November for *ingv* and similarly; e, f) for *mpi*. *Mri* was excluded since the model does not have specific humidity at the surface (1000hPa) in this region.

3.8 Summary

This chapter analyzed the projected regional changes in rainfall and associated circulation patterns. It also focused on extreme weather projections by use of extreme weather indices. Under the SRES A1B scenario, the mean of the three selected GCMs project an increase in rainfall in the LVB and East Africa as a whole. Analysis at the seasonal scale shows a similar increasing trend but more pronounced during the October-December season. Over the LVB, both seasons are suggested to experience an almost equal increase. The GCM projected anomalies show a pattern very similar to the seasonal migration of the ITCZ with regions that usually experience peak rainfall having more enhanced anomalies. It has previously been shown that westerly anomalies in the central western Indian Ocean have a strong correlation with East Africa's rainfall. Investigations reveal that, these westerly anomalies are projected to weaken in the future, a scenario associated with anomalously high rainfall in the region.

Extreme weather indices support Chapter 2's findings, that this region is likely to experience more extreme events. The mean of the three GCMs suggests more than 100% increase in days with amounts more than 40mm/day and a 2-20% increase in the intensity.

3.8.1 Projections of extreme events under climate change

Under the SRESA1B scenario, the number of wet days exceeding the 90% percentile of 1981-2000 is likely to increase by 20-40% in the whole region. An increase of about 5-20% is projected to occur in the LVB and the Congo basin with the highest changes of about more than 30% being projected for the Kenyan-Somali coast. This is also reflected in the number of wet days exceeding the 99% threshold with about 1-8% projected increase. This is accompanied by more than 100% increase on days with rainfall over 40mm east of Lake Victoria and central Kenya and 10% increase in the simple daily intensity index.

3.8.2 Mechanisms of extreme events under climate change

Anomalies from the 1981-2000 climatology show a pattern very similar to the seasonal migration of the ITCZ with peaks north of the equator. Investigations on mean sea level pressure and wind anomalies suggest anomalous low pressure over the region during these two seasons. For events occurring in MAM, a low pressure system is present all over East Africa extending from the South-west Indian Ocean to Central Africa. Moisture flux convergence during the two seasons remains high with the Indian Ocean providing the bulk during the MAM season. Mean sea level pressure anomalies for these events suggest an anomalously high pressure over the Madagascar (Mascarene high), strongly linked to stronger than usual southwest monsoons during the OND season. This, combined with above normal SST anomalies, provide favorable conditions for stronger than normal precipitation. On the MAM season when the NE monsoons dominate, a higher pressure gradient is suggested between the northern and southern hemispheres. A lined-up precipitation anomaly follows a belt of low pressure extending from the SW Indian Ocean to NE of central Africa. In both seasons, the anomalous easterly flow from the central Indian Ocean towards East Africa weakens the usual westerlies associated with subsidence in East Africa. Weakened westerlies, anomalous SST anomalies and a weakened Walker circulation cell over East Africa is associated with extreme rainfall in the region.

Chapter 4

NWP and downscaling of weather forecasts in the LVB

In a feasibility study commissioned by the LVBC (Semazzi et al., 2011), several aspects associated with extreme climate were reviewed through interviews, modeling, desk reviews and consultations with stakeholders in the LVB. They identified extreme weather as a big challenge to transportation in the LVB. The study included assessment of atmospheric and marine, monitoring and modeling requirements from which a Plan for a Navigation Early Warning System (NEWS) (CTOR1, CTOR3, and CTOR4) was one of the proposed interventions. This is in addition to a plan for a Hotspots Atlas (CTOR2), Marine and Atmospheric Observational Network and Water/Air Quality (CTOR3) and a plan for the Consultant's Proposal for a Centre for Meteorological Services (CMS) for the Lake Victoria Basin (CTOR5).

One key finding from this study was that there was a general lack of reliable and useful weather forecasts.

"The final daily forecast in each country is largely based on the analysis of output from a handful of regional Mesoscale models run daily in Nairobi and Dar es Salaam. These NWP systems are initialized using the analyzed output from global models such as the Global Forecast System (GFS) or the European Centre for Medium-Range Weather Forecasts (ECMWF). Numerical models can provide useful guidance for forecasters concerned with severe storms,

but their usefulness is conditioned on their ability to interpret the current weather scenarios and integrate the patterns forward in time. In the future, mesoscale models for the LVB region would be well served to utilize the surface data being collected to improve the initial conditions in the model. Additionally, any future radar or buoy data collected could be assimilated into the models to improve their predictive capabilities. " (Semazzi et al., 2011)

Some of the study recommendations are highlighted below :

1. *Project 1*: Navigation Early Warning System (NEWS) Pilot Project: The objective of this project is to test a pilot system for the provision of early warning alerts for fishermen navigational needs, based on the prediction of severe weather and hazardous marine conditions over Lake Victoria.

2. *Project 2*: Hotspots Atlas: Weather and climate information required for decision-makers and management of leading socioeconomic sectors in the EAC region is not currently available at any single collection center.

3. *Project 3*: Marine and Atmospheric Special Observing Period (SOP) for LVB: The results of the feasibility study have indicated the need for a major upgrade in the observational network for the marine and the meteorological conditions over the LVB.

Even though our study is not part of this project, improved weather prediction is one aspect we seek to provide an input in the LVB. In this chapter, we will introduce the concept of NWP, downscaling of weather forecasts and challenges therein, and evaluate the value added by data assimilation in simulating extreme weather in the LVB. Finally, we identify the current numerical weather needs that need improvement and suggest ways forward.

4.1 NWP: An historical overview

Humankind has always been fascinated by nature and how things work around him. For millennia people have tried to forecast the weather. As early as 650 BC, the Babylonians predicted the weather from cloud patterns as well as astrology. At the time of great scientific

evolution and study of the solar system, the Greek philosophers had much to say about meteorology, and many who subsequently engaged in weather forecasting no doubt made use of their ideas. Unfortunately, they probably made many bad forecasts, because Aristotle, who was the most influential, did not believe that wind is air in motion. He did believe, however, that west winds are cold because they blow from the sunset.

Scientific study of meteorology however did not develop much until the invention of the barometer and thermometer in the mid-17th century. A succession of notable achievements by chemists and physicists of the 17th and 18th centuries contributed significantly to meteorological research. The formulation of the laws of gas pressure, temperature, and density by Robert Boyle and Jacques-Alexandre-Csar Charles, the development of calculus by Isaac Newton and Gottfried Wilhelm Leibniz, the development of the law of partial pressures of mixed gases by John Dalton, and the formulation of the doctrine of latent heat (i.e., heat release by condensation or freezing) by Joseph Black are just a few of the major scientific breakthroughs of the period that made it possible to measure and better understand heretofore unknown aspects of the atmosphere and its behavior. During the 19th century, all of these brilliant ideas began to produce results in terms of useful weather forecasts.

The development of the electric telegraph in 1837 by Samuel F.B. Morse of the United States revolutionized weather data sharing. By 1849 Joseph Henry of the Smithsonian Institution in Washington, D.C., was plotting daily weather maps based on telegraphic reports, and in 1869 Cleveland Abbe at the Cincinnati Observatory began to provide regular weather forecasts using data received telegraphically. As early as 1814, U.S. Army Medical Corps personnel were ordered to record weather data at their posts, this activity was subsequently expanded and made more systematic. Actual weather-station networks were established in the United States by New York University, the Franklin Institute, and the Smithsonian Institution during the early decades of the 19th century. Within the next few decades, national meteorological services were established in such countries as the United Kingdom, Japan, India, and Brazil. The importance of international cooperation in weather prognostication was recognized by the directors of such national services and by 1880 they had formed the

International Meteorological Organization (IMO).

4.1.1 Numerical methods of weather prediction

The fundamental notions of NWP were first stated by Vilhelm Bjerknes as early as 1904. Shortly after the First World War, the first notable attempt at numerical experiment to predict weather was done. A British scientist named Lewis F. Richardson completed such a forecast that he had been working on for years by tedious and difficult hand calculations. Although the forecast proved to be incorrect, Richardson's general approach was accepted decades later when the electronic computer became available. He used a horizontal grid of about 200 km, and four vertical layers of approximately 200 hPa, centered over Germany. Using the observations at 7 UTC (Universal Coordinate Time) on 20 May 1910, he computed the time derivative of the pressure in central Germany between 4 and 10 UTC. The predicted 6-h change was 146 hPa, whereas in reality there was essentially no change observed in the surface pressure. This huge error was discouraging, but it was due mostly to the fact that the initial conditions were not balanced, and therefore included fast-moving gravity waves which masked the initial rate of change of the meteorological signal in the forecast (Kalnay, 2003). Richardson's attempt formed the basis for future numerical predictions

Charney et al. (1950) computed historic first one-day weather forecast using a barotropic (one-layer) filtered model. The work took place in 1948-9. They used one of the first electronic computers (the Electronic Numerical Integrator and Computer, ENIAC), housed at the Aberdeen Proving Grounds of the US Army in Maryland. Their results were quite remarkable. The 24-h forecast, though largely meteorological produced a reasonable pattern correlation between the predicted and the observed pressure field. In a later study, Charney (1962) observed that the filtered (quasi-geostrophic) equations, although very useful for understanding of the large-scale extra-tropical dynamics of the atmosphere, were not accurate enough to allow continued progress in NWP, and were eventually replaced by primitive equation models.

The primitive equations are conservation laws applied to individual parcels of air: con-

servation of the three-dimensional momentum (equations of motion), conservation of energy (first law of thermodynamics), conservation of dry air mass (continuity equation), and equations for the conservation of moisture in all its phases, as well as the equation of state for perfect gases (Kalnay, 2003). For example, in the earth's atmosphere, mass is assumed to have neither sinks nor sources. Stated another way, this concept requires that the mass into and out of an infinitesimal box must be equal to the change of mass in the box. This is the conservation of mass. The continuous equations of motions are solved by discretization in space and in time using, for example, finite differences. The resolution of the model is directly related to the accuracy of the forecasts. Higher resolution models tend to produce better predictions. However, increasing the resolution of any numerical model calls for more computing power and this yet remains to be one of the key challenges facing weather modelers.

4.1.1.1 Numerical models for weather prediction

Among the most significant scientific advances of the past century is our ability to simulate complex physical systems using numerical models and therewith to predict their evolution. One outstanding example is the development of general circulation models (GCMs) of the atmosphere and ocean, which have brought two great advantages: We can now predict the weather for several days in advance with a high degree of confidence, and we are gaining great insight into the factors causing changes in our climate, and their likely timing and severity (Lynch, 2008).Two types of models are in use for NWP: global and regional models.

(a) *General circulation models (GCM)*

A general circulation model (GCM) is a mathematical model of the general circulation of a planetary atmosphere or ocean and based on the Navier-Stokes equations on a rotating sphere with thermodynamic terms of various energy sources (radiation, latent heat). Figure 4.1 shows a schematic of a GCM. Atmospheric and oceanic GCMs (AGCM and OGCM) are key components of global climate models along with sea ice and land-surface components. GCMs and global climate models are widely applied for weather forecasting, understanding the climate, and projecting climate change. The most complete models of the climate system

are constructed by discretizing and then solving equations which represent the basic laws that govern the behavior of the atmosphere, ocean and land surface (McGuffie and Henderson-Sellers, 2005).

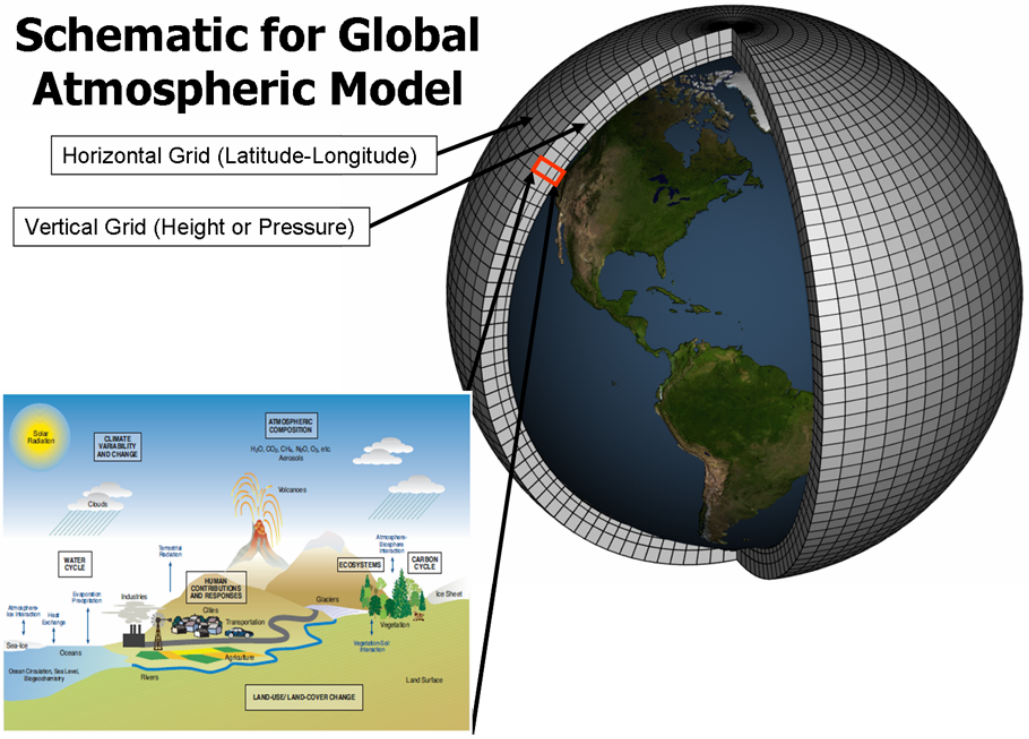

Figure 4.1: GCM Schematic, National Oceanic and Atmospheric Administration (NOAA).

In GCMs, three-dimensional, time-dependent equations govern the rate of change of the six basic model variables: surface pressure, two horizontal wind components, temperature, moisture and Geopotential height. The six basic equations solved to derive these variables are, the hydrostatic equation, two equations for horizontal motion, and the thermodynamic water vapor and mass continuity equations. Global models are generally used for guidance in medium-range forecasts (more than 2 days), and for climate simulations. Due to domain size and their global nature, global models can only be run at coarse scales.

(b) *Regional climate models (RCM)*

Regional models provide forecasts at a shorter range (1-3) days and due to their regionalized domains, they are run at two or more times higher resolutions than the global models. Due

to this, regional models provide more accurate forecasts and are able to reproduce small phenomena such as fronts, squall lines, and much better orographic forcing than global models. Unlike global models which are "self-contained", regional models require boundary conditions from the global models. These boundary conditions must be as accurate as possible, because otherwise the interior solution of the regional models quickly deteriorates. To counter this challenge it is universally accepted to "nest" a regional model with a coarser model, preferably a general circulation model (GCM). The GCM provides the boundary conditions and in the absence of observations, the initial conditions. This limits regional models to short term forecasts only.

(c) *Non-hydrostatic models*

The resolution of regional models has increased to just a few kilometers in order to resolve better storm-scale phenomena in recent years. Storm-resolving models such as the Advanced Regional Prediction System (ARPS) cannot use the hydrostatic approximation which ceases to be accurate for horizontal scales of the order of 10 km or smaller. At the National Center for Atmospheric Research (NCAR), the Weather Research and Forecasting (WRF) Model, a next-generation mesoscale NWP system designed to serve both operational forecasting and atmospheric research needs has been developed in the last decade. It features multiple dynamical cores, a 3-dimensional Variational (3DVAR) data assimilation system, and a software architecture allowing for computational parallelism and system extensibility. There is a tendency towards the use of nonhydrostatic models that can be used globally as well (Kalnay, 2003).

To meet expectations of predicting local meteorology, horizontal resolutions of operational mesoscale models in the world forecast centers have been becoming higher, approaching a few kilometers; the limit of validity of the hydrostatic approximation (Saito et al., 2007). Initially developed for small scale phenomena such as convection and nonlinear mountain waves, non-hydrostatic models have been advanced and used for operational weather forecasting. Several types of non-hydrostatic models exist; usually classified according to the treatment of the

basic equations and the continuity equation (e.g. the Anelastic (AE) model) which removes sound waves from solutions in the equation system by a scale analysis; the quasi-compressible model which considers the compressibility of air and predicts the pressure from divergence, while the reference density is used for momentum equations; and the fully compressible model that uses the compressible continuity equation without linearization with the reference atmosphere.

Generally, the state of dry air can be expressed by temperature T, pressure p, density ρ, and three components of wind u, v, w. As the physical laws, momentum equations in the three directions, the continuity equation, the thermodynamic equation and the state equation compose six basic equations corresponding to the six variables. Neglecting the Coriolis force and terms relating to the earth's curvature and diffusion, they are written as

$$\frac{dv}{dt} = -\frac{1}{\rho}\bigtriangledown p - gk \tag{4.1}$$

$$\frac{d\rho}{dt} = -\rho\bigtriangledown.v \tag{4.2}$$

$$\frac{d\theta}{dt} = \frac{Q}{\rho}C_p\pi \tag{4.3}$$

$$P = \rho RT \tag{4.4}$$

Where v is the wind vector, g the gravity acceleration, R the gas constant for dry air, Q the Adiabatic heating, $C_p = 7R/2$ the specific heat of dry air at constant pressure, and k denotes a unit vector in the vertical direction. The Exner function π and the potential temperature θ are defined as

$$\pi = (\frac{p}{p_0})^{\frac{R}{C_p}} \tag{4.5}$$

$$\theta = \frac{T}{\pi} \tag{4.6}$$

Where p_0 is the reference pressure (normally 1000 hPa) The momentum equation may be rewritten in the following form

$$\frac{dv}{dt} = -C_p\theta\bigtriangledown\pi - gk \tag{4.7}$$

The continuity equation 4.2 and the total differentiation can be written in the flux form as

$$\frac{d\rho}{dt} + \bigtriangledown.\rho v = 0 \tag{4.8}$$

$$\rho\frac{dA}{dt} = \frac{d\rho A}{dt} + \bigtriangledown.(\rho A v) \tag{4.9}$$

Also, the momentum equation 4.10 can be written in flux form as

$$\frac{d\rho v}{dt} + adv + \bigtriangledown p = -\rho g k \tag{4.10}$$

Where adv is the advection in the flux form.

4.1.1.2 Numerical model physical processes

The physical processes in GCMs and RCMs typically include the radiation scheme, the boundary layer scheme, the surface parameterization scheme, the convection scheme (including convective precipitation and clouds) and the large-scale precipitation scheme. All of these schemes, with the possible exception of the radiation scheme, are used at each location and each time step. The radiation schemes in GCMs usually incorporate both daily and annual solar cycles. Shortwave and longwave fluxes are usually treated separately. The solar radiation is absorbed and scattered by atmospheric gases, clouds and the Earths surface. Most

AGCMs have shortwave radiation schemes which explicitly consider scattering and absorption by clouds as a function of zenith angle (McGuffie and Henderson-Sellers, 2005).

The atmospheric boundary layer is the region in which surface friction has a large effect on the flow, typically a few kilometers above the surface. This layer suffers from fluctuations in temperature and humidity and its depth changes with the diurnal cycle. These features cannot be fully represented in most GCMs, primarily because the vertical resolution is inadequate and parameterization schemes are used to produce approximations of the processes involved. The cloud amount is important to the radiation scheme, but there is no single, simple law that governs the formation of clouds (McGuffie and Henderson-Sellers, 2005). Modern climate models diagnose the cloud amount and type from other model variables. Most models have schemes which differentiate between convective clouds and stratiform clouds, relating predictions of the former to the result of the convection scheme and the latter to large-scale condensation. For example Gu et al. (2011) introduced an improved radiation parameterization and showed that WRF is capable of generating reasonable cirrus cloud fields, their movement and dissipation processes.

A major challenge in NWP is the representation of convective processes. The major difficulty in modeling the result of this process is parameterizing the sub-grid scale nature of convection. Cumulus parameterization schemes have been the only way these sub-grid processes can be represented in GCMs, RCMs and hydrostatic models. Such schemes include: the Kuo scheme, Kessler warm rain microphysics, Kain and Fritsch cumulus parameterization and WRF Betts-Miller-Janjic cumulus parameterization. Precipitation (rain or snow) occurs as a function of the available moisture in the model atmosphere. Much of the climate model parameterization of precipitation is based on careful observation and modeling of the microphysical behavior of clouds. Factors such as the availability of condensation nuclei and the rate at which droplets coalesce must be parameterized or specified.

4.1.2 Data assimilation

Data assimilation is an analysis technique in which observed information is accumulated in the model state by taking advantage of consistency constraints with the laws of time evolution and physical properties (Bouttier and Courtier, 1999). There are two basic approaches to data assimilation: sequential assimilation, that only considers observation made in the past until the time of analysis, which is the case of real-time assimilation systems, and non-sequential, or retrospective assimilation, where observation from the future can be used, for instance in a reanalysis exercise. The four basic types of assimilation are depicted schematically in figure 4.14 (Bouttier and Courtier, 1999) .

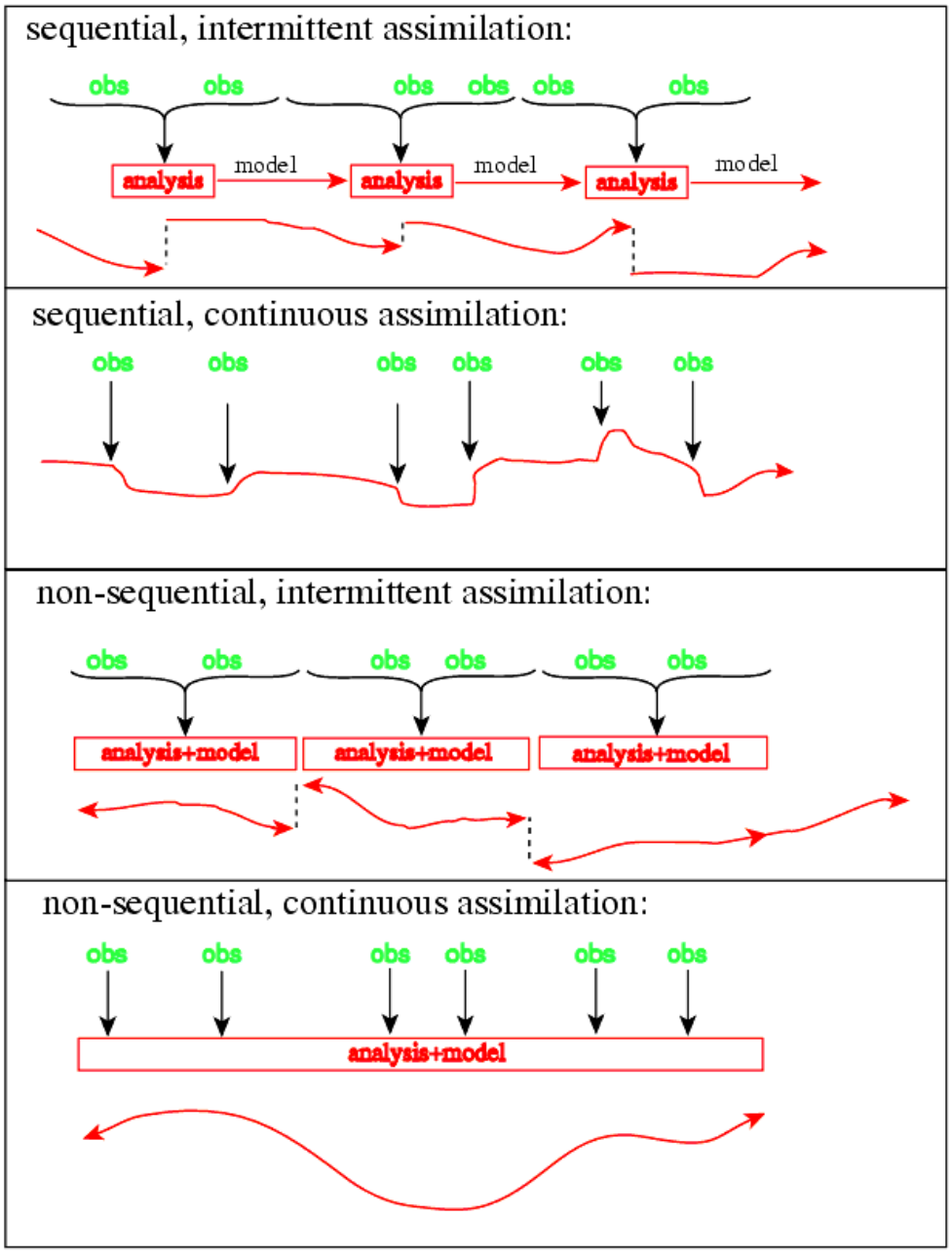

Figure 4.2: The four basic strategies for data assimilation, as a function of time.

NWP is an initial-value problem (Kalnay, 2003), given an estimate of the present state of the atmosphere, the model simulates (forecasts) its evolution. The problem of determination of the initial conditions for a forecast model is very important and complex, and has become

a science in itself. Several methods have been proposed and used for this purpose. These include successive correction method or SCM, optimal interpolation (OI), variational methods in three and four dimensions, 3D-Var and 4D-Var, and Kalman filtering (KF). In early experiments, the estimation of the initial conditions was done by hand and was rather time consuming.

With time, the need for objectivity became apparent and thus interpolation methods fitting data to grids were developed. These however could not solve the need for data adequacy i.e., there were never enough data to initialize the NPWs. It therefore became apparent that it was necessary to use additional information (background/first guess/prior information) to prepare the initial conditions before forecasting. In the early stages, climatology was used, but as the forecasts became better, a short-range forecast was chosen as the first guess in the operational data assimilation systems or "analysis cycles"(Kalnay, 2003). Since then several data assimilation schemes have been developed and used for many years. In this section a few selected of these are briefly highlighted.

4.1.2.1 Empirical analysis schemes

(a) *Nudging*

This is an empirical method of data assimilation first proposed by Kistler (1974), It consists of adding to the prognostic equations a term that nudges the solution towards the observations. This involves the selection of a relaxation term (nudging coefficient) based on empirical considerations and the variable. This method is not widely used for large-scale assimilation though some groups use it for small-scale observations (Kalnay, 2003).

In nudging, the model is pushed gently towards observed values or a gridded analysis in such a way that gravity wave noise is minimized. For example, let a be some prognostic variable of the model. The prognostic equation may be written as

$$\frac{da}{dt} = F(a,t) + G(t)\sum_{i}^{N} w_i(a_i - a) \tag{4.11}$$

Where the term on the left hand side of the equation is the model tendency, $F(a,t)$ is the model forcing, and the final term in the nudging term. $G(t)$ is the nudging coefficient, w_I is an analysis weight, a_I is an observed value, and a is the interpolated model's value.

(b) *Successive corrections method*

In the successive correction method (SCM), the field variables are modified by the observations in an iterative manner. A pass is made through every grid point, updating the variable at each grid point based on first guess field and the observations surrounding that grid point. After one pass is made through the domain, another pass is made, again modifying the field at each grid point based on the observations surrounding the grid point. There are two commonly used successive correction methods; the Cressman scheme and the Barnes scheme.

(c) *Optimal interpolation (OI) analysis*

The most common least squares method of data assimilation is the optimal interpolation (OI). Least squares methods differ from successive correction methods and nudging methods in that the observations are weighted according to some known or estimated statistics regarding their errors, rather than just by empirical values. Thus, observations from different sources can be weighted differently based on known instrument and other errors. For example, radiosonde measurements of temperature can be given a greater weight than satellite derived temperatures. The optimal interpolation method attempts to minimize the total error of all the observations to come up with an "ideal" weighting for the observations. With eight different variables and thousands of model grids and observations, the process can become quite complex.

4.1.2.2 Variational Methods

The variational methods have become the most commonly used data assimilation techniques in modern NWP models. This is due to the advantage of allowing one to eliminate the initialization step. Given a set of observations from satellites, radiosonde, and ground-based measurements, a 3D or 4D variational system can produce a "best" analysis of the atmo-

spheric state at desired resolutions in a statistically "optimal" way by assimilating them into an NWP model (Kalnay, 2003; Yan and Weng, 2011). The assumption in the variational approach is that 1) the observation errors are non-biased and 2) they follow Gaussian distributions. The best state of the atmosphere (analysis X) is computed by minimizing a cost function of J (X);

$$J(X) = (X - X_b)^T B^{-1}(X - X_b) + [H(X) - Y_0]^T (E + F)^{-1}[H(X) - Y_0] + J_c \qquad (4.12)$$

Where X_b is the background, B is the background error covariance matrix, H the forward model (e.g., a radiative transfer model), Y_0 is the observations, E is the instrument error covariance matrix, F is the error covariance matrix, and the constraint term. In an assimilation window, the background field is a previous model forecast. To obtain the background or first guess "observations", the model forecast is interpolated to the observation location, and if they are different, converted from the model variables to observed variables (such as satellite radiances, brightness temperature or radar reflectivity) through an appropriate operator, like the Radiative Transfer Model.

The difference between the observations and the first guess is known as the innovations / observational increments. The analysis is calculated by adding the innovations to the model forecast (first guess) with weights determined based on the estimated statistical error covariance of the forecast and the observations. In the 3D-Var approach, a cost function is defined proportional to the square of the distance between the analysis and both the background and the observations. The minimum of the cost function is obtained for which is defined as the analysis. An analysis is the production of an accurate image of the true state of the atmosphere at a given time, represented in a model as a collection of numbers. An analysis can be useful in itself as a comprehensive and self-consistent diagnostic of the atmosphere. It can also be used as input data to another operation, notably as the initial state for a numerical weather forecast, or as a data retrieval to be used as a pseudo-observation(Bouttier and Courtier, 1999). It can provide a reference against which to check the quality of observations.

(a) *Three-dimensional variational analysis (3D-Var)*

The principle of 3D-Var is to avoid the computation of the gain completely by looking for the analysis as an approximate solution to the equivalent minimization problem defined by the cost function. The solution is sought iteratively by performing several evaluations of the cost function. The popularity of 3D-Var stems from its conceptual simplicity and from the ease with which complex observation operators can be used, since only the operators and the adjoints of their tangent linear need to be provided. Weakly non-linear observation operators can be used, with a small loss in the optimality of the result. As long as is strictly convex, there is still one and only one analysis.

(b) *Four-dimensional variational assimilation (4D-Var)*

4D-Var is a simple generalization of 3D-Var for observations that are distributed in time. The equations are the same, provided the observation operators are generalized to include a forecast model that will allow a comparison between the model state and the observations at the appropriate time (Bouttier and Courtier, 1999).

4.1.2.3 The ensemble Kalman Filter assimilation

In the 1960's, Rudolf Kalman developed a theory of how to optimally combine measurements and modeling forecasts together to give the best estimate of a systems state. This was motivated by the need to estimate the location of the rocket during the Apollo moon landing project. Kalman produced the mathematical theory on how to combine radar measurements and the predicted estimate of position together to give the best location of the rocket at any given time. His methodology and theory was found useful not only in that project but also in weather forecasting. The Ensemble Kalman Filter is a Monte-Carlo optimal data assimilation method originally proposed by Evensen (2003). The advantage is mainly computational, in that the calculation and storage of large covariance matrices are not needed - they are approximated by running a large number of calculations simultaneously.

4.1.3 Ensemble forecasting

Quantitative precipitation forecast (QPF) is one of the more difficult tasks in the weather forecasts, and any attempt in evaluating the uncertainty of the precipitation forecast contributes to a better characterization of the weather effects on the territory (Cane and Milelli, 2010). Uncertainties in QPF usually propagate to the intended local scale application like hydrological modeling. To reduce this uncertainty, ensemble forecasting is used. Ensemble forecasting is a numerical prediction method that is used to attempt to generate a representative sample of the possible future states of a dynamical system. The ultimate goal of ensemble forecasting is to predict quantitatively the probability density of the state of the atmosphere at a future time (Leutbecher and Palmer, 2008). Usually, ensemble forecasts consist of multiple integrations of NWP models, different configurations and even different initial conditions.

Ensemble forecasting methods differ mostly in the way the initial perturbations are generated, and can be classified into essentially two classes: those that have random initial perturbations and those where the perturbations depend on the dynamics of the underlying flow (Kalnay, 2003). Those using random perturbations are referred as Monte Carlo forecasting and the initial perturbations are chosen to be "realistic". They have horizontal and vertical structures statistically similar to forecast errors, and amplitudes compatible with the estimated analysis uncertainty. The amplitudes are realistic but the perturbations themselves are chosen randomly, without regard to the "dynamics of the day". The second class methods include errors of the day and have been developed, tested, and implemented at several operational centers. These methods include the "breeding" and "singular vector" methods which are characterized by including in the initial perturbations growing errors that depend on the evolving underlying atmospheric flow.

4.1.4 Downscaling of weather forecasts

One goal of weather forecasting is to provide input for early warning systems especially extreme weather-related events. One application that weather forecasts have been found very useful is the prediction and adaptation to floods. It is typical that the resolution of present day operational weather and climate prediction models is much coarser than that required for hydrological and water resources applications. Output from these coarse resolutions must be interpreted at a finer resolutions and local schools through downscaling. Downscaling is the process of deriving finer resolution information from larger scale weather or climate model output for use in applications (e.g., hydrological modeling and water resources management). There are primarily two kinds of downscaling methods: statistical and dynamical downscaling methods.

Statistical downscaling methods use historical data and archived forecasts to produce downscaled information from large scale forecasts. These methods may be based on parametric regressions or on nonparametric probabilistic formulations. Their advantage is that they are simple to implement and use and, for regions with large data sets, they produce unbiased and reliable estimates for periods similar to those used for their calibration. However, they require large historical data sets for calibration and that their ability to reproduce the relationships between large and small scales diminish as the future weather and climate conditions change with respect to those used for calibration.

Dynamical downscaling methods involve the use dynamical models of the atmosphere nested within the grids of the large-scale forecast models. Typically, one way nested limited area weather or regional climate models are implemented to produce a finer resolution gridded information for applications, with coarse resolution models providing initial and lateral boundary conditions. The advantage of using dynamic downscaling is that the physics of the models provides justification for their application under a variety of weather and climate conditions in a changing climate, especially for situations with strong boundary forcing. However, they are expensive in terms of computational time and data requirements, they require

three dimensional boundary and initial conditions, and in most cases they require output bias adjustment procedures for good reproduction of the conditions at higher resolution.

4.2 Short-term mesoscale extreme event downscaling and forecasting

Global weather forecasts are usually provided at coarse scales (25-100km); local features (e.g. Land/lake breezes and localized convectional rainfall), that determine the weather of a place are not well represented in the GCMs. It becomes therefore necessary for any application where reasonable accuracy is desired, to downscale QPF forecasts for localized application. This is achieved through downscaling. The term "downscaling" refers to the use of either fine spatial-scale numerical atmospheric models (dynamical downscaling), or statistical relationship (statistical downscaling) in order to achieve detailed regional and local atmospheric data (Castro, 2005). Downscaling global weather prediction model outputs to individual locations or local scales is a common practice for operational weather forecast in order to correct the model outputs at sub grid scales (Do Hoai et al., 2011).

The primary goal of downscaling is to create local scale forecasts aimed at applications at fine scales and also creating forecasts that are realistic and representative of the area of interest. One application that needs reliable and localized forecasts is flood monitoring. Reliable QPF forecasts when used to force hydrological models can provide timely flood forecasts and hence form part and parcel of a flood early warning system. Regional climate models, limited area models and mesoscale models are some of the systems that are you used to achieve dynamic downscaling. Dynamic downscaling is advantageous in that, local effects of terrain and other land surfaces are factored in the model parameterization. Usually, initial and boundary conditions are provided by the mother GCM (global forecast). Castro (2005) reviewed the value of dynamical downscaling using a Regional Atmospheric Modeling System (RAMS) and concluded that the value added is the resolution of the small-scale

features which have a greater dependence on the surface boundary. Similar studies using Mesoscale scale models have also provided useful inputs for practical applications. However, model parameterization, computational needs and predictability of the weather limits use of these models for a few hours and this also dependents on the weather phenomena.

ARPS, a mesoscale model, was applied to downscale global forecasts from 100Km to 5km to assess the applicability of the model output (especially QPF) for hydrological flood monitoring in the LVB.

4.2.1 Methodology and tools

4.2.1.1 ARPS mesoscale model

The simulations were made using the Advanced Regional Prediction (ARPS) (Xue et al., 2000, 2001, 2003; Gao et al., 2004) developed by the Center for Analysis and Prediction of Storms (CAPS), University of Oklahoma. ARPS is a non-hydrostatic atmospheric prediction model and is appropriate for use on scales ranging from a few meters to hundreds of kilometers. It is based on compressible Navier-Stokes equations describing the atmospheric flow, and uses a generalized terrain-following coordinate system. The ARPS model has been used widely in storm studies all over the world including (Vaidya et al., 2004; Sun, 2005; Collischonn et al., 2005; Srivastava et al., 2010; Schenkman et al., 2011; Clark et al., 2011; Jung et al., 2012).

(a) *The model base state*

In ARPS, wind components and the state variables are defined as the sums of base-state variables and the deviations from the base state. The base state is assumed to be horizontally homogeneous, time invariant and hydrostatically balanced. For this reason, the base-state mass and wind fields are, in general, not in a geostrophic balance, except when the base-state winds are zero. In the model, the base state can be initialized using prescribed analytical functions or an external sounding. The simulations used NCEP FNL (Final) Operational Global Analysis data (http://rda.ucar.edu/datasets/ds083.2/). The base state is usually constructed as the horizontal domain average.

$$u(x, y, z, t) = u(z) + u'(x, y, z, t) \tag{4.13}$$

$$v(x, y, z, t) = v(z) + v'(x, y, z, t) \tag{4.14}$$

$$\theta(x, y, z, t) = \theta(z) + \theta'(x, y, z, t) \tag{4.15}$$

$$w(x, y, z, t) = w'(x, y, z, t) \tag{4.16}$$

$$p(x, y, z, t) = p(z) + p'(x, y, z, t) \tag{4.17}$$

$$\rho(x, y, z, t) = \rho(z) + \rho'(x, y, z, t) \tag{4.18}$$

$$qv(x, y, z, t) = qv(z) + qv'(x, y, z, t) \tag{4.19}$$

$$qli(x, y, z, t) = qli'(x, y, z, t) \tag{4.20}$$

Where u, v, and w, are the Cartesian components of velocity (momentum), θ the potential temperature, p, the pressure, ρ the density, qv, the water vapor mixing ratio, and qli, one of the hydrometer categories. The over-barred variables represent the base state and the primed variables are the deviations. The base state for w, and qli, is assumed zero.

In the transformed coordinate system,

$$u(\xi, \eta, \zeta, t) = u(\xi, \eta, \zeta) + u'(\xi, \eta, \zeta, t) \tag{4.21}$$

$$v(\xi,\eta,\zeta,t) = v(\xi,\eta,\zeta) + v'(\xi,\eta,\zeta,t) \tag{4.22}$$

$$w(\xi,\eta,\zeta,t) = w'(\xi,\eta,\zeta,t) \tag{4.23}$$

$$\theta(\xi,\eta,\zeta,t) = \theta(\xi,\eta,\zeta) + \theta'(\xi,\eta,\zeta,t) \tag{4.24}$$

$$p(\xi,\eta,\zeta,t) = p(\xi,\eta,\zeta) + p\prime(\xi,\eta,\zeta,t) \tag{4.25}$$

$$\rho(\xi,\eta,\zeta,t) = \rho(\xi,\eta,\zeta) + \rho'(\xi,\eta,\zeta,t) \tag{4.26}$$

$$qv(\xi,\eta,\zeta,t) = qv(\xi,\eta,\zeta) + qv'(\xi,\eta,\zeta,t) \tag{4.27}$$

$$qli(\xi,\eta,\zeta,t) = qli'(\xi,\eta,\zeta,t) \tag{4.28}$$

(b) *The governing equations*

ARPS solves prognostic equations for u, v,w,θ', $\rho'$and $q\psi$, which are, respectively, the x, y and z components of the Cartesian velocity, the perturbation potential temperature and perturbation pressure, and the six categories of water substance (water vapor, cloud water, rainwater, cloud ice, snow, and hail). Among the three state variables (density, temperature and pressure), two should be predicted and the other diagnosed. Since the pressure is directly responsible for the mass balance in the system through the pressure gradient forces in the momentum equations, ARPS computes pressure. The pressure equation is obtained by taking the material derivative of the equation of state and replacing the time derivative of the density by velocity divergence. The continuous equations are solved numerically using finite difference methods on a rectangular computational grid. The model variables are staggered

on an Arakawa C-grid, with scalars defined at the center of the grid boxes and the normal velocity components defined in the corresponding box faces. The coordinate variables x, y and z are also staggered and are defined at the u, v and w points, respectively.

Since the model atmosphere described by the governing equations is compressible, meteorologically unimportant acoustic waves are also supported by the model. The presence of acoustic waves severely limits the time step size of explicit time integration schemes. To improve the model efficiency, the mode-splitting time integration technique is employed. This technique divides a big integration time step into a number of computationally inexpensive small time steps and updates the acoustically active terms every small time step while computing all the other terms only once every big time step. Consequently, only the small time step size is limited by the acoustic wave speed.

For each big time step, the u, v,w,θ',and p' equations are integrated forward from $t - \Delta t$ and $t + \Delta t$ during n_s number of small time steps, where Δt is the big time step size. The small time step size, $\Delta\tau$, satisfies equation $2\Delta t = n_s\Delta\tau$. The superscripts t and τ indicate the time level at which the terms are evaluated. The terms with superscript τ or $\tau + \Delta\tau$ are evaluated every small time step and those with superscript t are evaluated once every big time step and kept fixed throughout the small steps.

(c) *Subgrid scale turbulence closure*

Turbulence parameterization, the closure linking the resolved scales and the unresolved subgrid-scale (SGS), is critical to the successful simulation of many flows. Three available options in ARPS for parameterizing the subgrid scale turbulence - the Smagorisky, 1.5 order turbulent kinetic energy (TKE) and Germano dynamic subgrid-scale (SGS) closure schemes. The Smagorinsky scheme is a special case of the TKE equation. The Germano dynamic SGS closure converts previously prescribed SGS model coefficients to self-determined parameters that vary with time and space.

(d) *Grid structure and boundary conditions*

In a regional atmospheric model, only the lower boundary is physical. The boundaries at

the top and sides are usually artificial. ARPS permits the user to choose different types of boundary conditions for the lateral, top and bottom boundaries. Five types of lateral boundary conditions are available in ARPS: rigid wall, periodic, zero normal gradient, wave-radiating open boundary, and externally specified boundary conditions. All five options can be specified independently for each lateral boundary. Three types of boundary conditions are available at the top and bottom boundaries: rigid top lid (impermeable ground), periodic, and zero-normal gradient. Wave reflection from the rigid top boundary can be suppressed by use of a Rayleigh damping layer near the top boundary. The periodic boundary condition assumes that the solution outside the computational domain replicates itself indefinitely. The solution at a distance d to the left of the computational domain boundary equals the solution a distance d to the left of the right boundary.

4.2.2 Study area

The LVB has a size of 194,000 km^2, with the Lake surface covering an area of about 68,800 km^2, (Figure 4.3). The Basin area is shared between riparian states of Tanzania (44%), Kenya (22%), Uganda (16%), Burundi (7%) and Rwanda (11%). The LVB holds world leading status for freshwater lake size, elaboration of vertebrate species diversity, species extinctions, exotic species invasions, and freshwater fishery production(LVBC, 2007). The Lake is high in elevation, mostly enclosed by highlands and mountain ranges.

4.2.3 Model data

The National Center for Environmental Prediction (NCEP) Global Forecast System (GFS) final (FNL) gridded analysis dataset is used both for initial and boundary conditions. The Tropical Rainfall Measuring Mission (TRMM) 3-hourly rainfall dataset is used for validation partly due to lack of adequate observations in this region. The Globally-merged, full-resolution (4 km) IR data((Janowiak et al., 2001)) formed from the 11 micron IR channels aboard the GMS-5, GOES-8, Goes-10, Meteosat-7 and Meteosat-5 geostationary satellites

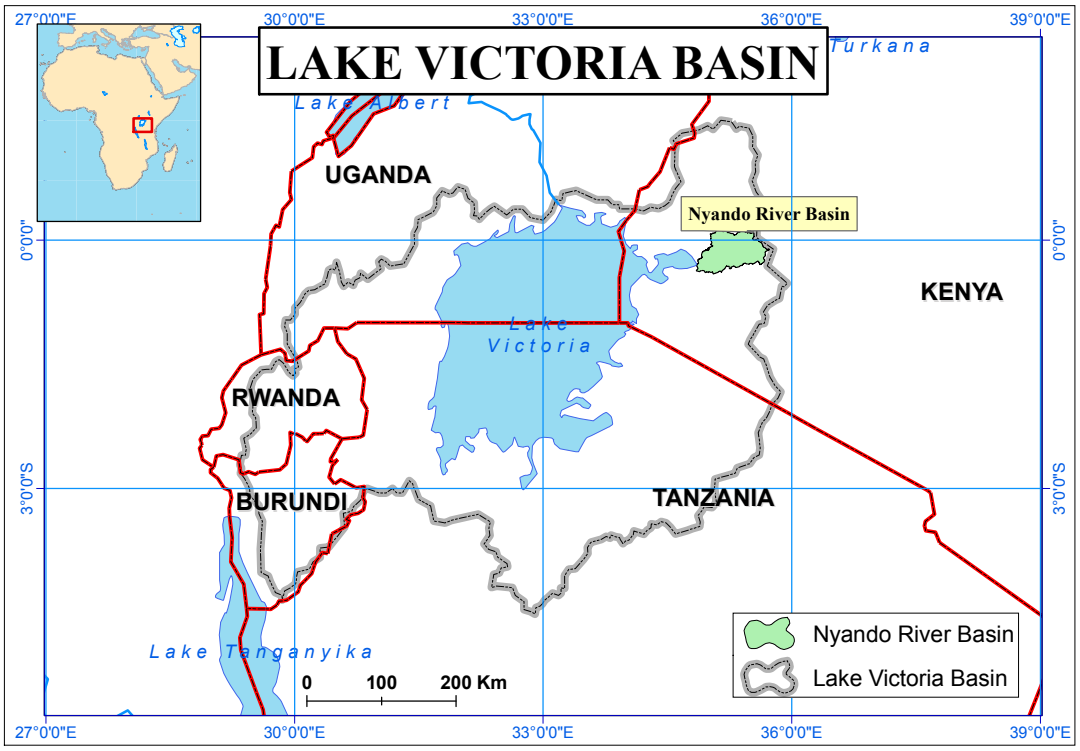

Figure 4.3: Lake Victoria basin, East Africa: adapted from Strategic Action Plan (SAP) for the LVB.

available every 1/2 hour was used to validate cloud top temperature as well as simulated integrated condensate. For land use, terrain and soil we used the 30s USGS global data set.

4.2.4 Numerical experiment

This study sought to downscale the global weather forecasts from GCM scale to hydrological scales (100km to 5km). This is targeted to provide fine resolution meteorological variables that can be used as forcing for hydrological models for flood warning systems. In addition, AMSR-E satellite data assimilation was done to improve the prediction. Three factors were taken into consideration in selecting the extreme event to investigate. 1) AMSR-E coverage; being located at the equator the coverage is limited to once in a few days for full domain, 2) A recorded coincidence of rainfall covering at least a quarter of the basin with maxima over

the lake or adjacent areas and 3) a day(s) with continuous mesoscale cloud system lasting at least 6 hours. The Globally-merged, full-resolution (4km) infrared (IR) data set was used for this purpose. Based on this and extensive screening, 4^{th} April, 2004 was selected for the numerical experiment. The accumulated daily rainfall for this day at *Kitale* station (35E, 1N) exceeded 85mm. This is above the 99^{th} percentile (71.70 mm/day) for the period 1973-2004 and also the 26^{th} highest amount recorded at this station for the same period. This is also the highest rainfall recorded at this station for 2004.

4.2.4.1 Model and domain setup

A nested model set up approach was employed with the outer domain of 30km, a second domain of 10km and a finer domain of 5km. Nesting of NWP models has been shown to produce better forecasts (e.g (Koch and Mcqueen, 1987; Rasmy et al., 2012; Talbot et al., 2012)). Figure 4.4 shows the location and domain setup. The mesoscale model was configured with 1.5 TKE-based closure system, SiB2(Sellers et al., 1996) land surface scheme, turbulent mixing, Lin ice microphysics scheme and cumulus parameterization for Grid1 and Grid2. The simulation was initiated at 06UTC on 4^{th} for the outer grid, 12UTC for the second grid and 18UTC for the fine grid. In the successive nesting, the boundary conditions were provided by the preceding grids and the initial conditions interpolated at the start of integration time corresponding to the preceding grid also.

4.2.5 Validation of QPFs

In the assessment of quantitative precipitation forecasts, point validations are far more common than validation relying on values integrated in space. Point validations merely compare the values measured at the locations of the rain gauges to the values simulated at the nearest grid element (Yates et al., 2006). The concept of "super-observations" has also been introduced in previous studies (e.g. (Cherubini et al., 2002)) where the observations are "up scaled" to the model scales and the observations are interpolated to each model grid

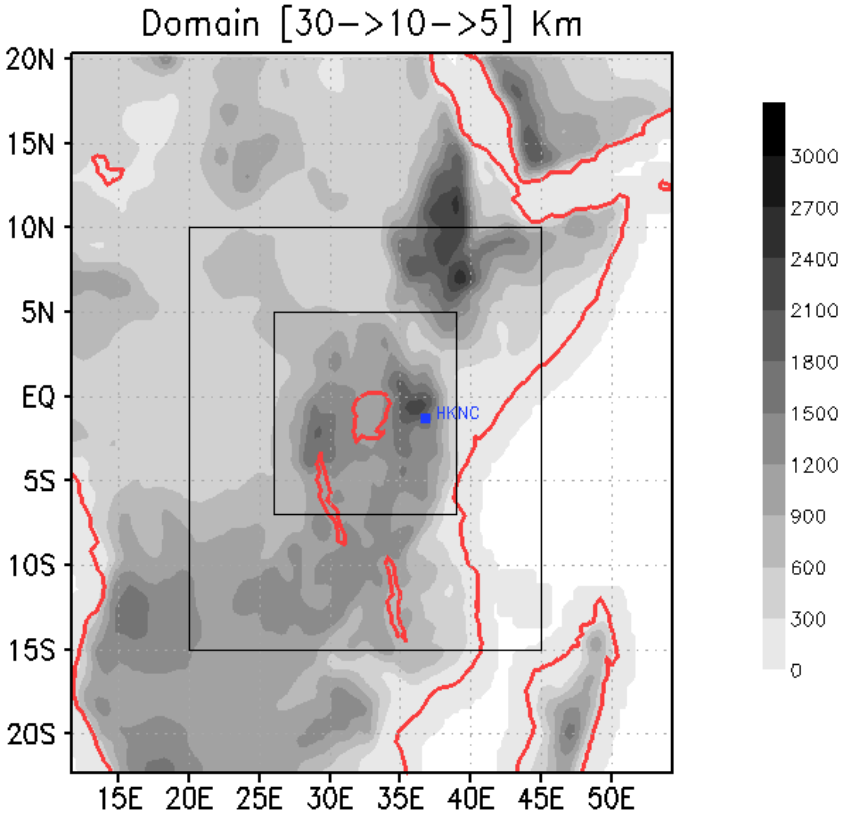

Figure 4.4: Nested domain set up (30 Km, 10 Km, and 5 Km).

box. Validationwas conducted using continuous statistics as well as contingency tables since ground based data was not available.

It is complemented by the use of scatter diagrams, maps, and correlation charts. The comparison is reduced to bulk scores, such as the root mean square error (RMSE) (respectively the mean and the root of the quadratic mean of the differences between observed and simulated values) or the square of the correlation coefficient (R^2). We use binary criteria relying on contingency a table established for a given threshold, following the format given in table 4.1 in a similar fashion as Yates et al. (2006).

Table 4.1: Contingency score table, "obs" stands for observations.

	Forecast $<$ threshold	Forecast $\geq$ threshold
Obs. $<$ threshold	a	b
Obs. $\geq$ threshold	c	d

In Table 4.1 a is the number of points where both the reference and the simulation are under the threshold; b is the number of points where the forecast is above but the reference is under the threshold; c is the number of points where the forecast is under whereas the reference is above the threshold; d is the number of points where both the reference and the forecast are above the threshold. From the contingency table, the following measures were computed: Forecast accuracy (ACC), frequency bias (FBIAS), probability of detection (POD), false alarm ratio (FAR), threat score (TS) and Heidke skill score (HSS). To match temporal resolution of TRMM, we aggregated forecasted precipitation into 3-hourly rates as well as cumulative rates for the 12 hours under investigation. Statistics are presented for 21Z, 00Z, 03Z and 06Z.

- POD gives the rate of well-predicted locations among the locations where the reference is over the threshold; a perfect forecast has POD=1
- FAR gives the rate of ill-predicted locations among the locations where the forecast is over the threshold; a perfect forecast has FAR=0.
- ACC gives the rate of all well-predicted locations with respect to the threshold; a perfect forecast has ACC=1. The POD, FAR and ACC scores need generally to be examined together
- TS gives the rate of well-predicted locations among the locations where the reference or the simulation is above the threshold. A perfect forecast has TS=1.

- HSS measures the ability to predict precipitation above a given threshold at a specific location; a perfect prediction has HSS=1, a random prediction has this score equal to zero

These scores are computed as shown below:

$$POD = \frac{d}{c+d} \tag{4.29}$$

$$FAR = \frac{b}{b+d} \tag{4.30}$$

$$ACC = \frac{a+d}{a+b+c+d} \tag{4.31}$$

$$FBIAS = \frac{b+d}{c+d} \tag{4.32}$$

$$TS = \frac{d}{b+c+d} \tag{4.33}$$

$$HSS = \frac{a+d-T}{a+b+c+d-T} \tag{4.34}$$

With ;

$$T = \frac{(a+b)(a+c)+(b+d)(c+d)}{a+b+c+d} \tag{4.35}$$

4.2.6 Downscaling: Results and discussions

This section presents the results of the downscaling experiment. The results for data assimilation are presented in section 4.3.2.

4.2.6.1 Synoptic conditions, 4^{th} April, 2004

Figure 4.5 shows the observed cloud top temperature from 21UTC 4^{th} to 00UTC 5^{th} April. A strong Mesoscale system existed over the lake region and this is strongly related to the synoptic pattern of the migration of the ITCZ.

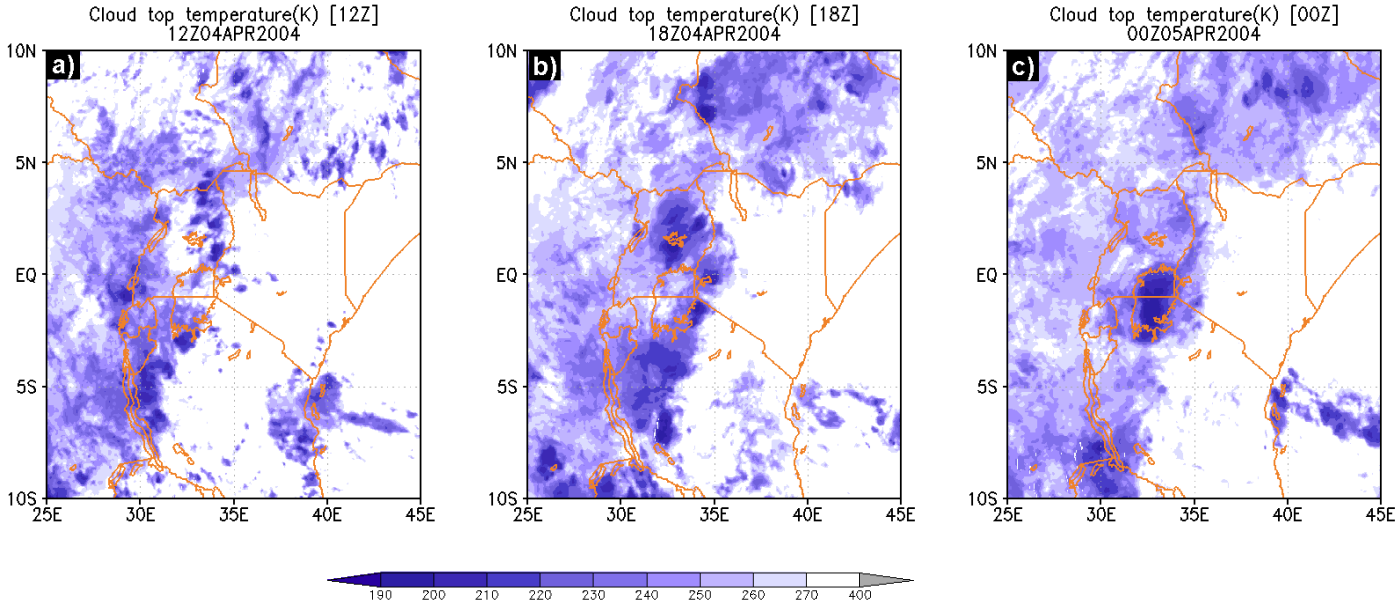

Figure 4.5: Observed cloud top temperature (a) 21UTC, (b) 18UTC, (c) 00UTC (5^{th} April).

A low pressure system existed in the region (Figure 4.6), the Ethiopian highlands, the Nandi Hills (East of Lake Victoria) and western sides of the lake. This twin pressure system continued strengthening at about 18UTC. Also, a synoptic scale surface convergence (not shown) was present from about 12UTC and continued over the lake until about 12UTC on 5^{th} April when the circulation developed into a predominantly southeasterly flow around the Ethiopian highlands.

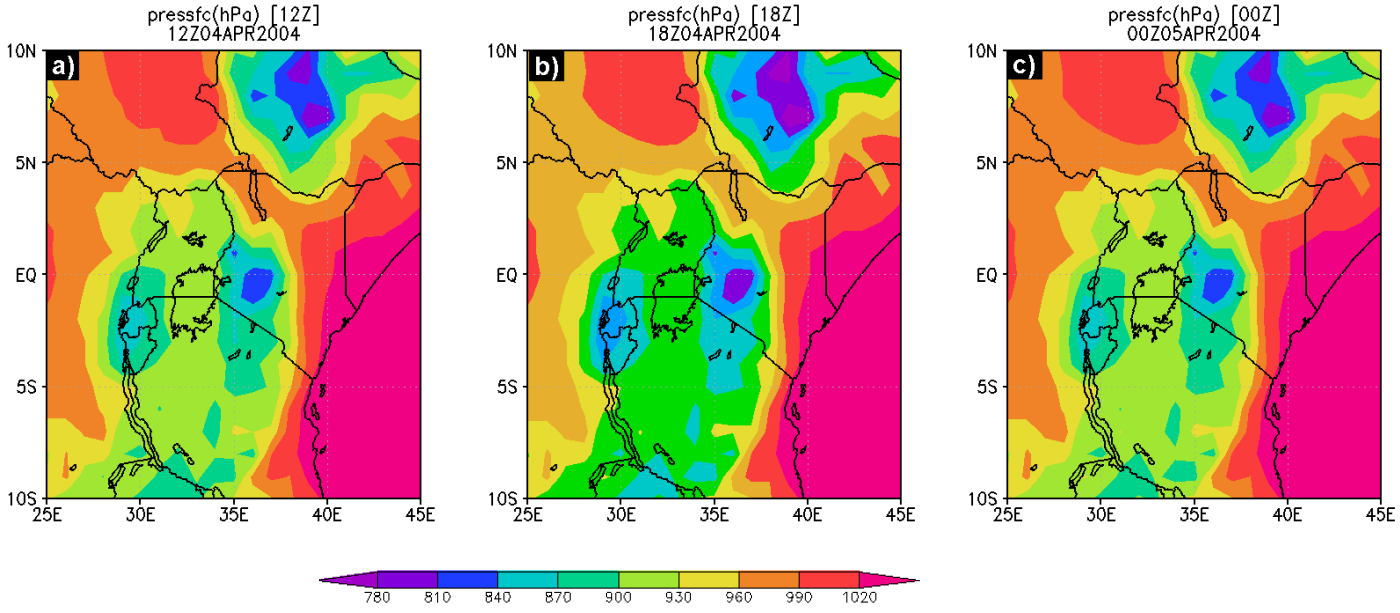

Figure 4.6: Surface pressure (a) 21UTC , (b) 18UTC , (c) 00UTC (5^{th} April).

4.2.6.2 Simulation of rainfall

Figure 4.7 shows the simulated 3-hour accumulated rainfall for the this experiment as compared to TRMM. This ARPS downscaling experiment was able to reproduce this extreme event to some degree of accuracy. At 21UTC, the ARPS run simulated rainfall northwest (NW) of the domain. The TRMM observations recorded rainfall over the lake at 00UTC (5^{th} April) and this event continued for about six hours. During this time, the ARPS run was not able to produce this pattern well and was characterized by excess rainfall NW of the domain. However, at 03UTC on 5^{th}, the system was able to reproduce some rainfall though the regions of maxima are further north compared to TRMM. In addition, the semi-autonomous event at around (35E,1N) was absent in this run. The lined up pattern evident in the TRMM observations was reproduced in this experiment albeit with about 200km displacement westwards.

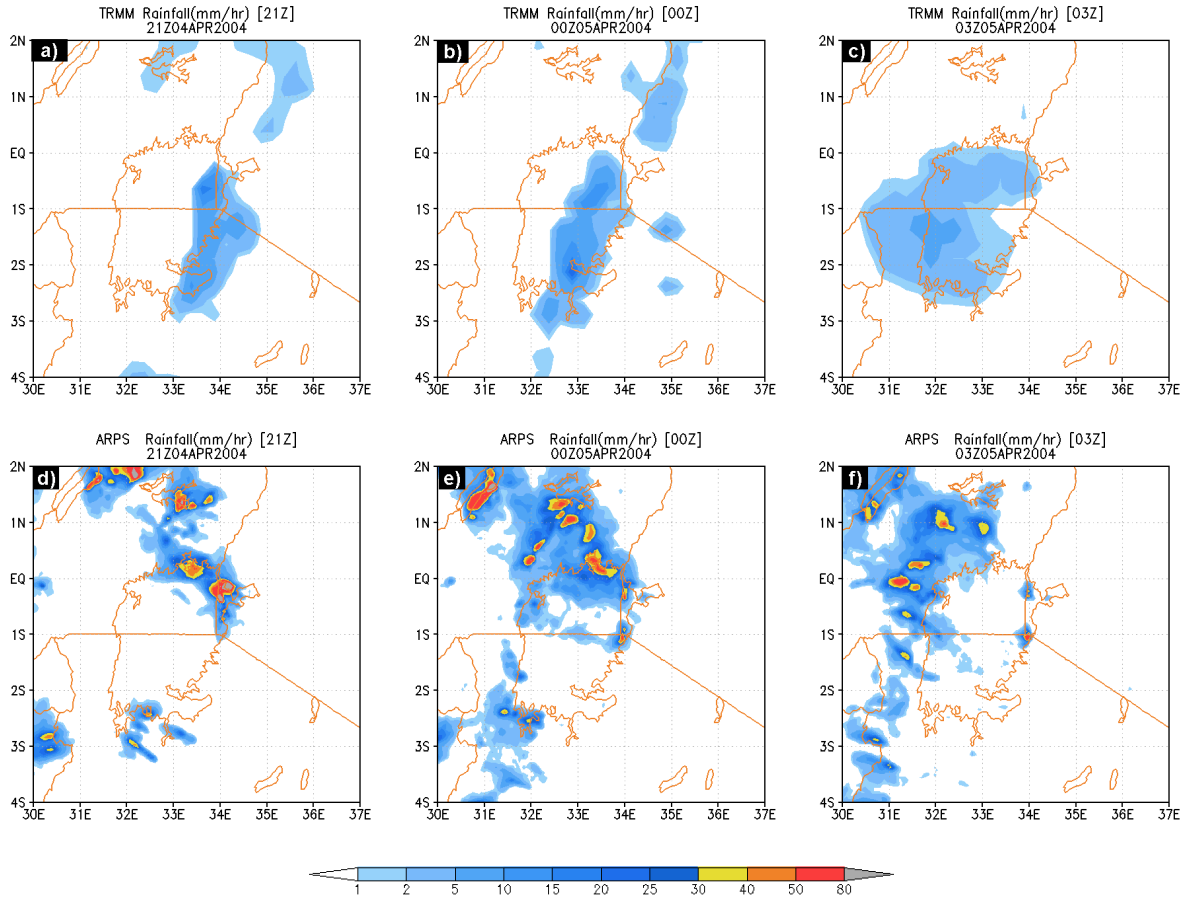

Figure 4.7: Comparison between ARPS simulated 3-hourly rainfall and TRMM estimates over LVB (a)21UTC TRMM ,(b) 00UTC TRMM(5^{th} April) ,(c) 03UTC TRMM, (d) 21UTC ARPS ,(e) 00UTC ARPS ,(f) 03UTC ARPS

(a) *Continuous statistics*

Table 4.2 shows the comparison of the predicted versus observed mean precipitation for the first 12 hours under investigation. On average the model overestimates QPF by more than 100% with a basin average of 3.2mm at 03UTC compared to TRMM's 0.5mm. Though some aspects of this prediction at specific times is presented reasonably, the spatial correlation between the predicted and observed is very weak (-0.02) with only prediction at 06UTC 5^{th} reaching a coefficient of 0.02.

Table 4.2: Comparison of statistics.

Statistic		*3-hour*	*6-hour*	*12-hour*
Mean	Observation	0.50	0.50	0.25
	Forecast	3.15	2.93	0.90
Standard Dev.	Observation	–	–	0.60
	Forecast	–	–	2.83
R^2	-	-0.02	-0.07	0.02

Figure 4.8 shows the scatter diagrams for the selected analysis times. The scatter diagrams show complex patterns with the displayed lines of fit far from representative. Overall, the simulated rainfall is too weak (bias $\tilde{5}$mm/hr).

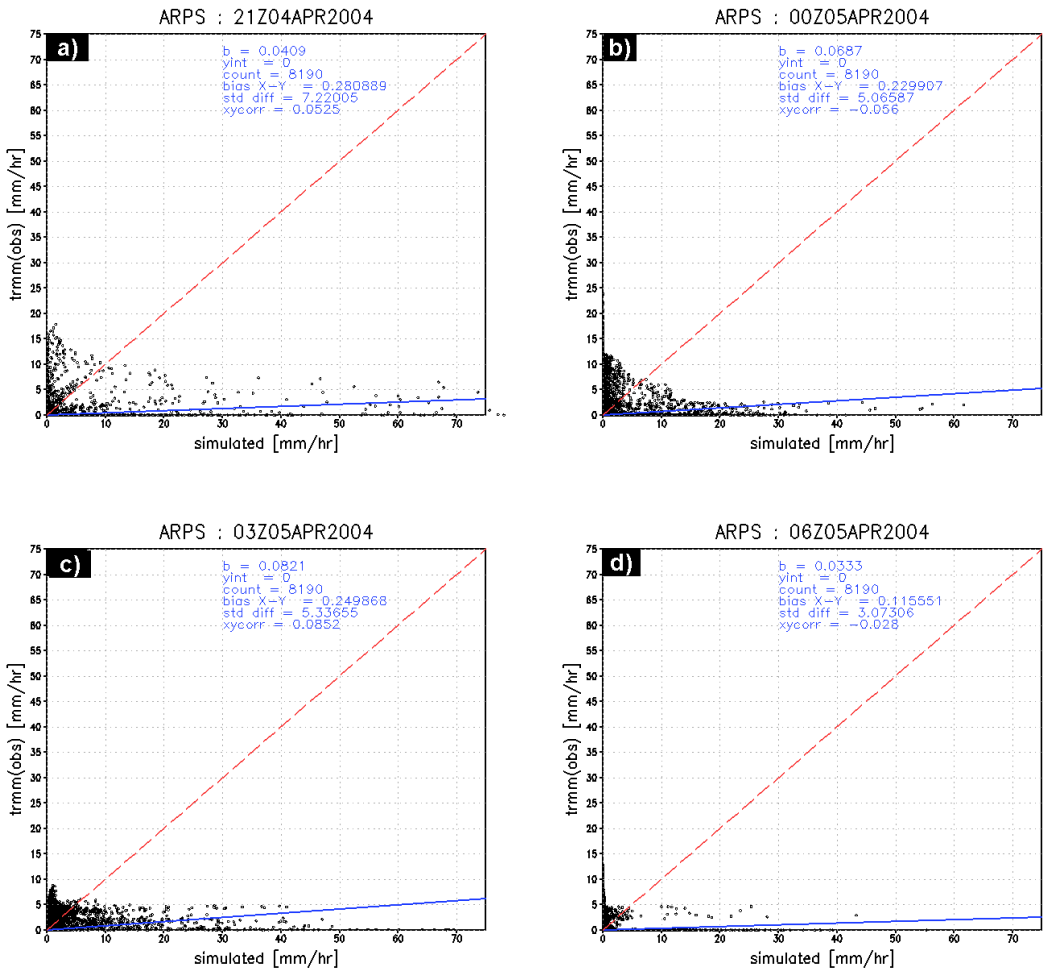

Figure 4.8: Scatter plots for the ARPS experiment (a) 21UTC, (b) 00UTC, (c) 03UTC (5^{th} April), and (d) 06UTC.

(b) *Scores computed based on the contingency table*

Generally, there are no rules with regard to thresholds in contingency tables. Previous studies have used 70,80 and 90 percentiles to evaluate the probabilities. We applied a slightly different approach by using thresholds selected between 2-7 mm since the observation rarely exceeds 10mm/hour in the observations. Further, this range is representative of most of the possibilities of prediction and observation. Figure 4.9 shows the scores based on the contingency table. High thresholds are characterized by below average scores on POD, (e.g.

at 0.3 for 2 mm/hr and almost zero for 7 mm/hr). However, forecast accuracy is slightly better for lower thresholds. FBIAS is also higher for large thresholds with about 30mm/hr for 7mm/hr threshold. The false alarm ratio (FAR), an indicator for ill-predictions, is very high for all the thresholds. FAR is almost 1.0 for 7mm/hr threshold, 0.9 for 3mm/hr and only about 0.8 for 2mm/hr. This shows the model performance is very poor.

The model scores poorly on HSS (not shown) indicating failure to predict rainfall amounts higher than the average threshold. The performance of the model varies with time, three hours after integration, the POD and ACC are very low and this could be attributed to model spin up. At 03UTC, the model performs slightly better and the maps (figure 4.7) show a reasonable pattern. This performance deteriorates with time and the scores of POD reduces to almost zero after 12 hours of integration. It is worth noting that, for this event, dissipation starts after about 03UTC and this could partly explain the degradation of the scores.

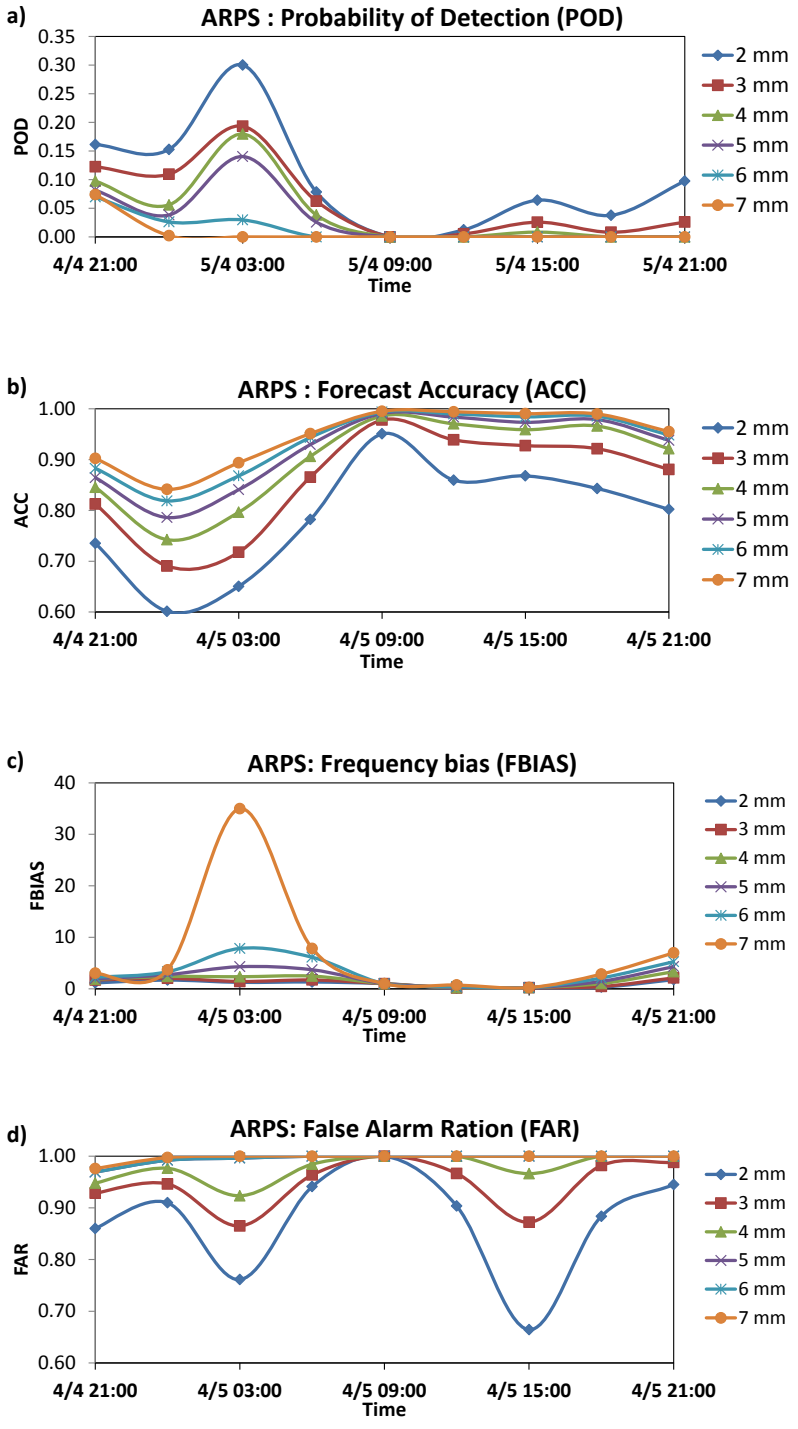

Figure 4.9: Scores computed based on the contingency table for the simulation. Each 3-hour accumulation is presented by one value; a) POD b) ACC, c) FBIAS and c) FAR.

4.2.6.3 Simulated cloud pattern

Since precipitation validation in this experiment was limited to TRMM, this study also evaluated the simulated cloud pattern against observed cloud top temperature pattern by the globally merged Infra-Red (IR) hourly product. IR cloud top temperature can be used to identify the spatial distribution of clouds with regions of dense clouds having lower temperatures. We compared the pattern as well as the coefficient of correlation and figure 4.10 summarizes the findings. In a similar fashion to the simulated rainfall, the model was able to reproduce a reasonable cloud pattern for this event with the lined up cloud pattern in the observations showing some signal in the ARPS results at 00UTC on 5^{th}. However, over the lake, there appears to have weak or no cloud simulated at all.

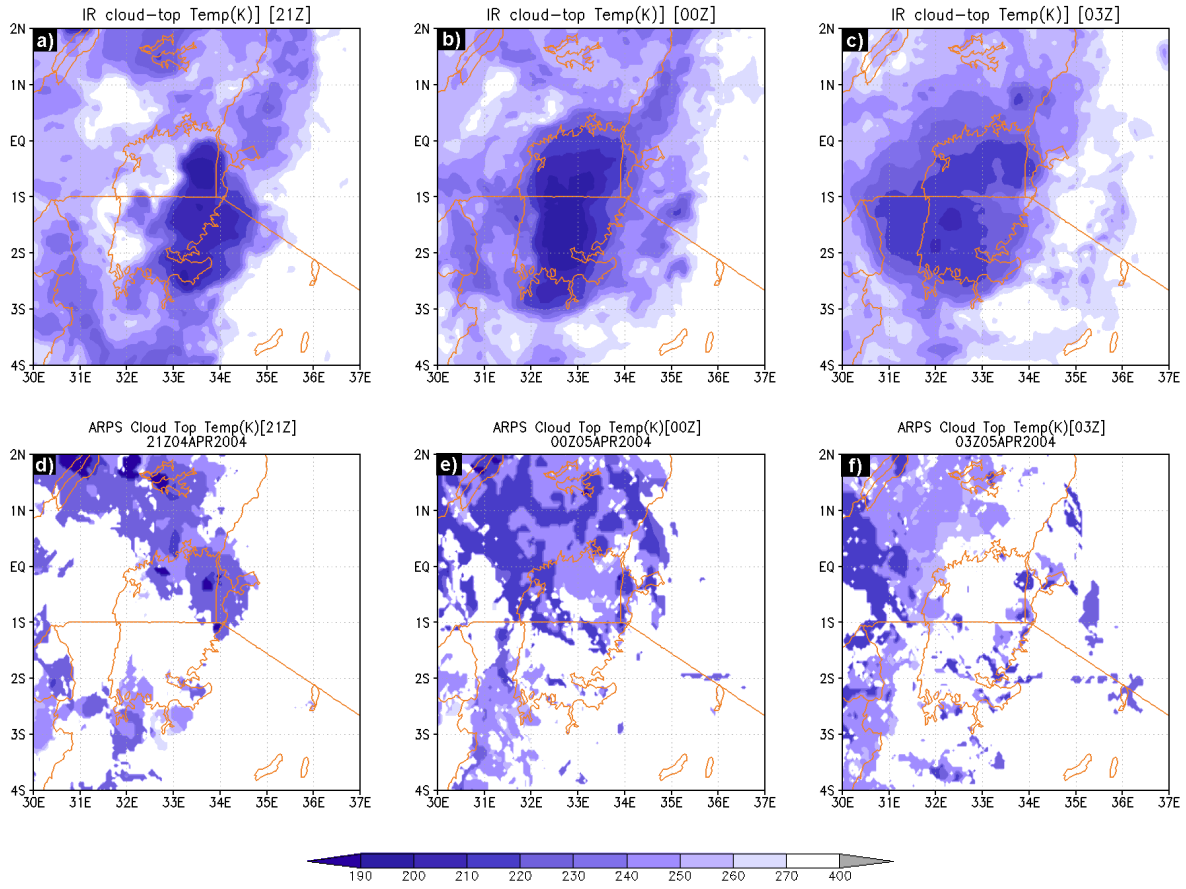

Figure 4.10: Comparison between simulated and observed cloud top temperature (a) 21UTC IR, (b) 00UTC IR, (c) 03UTC IR (5^{th} April), (d) 21UTC ARPS, (f) 00UTC ARPS, (f) 03UTC ARPS (5^{th} April) .

We also computed the temporal evolution of correlation between the simulated and observed cloud top temperature and figure 4.11 summarizes the findings. Up to about 4 to 6 hours after integration, the model simulates a weak cloud pattern and it closely resembles the observed pattern with a correlation coefficient of about 0.1. However, the performance deteriorates afterwards and the model further diverts away from the observation. After ten hours, the event has dried up and the model is able to recreate a dry LVB. This is reflected by the positive strong correlation from 12 to 36 hours. However, since the focus of this study is extreme events, this may not be very relevant as assessment of skill. Reasonable analysis

is limited to the first twelve hours of integration (duration of the extreme event).

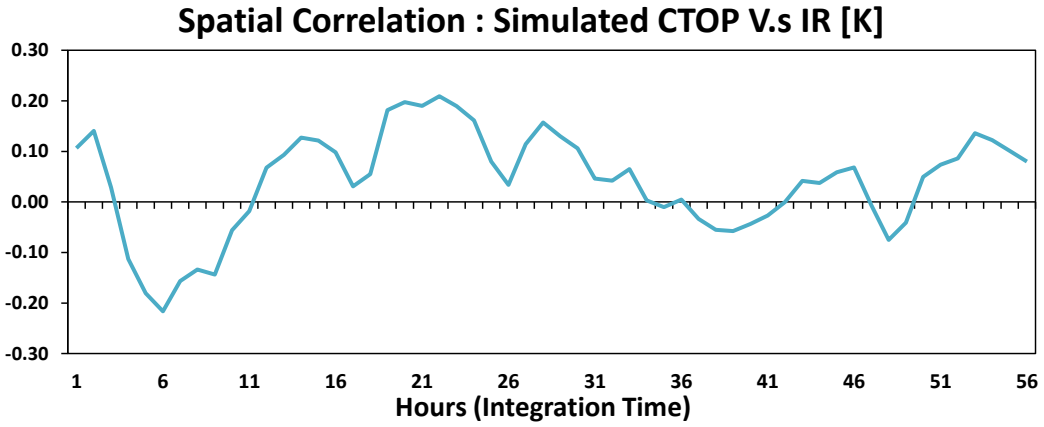

Figure 4.11: Temporal evolution of simulated vs. observed ARPS cloud top temperature from 18:00 hours on 4^{th} April, 2004.

Figure 4.12 shows the spatial evolution of integrated cloud condensate with time and how it compares with the observed cloud pattern by IR cloud top temperature. From about 21UTC on 4^{th}, the concentration of integrated cloud water starts to develop over the north-eastern parts of the lake which also coincides with region of rainfall maxima. This system continues to develop but does not reach full potential even after 3 hours. The continuous cloud system development in this region leads to the release of latent energy by conversion of water vapor to cloud water. Conversely, this leads to strengthening of updraft and convection occurs.

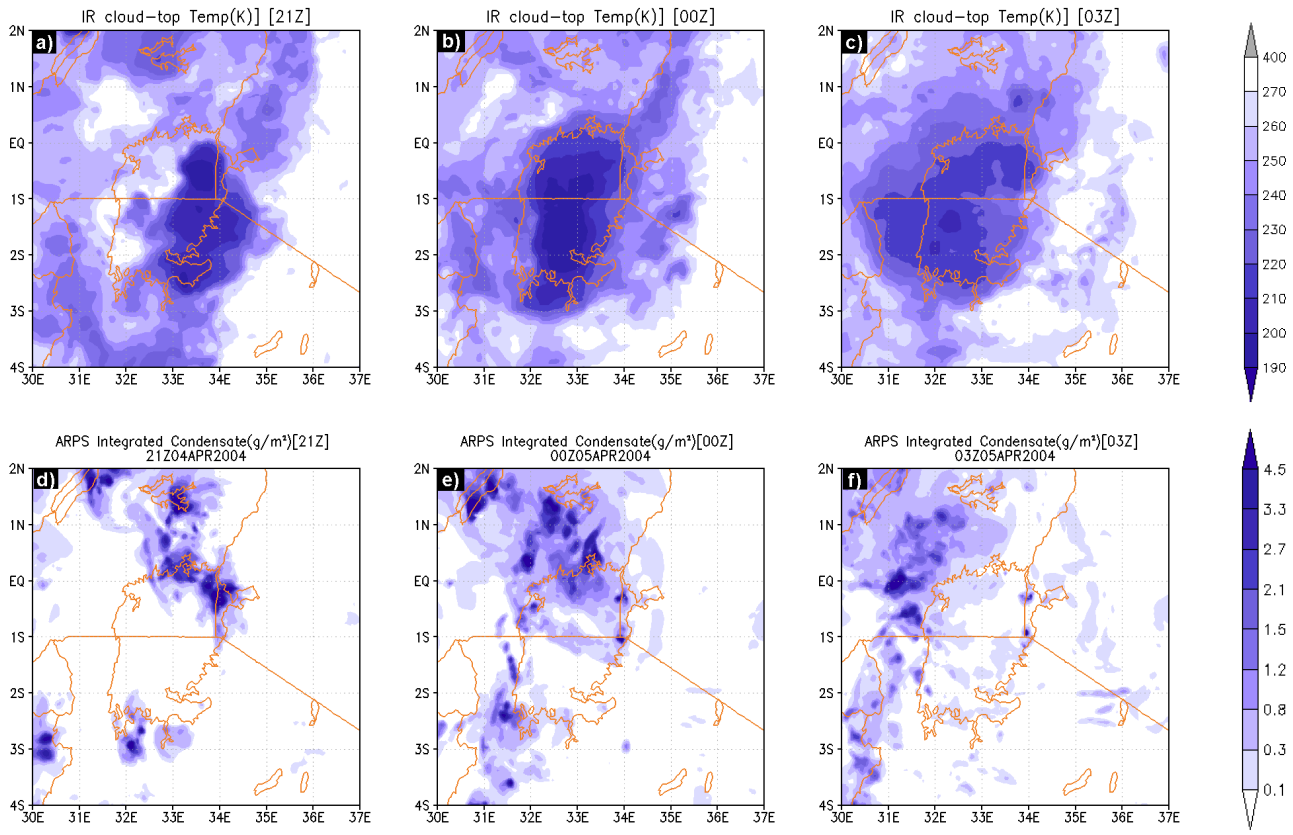

Figure 4.12: Comparison between simulated integrated cloud condensate and observed cloud top temperature (a) 21UTC IR,(b) 00UTC IR,(c) 03UTC IR(5^{th} April),(d) 21UTC ARPS,(e) 00UTC ARPS, (f)03UTC ARPS .

4.3 Data assimilation and wind bogussing for extreme event forecasting

In the previous sections, we investigated the merits and limitations of downscaling only (ARPS) by using the mesoscale model only. As an initial step to approach the problem gradually, we further extended our modeling framework to assimilate the passive microwave higher frequency observations that contain atmospheric moisture information over land surface as well as over water (in this case Lake Victoria). This is achieved by coupling land data assimilation at the lower frequencies with cloud assimilation at higher frequencies (sensitive

to water vapor and cloud water).

The Coupled atmosphere and land data assimilation system (CALDAS)(Rasmy et al., 2012) is an integrated system of a Mesoscale storm model (ARPS), a Land data assimilation system(LDAS-A)(Rasmy et al., 2011) and a cloud microphysics data assimilation system (CMDAS) (Mirza et al., 2008). The Land data assimilation system (LDAS-A) component consists of a mesoscale atmospheric model, a land surface model (SiB2) that acts as a land surface driver for the atmospheric model and as a model operator of the assimilation system, a microwave Radiative Transfer Model (RTM) as an observation operator, and an ensemble Kalman filter (EnKF) as an assimilation algorithm. The LDAS-A was developed to improve the surface moisture heterogeneity through the assimilation of lower frequency satellite passive microwave observations such as those at 6.9 and 10.65GHz. On the other hand the CMDAS component assimilates microwave satellite data at the 23GHZ (sensitive to water vapor) and 89GHZ for the cloud. Brightness temperature from the AMSR-E microwave sensor is used in the CALDAS system. The AMSR-E is a twelve-channel, six-frequency, total power passive-microwave radiometer system. It measures brightness temperatures at 6.925, 10.65, 18.7, 23.8, 36.5, and 89.0GHz. Vertically and horizontally polarized measurements are taken at all channels.

Since LDAS-A can reasonably represent the land surface emission using lower frequency passive microwave observations (Rasmy et al., 2012), the atmospheric contributions in the satellite microwave higher frequency observations can be computed separately. To accomplish the atmospheric observation over the land surface, LDAS-A system incorporates passive microwave higher frequency (23 and 89GHz) observations to bridge the AMSR-E lower frequency (land surface) information with same footprint higher frequency observations to obtain the atmospheric information, while data assimilation components of land and atmosphere maintain the consistency between model variables and assimilated variables. This is done through the coupled atmosphere and land data assimilation system.

In this way, a synchronized land–atmosphere initialization can be performed in a land-atmosphere coupled model and can eliminate the biased forcing to the land surface or vice

versa. The concurrent and near-real time initialization of both land and atmosphere introduces the near-real time condition of both land and atmosphere in numerical weather forecast, and therefore is a promising method to improve the future predictability of land and atmospheric water and energy budgets.

4.3.1 System overview

A brief overview of the CALDAS is given in this section. More detailed information can be found in Rasmy et al. (2012). Figure 4.13 illustrates the schematic diagram of the CALDAS, its principal components and the connections between individual sub-components. The CALDAS has fundamentally three sub-systems : (1) a land–atmosphere coupled mesoscale model (ARPS), (2) a land data assimilation system (LDAS), and (3) a cloud microphysics data assimilation system (CMDAS).

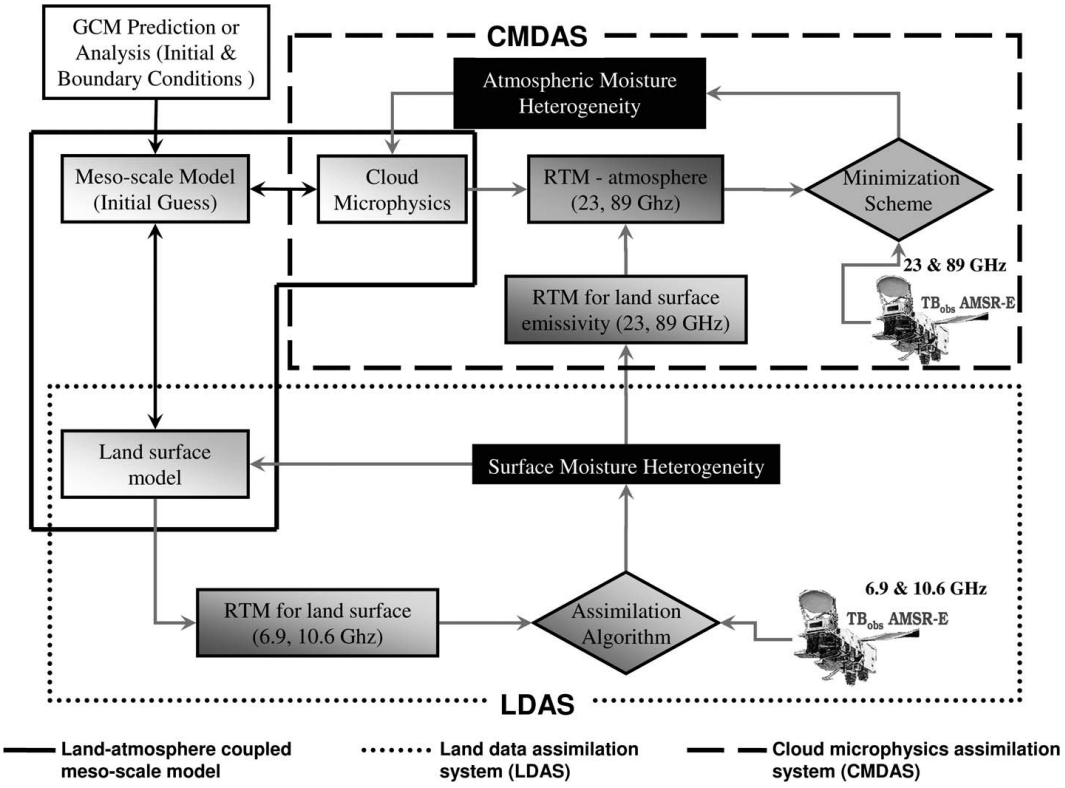

Figure 4.13: CALDAS on and its main components.

The LDAS comprises a land surface scheme as a model operator, a RTM for land surface, an observation operator, and a sequential assimilation algorithm to directly assimilate 6.9 and 10.6 GHz of AMSR-E brightness temperature observations. The CMDAS consists of the cloud microphysics scheme as a model operator, a RTM for both land and atmosphere as observation operator, and a minimization scheme to assimilate 23 and 89 GHz of AMSR-E brightness temperature observations.

CALDAS utilizes the improved land surface emission by LDAS as the lower boundary conditions and thereby improves the atmospheric moisture heterogeneities including those of water vapor, cloud liquid water, hail, rain, snow. The land-atmosphere coupled mesoscale model operates as an *atmospheric driver*, simulates the evolution of land and atmospheric states and provides initial and boundary conditions that are required for LDAS and CMDAS for each layer of soil and atmosphere, while the model operators in both LDAS and CMDAS maintain the consistency between assimilated variables and model variables. The model operators (i.e., land surface model and cloud microphysics scheme) are kept common between land-atmosphere mesoscale model and the assimilation systems to maintain the consistency between assimilated variables and model variables. As CALDAS is on-line based system, the assimilated variables are immediately fed back to the land-atmosphere mesoscale model. With the improved land and atmospheric conditions, the mesoscale model is integrated forward in time for prediction of land and atmospheric evolution.

4.3.1.1 Cloud Microphysics Data Assimilation System (CMDAS)

The earlier version of Cloud Microphysics Data Assimilation System (CMDAS) that was referred to as 1-Dimensional variational (1D-Var) Ice Cloud Microphysics Data Assimilation System (IMDAS) was initially developed by Mirza et al. (2006) to improve the atmospheric conditions over ocean and sea surface using AMSR-E 23 and 89 GHz frequency brightness temperatures. IMDAS had only considered Water Vapor (WV) and Cloud Liquid Water Content (CLWC) as assimilation parameters. However, due to the nature of cloud systems, clouds are generally in mixed-phase that composed of a mixture of cloud droplets and ice

crystals. The partitioning of condensed water into liquid droplets and ice crystals in clouds varies throughout the life cycle of clouds, with droplets forming initially but crystals dominating later as ice forms first by crystal nucleation and then by vapor deposition. To account for better precipitation estimation and to include the effect of the liquid and solid phase of the cloud on microwave frequency (89 GHz), Kuria et al. (2007) modified the CMDAS to allow direct estimation of snow and rain rate as additional assimilation variables.

(a) *Cloud Microphysics Scheme*

In the NWP, the portion of precipitation from a prognostic cloud and its precipitation processes is regarded as grid-resolvable precipitation. The other portion is from sub-grid scale precipitation and it is due to parameterized cloud and precipitation processes from the cumulus parameterization scheme. Various parameterizations have been developed to represent microphysical properties of the clouds and precipitation. A bulk parameterization of cloud particles and precipitation drops is primarily based on the works of Lin et al. (1983) and it has been a core part of representing cloud and precipitation processes in both GCM and mesoscale models. In this research, we adopted Lin's ice microphysics scheme as a model operator for atmospheric data assimilation to represent the formation, growth and sedimentation of liquid and solid particles.

(b) *Microwave Radiative Transfer model*

The AMSR-E microwave sensor does not observe soil moisture, water vapor, rain water or cloud water. There is a need for a transformation between observed brightness temperature and these variables. Based on the emission behavior of dry soil and liquid water in the microwave region, a radiative transfer algorithm, allowing the estimation of soil moisture from the land surface, was considered. This model is characterized by its low computational cost and physically based formulation which are convenient specificities for an assimilation system. Based on the soil moisture values derived from SiB2, the radiative transfer model (RTM), as the observation operator, estimates the brightness temperature, which is then compared with the satellite observation through a cost function. Due to the applicability of

RTM for wider frequency range, the same RTM that was used to calculate the surface emission and scattering effect of upwelling radiation at lower frequencies, was used to estimate the the surface emission and scattering effect of upwelling radiation at higher frequencies.

To estimate the atmospheric emission and scattering effect of upwelling radiation at higher microwave frequencies, GUOSHENG (1998) proposed a model referred to as 4-stream fast model. In the 4-stream fast model, radiances at any direction were expressed by formal solution while the scattering source term was determined by a 4-stream discrete ordinate solution using Henyey-Greenstein scattering phase function. They showed that the model was fast and accurate enough for practical use in microwave remote sensing and data assimilation, where many model simulations are required, and the error being less than 3K compared to the accurate polarized 32-stream model. They further compared with a 2-stream Eddington model and the results showed that it was more accurate than the Eddington model, especially for ice cloud conditions(Rasmy et al., 2012).

(c) *Minimization scheme*

For atmospheric data assimilation (CMDAS), a minimization scheme (Shuffled Complex Evolution (SCE) Method) that was developed by Duan et al. (1993) was chosen to minimize the cost function between model brightness temperatures and observed brightness temperatures of AMSR-E at 23 and 89GHz. The SCE method is a global optimization strategy that combines the best features of multiple complex shuffling and competitive evolution. This method is capable of finding the global optimum and does not rely on the availability of an explicit expression of the objective function or the derivatives. For complete information, please refer to Duan et al. (1993).

4.3.1.2 Datasets and methods

(a) *Initial and boundary conditions*

For this is the extension of the first downscaling experiment, the same model domain, initial and boundary conditions were used.

(b) *Advanced Microwave Scanning Radiometer (AMSR-E)*

CALDAS utilizes the AMSR-E higher frequency brightness temperature observations at 23 and 89 GHz for assimilation. AMSR-E is a twelve-channel, six-frequency, passive-microwave radiometer system. It measures horizontally and vertically polarized brightness temperatures at 6.9 GHz, 10.7 GHz, 18.7 GHz, 23.8 GHz, 36.5 GHz, and 89.0 GHz. Spatial resolution of the individual measurements varies from 5.4 km at 89 GHz to 56 km at 6.9 GHz. AMSR-E is developed and provided by the Japan Aerospace Exploration Agency (JAXA, Contractor: Mitsubishi Electric Corporation) with close cooperation of U.S. and Japanese scientists. AMSR-E was modified for Aqua from the design used for AMSR, which is onboard, the Japanese ADEOS-2 satellite. The AMSR-E radiometer is an advancement of previous microwave radiometers. The spatial resolution is twice better that of Scanning Multichannel Microwave Radiometer (SMMR) and Special Sensor Microwave/Imager (SSM/I) data. Additionally, AMSR-E combines several channels together that were used individually like in the SMMR and SSM/I satellites.

AMSR-E uses an offset parabolic reflector, 1.6 m in diameter, to focus Earth-emitted microwave radiation into an array of six feedhorns, which then feed the radiation to the detectors. The AMSR-E instrument rotates continuously about an axis parallel to the Aqua satellite at 40 RPM. At an altitude of 705 km, it measures the Upwelling scene brightness temperatures over an angular sector of 61 about the sub-satellite track, resulting in a swath width of 1445 km. AMSR-E records active scene measurements at equal intervals of 10 km (5 km for the 89 GHz channels) along the scan. The reflector is fixed at a 47.4 degree half-cone angle, which results in an Earth incidence angle of 55.

The AMSR-E instrument measures geophysical variables related to the earth's water cycle, including: precipitation rate, cloud water, water vapor, sea surface winds, sea surface temperature, sea ice concentration, snow water equivalent, and soil moisture. The AMSR-E antenna stopped spinning at 0726GMT 4^{th} October, 2011 most likely due to aging lubricant in the mechanism. AMSR-E currently is not producing any data and has been replaced with

AMSR-2 launched on 18^{th} May, 2012. The Advanced Microwave Scanning Radiometer 2 (AMSR2) on-board the GCOM-W1 satellite is a remote sensing instrument for measuring weak microwave emission from the surface and the atmosphere of the Earth. From about 700 km above the Earth, AMSR2 will provide highly accurate measurements of the intensity of microwave emission and scattering. The antenna of AMSR2 rotates once per 1.5 seconds and obtains data over a 1450 km swath. This conical scan mechanism enables AMSR2 to acquire a set of daytime and nighttime data with more than 99% coverage of the Earth every 2 days.

4.3.2 Assimilation: Numerical experiment

Two numerical experiments were considered: (1) ARPS run (in section 4.2.4),one-way nesting procedure employing the land–atmosphere mesoscale model without any assimilation, and (2) CALDAS run, in which ARPS runs accompanied by a sequential land data and a cloud microphysics data assimilation. The study domain was kept same as described in section 4.2.4. In addition a set of seven more experiments was set up to investigate the assimilation of water vapor and the challenges therein.

4.3.3 Model configuration and parameter settings

The model configuration and parameter settings for ARPS and SiB2 were kept same as for the ARPS experiment as described in section 4.2.4. In the following section, the model settings for CMDAS are as outlined.

4.3.3.1 Assimilation Parameters

Four atmospheric moisture variables; cloud liquid water, water vapor, rain water, and snow water were used as the assimilation parameters. To assimilate those parameters, lower and upper limits of vertically integrated values of cloud liquid water (ICLW), water vapor (IWV), rain water (IRW), and snow water (ISW) have to be defined explicitly. Though there were

no direct measurements available for these parameters, consideration was done to give more room since this region is predominantly wet. For example, $80 kgm^{-2}$ was set as the maximum range for integrated water vapor. The lower and upper bound of the cloud liquid water content were obtained from literature and for different types of clouds, such as those given at ($http://www-das.uwyo.edu/\ geerts/cwx/notes/chap08/moist_cloud.html$).

The upper bound for other parameters (IRW and ISW) was selected arbitrarily since no information was available. The accurate representation of upper bound of each parameter can only be selected based on thorough detailed field campaign, which will be the future target for the extended model validation. Table 4.3 summarizes the ranges of parameters used in CMDAS.

Table 4.3: Upper and lower bounds of assimilation parameters.

Parameter	Unit	Lower limit	Upper Limit
Integrated Water Vapor (IWV)	kgm^{-2}	4.0	80.0
Integrated Cloud Liquid Water (ICLW)	kgm^{-2}	0.0	3.5
Integrated Rain Water (IRW)	kgm^{-2}	0.0	5.5
Integrated Snow Water (ISW)	kgm^{-2}	0.0	2.0

4.3.3.2 Cloud bottom and cloud top

CMDAS was formulated to consider only one layer of clouds. The cloud depth is defined by a *cloud bottom* and a *cloud top* height, relative to the ground elevation and it has to be specified explicitly before the assimilation takes place. Due to the unavailability of radiosonde observations in this region, empirical cloud height values were used. The cloud bottom was assumed to be at 1,600m above the surface and cloud top at 6,000m.

4.3.3.3 Profiles of assimilation parameters

ICLW was transformed to the parabolic distribution with maximum cloud content at the center of the cloud and has zero values above the top and below bottom of the cloud layer. For integrated water vapor, a (SCE/model) IWV factor was computed and applied to the model profile to retain model consistency. Further experiments of saturation instead of factor method were also considered.

The profiles of rain and snow follow a skewed profile and begin to form at the cloud top and reaching a maximum at the cloud bottom, after that it decreases due to evaporation and breakup of raindrop or snowflakes. Kuria et al. (2007) added a constraint for qr and qs in the following form. It is assumed that for temperatures colder than -20^o C, only snow exists, and for temperatures above 4^o C, only rain exists. For temperatures between these two extremes, we assume a linear conversion function of precipitation to rain and snow, according to the equation given below

$$q_p = \begin{cases} \frac{T_u - T}{T_u - T_l} q & \text{snow} \\ \frac{T - T_l}{T_u - T_l} q & \text{rain} \end{cases}$$

Where T is the temperature of a layer, T_u is an upper temperature threshold (4^o C), T_l is a lower temperature threshold (-20^o C), q_p is respective precipitation variable and q is total precipitation in the layer. Using this strategy the retrieved profiles can be made physically consistent. Cloud ice and hail are not explicitly assimilated, but those are the by-products of the assimilation exercise (by-products from Lin's Microphysics). However, both ice and hail will have to be considered in the future modeling framework for accurate assimilation.

4.3.4 Cost function

The SCE algorithm is based on an iterative method, where a cost function is minimized by adjusting the state vector or assimilation parameters. The cost function J (X) is given by

$$\begin{aligned} J(X) =& J_b(X) + J_0(X) \\ =& \frac{1}{2}\left[(X_b - X)^T B^{-1}(X_b - X) + [Y_0 - H(X)]^T R^{-1}[(Y_0 - H(X)]\right] \end{aligned} \tag{4.36}$$

Where, the subscripts b and 0 denotes the background and observation respectively. B is the background error covariance matrix and R is the observation error covariance matrix.

Mirza et al. (2008) assumed that the background error term (J_b) is equal to zero since the information of the background error covariance matrix (B) is unknown. A further assumption was made for observations, where all the observations have same error and that is equal to a unit matrix ($R = I$). Considering these assumptions, the cost function can be written as

$$J(X) = \frac{1}{2}\sum_{i=1}^{N}[Y_0 - H(X_i)]^T[Y_0 - H(X_i)] \tag{4.37}$$

$$X_i = M(X_o) \tag{4.38}$$

Where Y_o is the observations (23.8 and 89 GHz), N is the number of brightness temperature observations, H is the radiative transfer model that represents land and the atmosphere, M is Lin's ice microphysical scheme, and X is the atmospheric states. J is minimized using SCE-UA method that guarantees asymptotic convergence to the global minimum (or optimum).

4.3.5 Assimilation: Results and discussion

Due to the large size of the LVB (194,000 km^2) there was a limitation on the available AMSR-E passes (data). Assimilation was only possible at 23:10 pm on 4^{th} April, 2004. Figure 4.14 shows the observed TRMM rainfall, observed IR cloud top temperature and AMSR-E brightness temperature for this day. The AMSR-E observation shows a lined up pattern of low brightness temperature values indicating the presence of deep clouds, which by using CMDAS would be assimilated into the NWP and possibly produce better forecasts. Also, part of the clouds exist over the lake and a small portion on land which provided a good test-bed for the validation of the LDAS-A over wet and humid areas.

The CALDAS run was initiated in a similar way to the ARPS experiment. It was started at 06UTC 4^{th} for the outer grid (grid1), 12UTC for second nesting grid (grid2) and 18UTC for the inner nest (grid3) on which data assimilation was done. Assimilation occurred at 23:10 UTC followed by a forecast run lasting 36 hours.

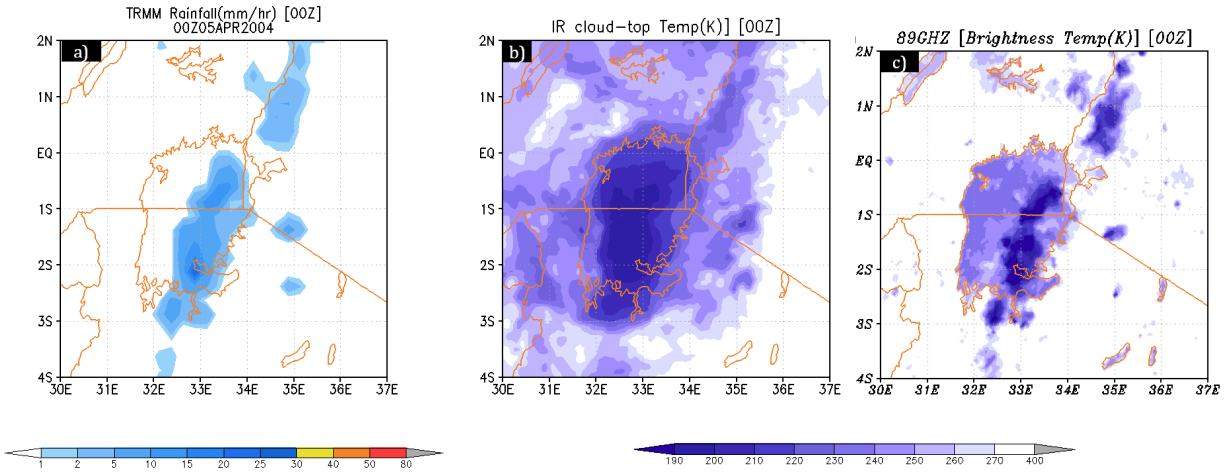

Figure 4.14: (a) Observed rainfall (TRMM), (b) observed cloud top temperature (IR), and (c) AMSR-E brightness temperature at 00UTC (5^{th} April).

Figure 4.15 shows the observed and the assimilated brightness temperature and the differences. The CALDAS system was able to assimilate AMSR-E observations successfully and the assimilated brightness temperature closely resembles observations. However, CALDAS assimilates higher brightness temperature compared the observed at 23GHz frequency. Sensitivity experiments were conducted to investigate this occurrence and will be highlighted in the next section. The assimilation of lower brightness temperature over the lake by the 23GHz shows that CALDAS was able to introduce clouds and to an extent, overestimated the cloud activity over the lake.

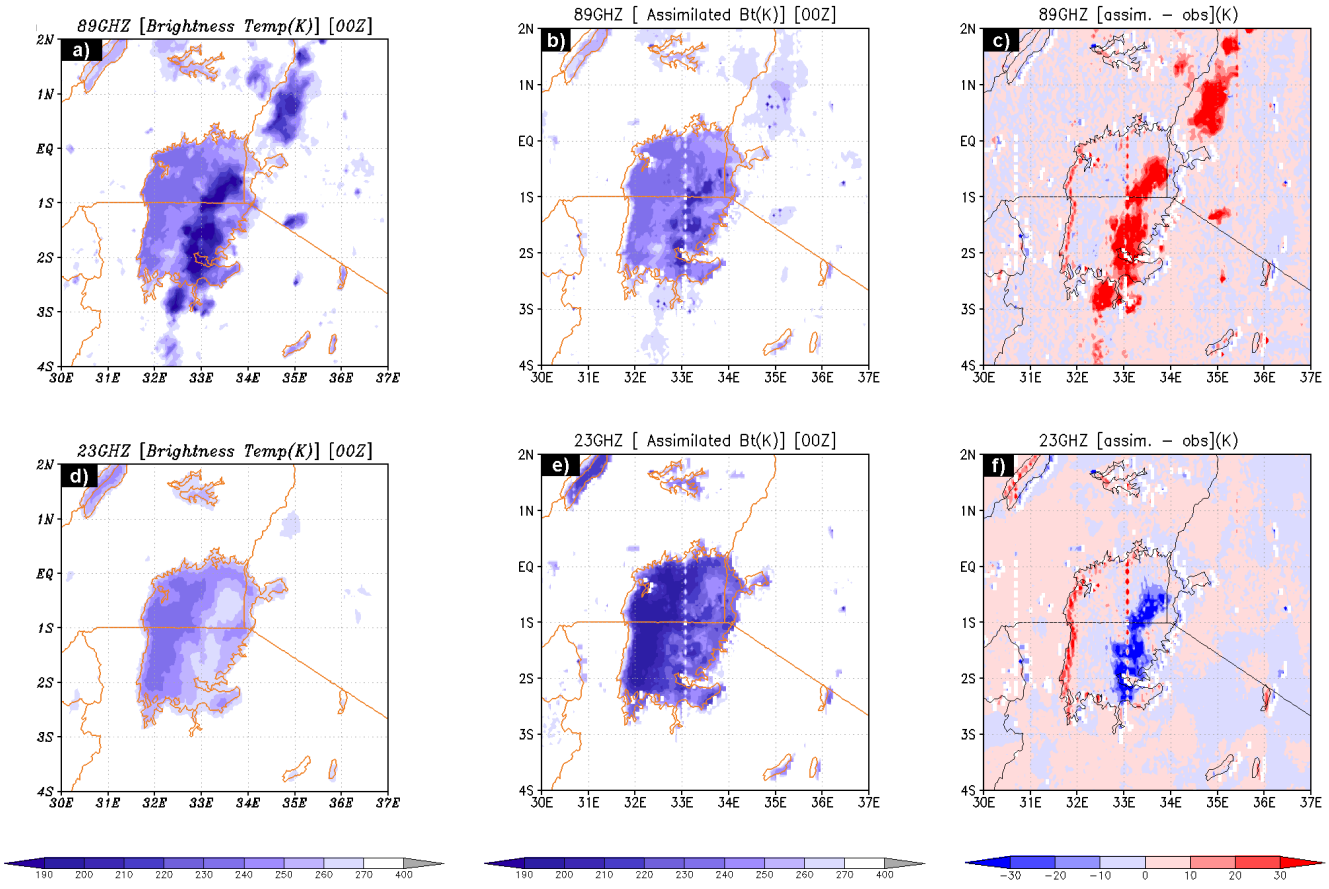

Figure 4.15: Brightness temperature (a) Observed 89GHz, (b) assimilated 89GHz, (c) 89GHz assimilated-obs difference, (d) Observed 23GHz, (e) assimilated 23GHz, (f) 23GHz assimilated-obs difference

To investigate the value added by assimilation, the performance of CALDAS and ARPS run was validated against TRMM rainfall and observed cloud top temperature. Figure 4.16 shows the simulated pattern of cloud top temperature as compared to observed IR.

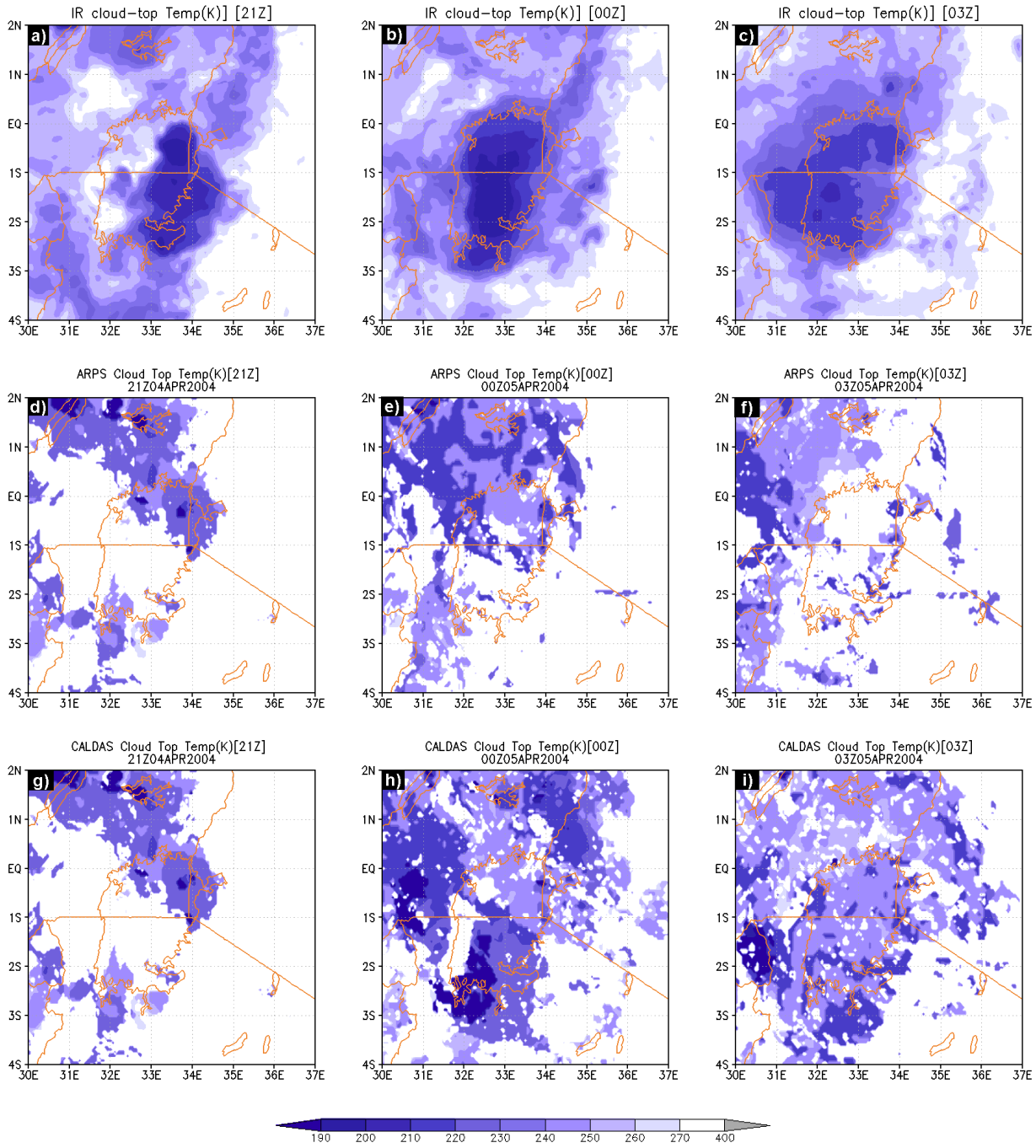

Figure 4.16: Comparison of simulated against observed cloud top temperature (a) 21UTC IR, (b) 00UTC IR(5^{th} April), (c) 03UTC IR, (d) 21UTC ARPS, (e) 00UTC ARPS, (f) 03UTC ARPS, (g) 21UTC CALDAS, (h) 00UTC CALDAS, (i) 03UTC CALDAS

After assimilation at 23:10 UTC, the performance of CALDAS improves considerably and this is demonstrated by the simulation of cloud top temperature very similar to observations ($R^2 = 0.3$). In particular the lined up pattern is introduced into the system and also an intensification of clouds over the lake. However, the simulated cloud is rather spotty and inhomogeneous compared to observations. Three hours after assimilation the cloud system is still present over the lake and though weaker than observations, it is far much better than the ARPS run. This shows that assimilation of AMSR-E improves the simulation of cloud water.

4.3.5.1 Representation of rainfall

The ARPS downscaling experiment is able to reproduce this extreme event to some degree of accuracy. The TRMM observations recorded rainfall over the lake at 00UTC (5^{th} April) and this event continued for about six hours. During this time, the ARPS run is not able to produce this pattern well and is characterized by excess rainfall NW of the domain. However, at 03UTC on 5^{th}, the system is able to reproduce some rainfall though the regions of maxima are further north compared to TRMM. In addition, the semi-autonomous event at around (35E, 1N) is absent.

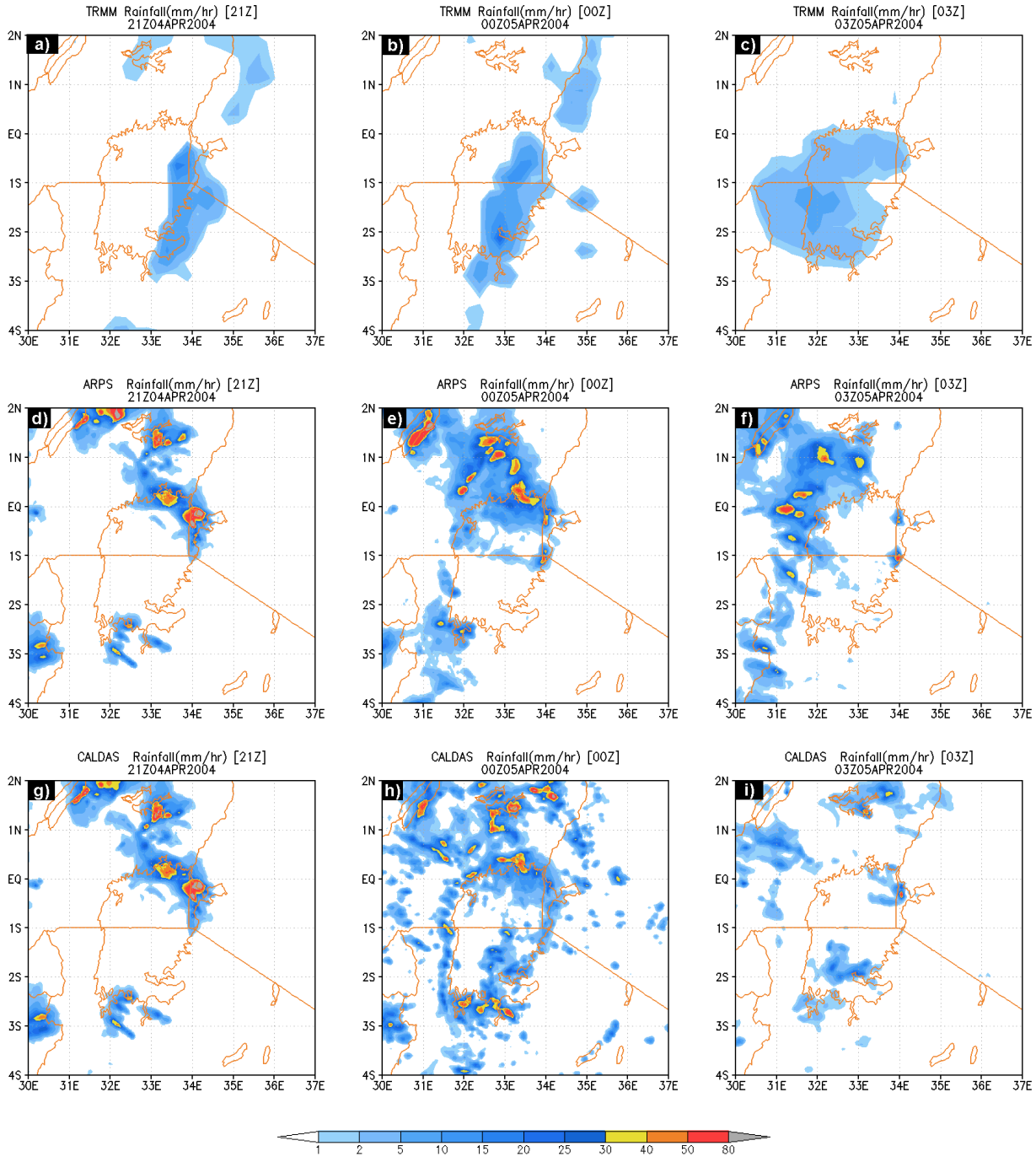

Figure 4.17: Comparison of 3-hourly simulated against observed rainfall (a)21UTC TRMM, (b) 00UTC TRMM(5^{th} April), (c) 03UTC TRMM, (d) 21UTC ARPS, (e) 00UTC ARPS, (f) 03UTC ARPS, (g) 21UTC CALDAS,(h) 00UTC CALDAS, (i)03UTC CALDAS

.

With improvement in cloud activity simulation, the CALDAS prediction of this rainfall event shows better performance compared to the ARPS experiment (Figure 4.17). The CALDAS run produces slightly improved results after the assimilation of AMSR-E data at 23:10 UTC on 4^{th} April. In particular, the performance is considerably improved at 00UTC on 5^{th}. This run was able to introduce the semi-autonomous event at around (35E, 1N). In addition, the lined up pattern in the TRMM observation is reproduced weakly in this run. The model is not able to sustain this event and at 03UTC, we only see some "over the lake" Erainfall with the overestimation NW of the domain seen in the ARPS run reduced. The regions of maxima in this run match closely that of TRMM but characterized by overestimation at 00UTC and almost no rainfall at 03UTC.

The peak of the event at 03UTC on 5^{th} was not well simulated by both experiments. Despite the improvement by CALDAS, the NWP was not able to sustain the induced model state for long. Investigations revealed that the assimilated water vapor dried up immediately after assimilation. Figure 4.18 shows the integrated water vapor for the ARPS and CALDAS experiments. The spatial distribution of IWV in the CALDAS shows some strange pattern with higher amounts of water vapor assimilated over the land-lake boundary as well as reduction of water vapor in the North-East and South-West parts of the domain. This leads to dry air mass which when it converges over the lake produces no rainfall. This explains the drier state of the model at 03UTC.

The lake boundary problem is associated with mixed pixels (land/water) as a result of the coarse resolution of AMSR-E footprint and at the moment a solution has not been formulated.

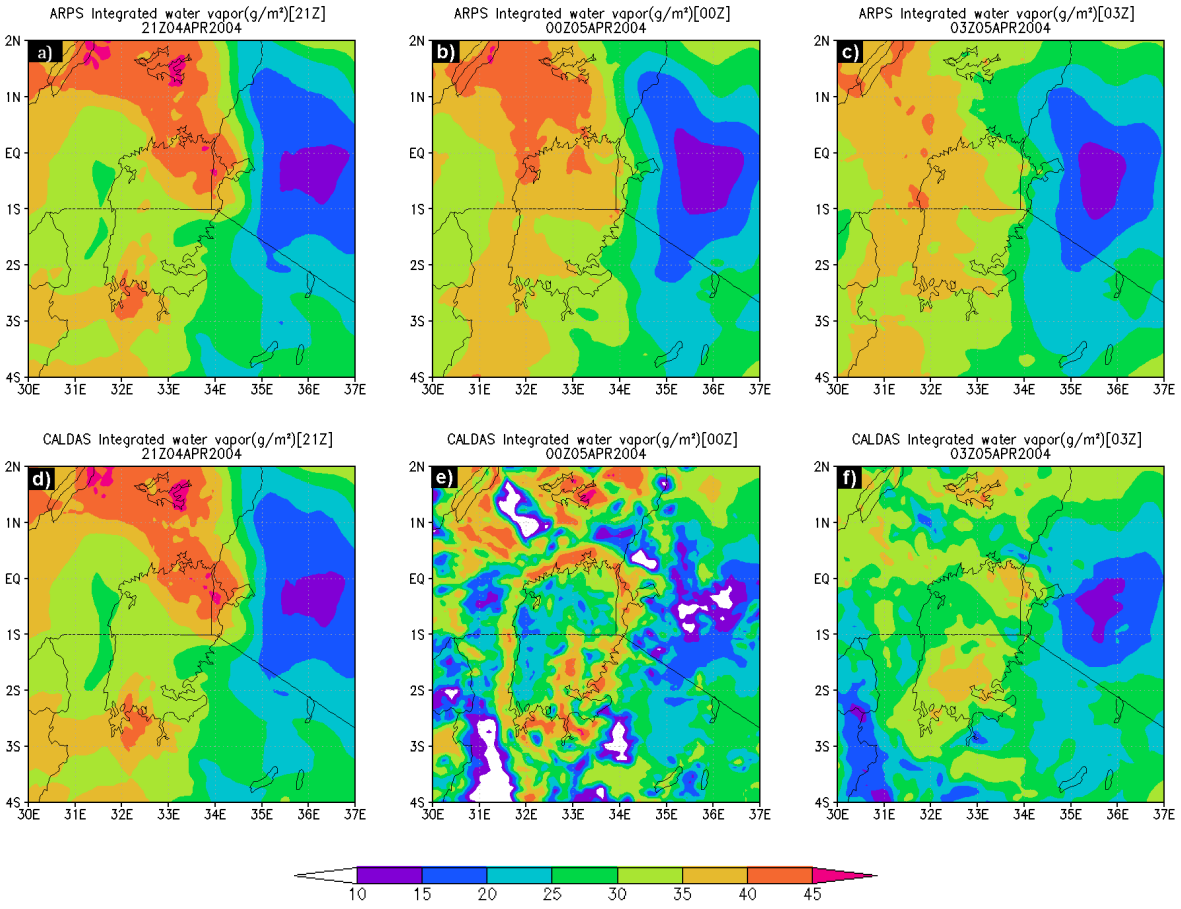

Figure 4.18: Comparison of integrated water vapor (a) 21UTC ARPS,(b) 00UTC ARPS,(c) 03UTC ARPS, (d) 21UTC CALDAS, (e) 00UTC CALDAS, (f) 03UTC CALDAS

4.4 Water vapor assimilation: CMDAS and RTM sensitivity experiments

Since LVB lacks high resolution soil moisture data, we assume that assimilation of soil moisture is correct and focus only on the atmosphere component. In addition, we choose to apply these experiments for an extreme event in which surface fluxes may not play a very important role in atmospheric modulation. Our experiments mainly focus on CMDAS *(set #1, 2)* assimilation and the radiative transfer model *(set #3)* used in CALDAS. These focused

on the significance and the approaches to assimilation of water vapor and the relevance of rain water as well as the sensitivity of the RTM to variations in surface temperature and soil moisture. The experiments were designed to identify the reason why the induced model state was not being kept for long. This involved testing the relevance of the assimilation of all CALDAS hydrometers and the general approach to the assimilation of cloud water and water vapor. By default, water vapor assimilation uses a factor approach between the model and SCE-UA IWV so as to retain the model state integrity and stability. Rainwater, cloud water and snow water are also assimilated in CALDAS default settings. The impact of each of these was investigated and Table 4.4 summarize these experiments.

Table 4.4: Set 1 : Water Vapor saturation and bogus assimilation experiments.

Experiment	**Settings**
CALDAS	The default run; rain water, cloud water, snowater and water vapor variables are assimilated
QVSAT	Water vapor was not assimilated, rather saturated whenever a cloud is found in the NWP
BOGUS	Wind modification on the lower and upper model levels to enhance convection

4.4.1 Water vapor saturation experiment (QVSAT)

The QVSAT experiment hypothesizes that to ensure consistency in energy and model state, integrated water vapor should not be assimilated through the shuffled evolution complex used in CMDAS. Instead, the vertical profile of the grid should be saturated whenever a cloud is found. This was achieved by setting a threshold of 1.2 kgm^{-2} in integrated cloud condensate, then saturating model water vapor profile between the cloud top and cloud bottom whenever this threshold is exceeded. This would ensure model state integrity and conservation of energy. It is hypothesized that introducing high relative humidity might

help induce condensation processes which in turn would produce latent heat release (adding buoyancy) in addition to the creation of cloud and rain water.

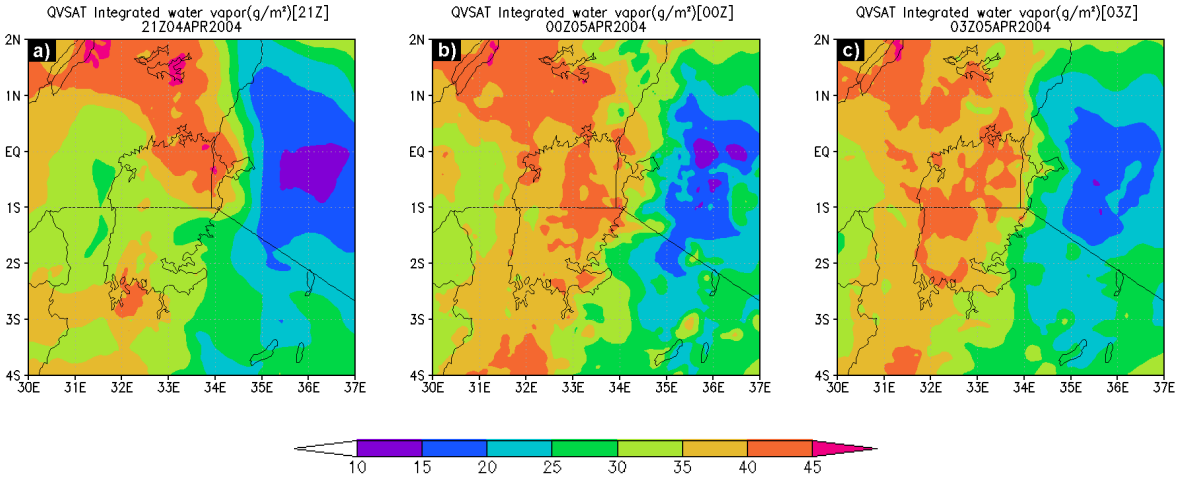

Figure 4.19: Integrated water vapor for QVSAT (a) 21UTC, (b) 00UTC, (c) 03UTC

Figure 4.19 shows the integrated water vapor for the QVSAT experiment at 21UTC, 00UTC and 03UTC. The drying up evidenced in the CALDAS run has disappeared and the model water vapor seems uniform and heterogeneous. Over the lake AMSR-E observed a dense cloud pattern (figure 4.15)and this is reflected by the high amounts of water vapor around (33E,1S). However, the regions NW of the lake has more moisture assimilated compared to the ARPS experiment while there is no discernible change NE of the domain.

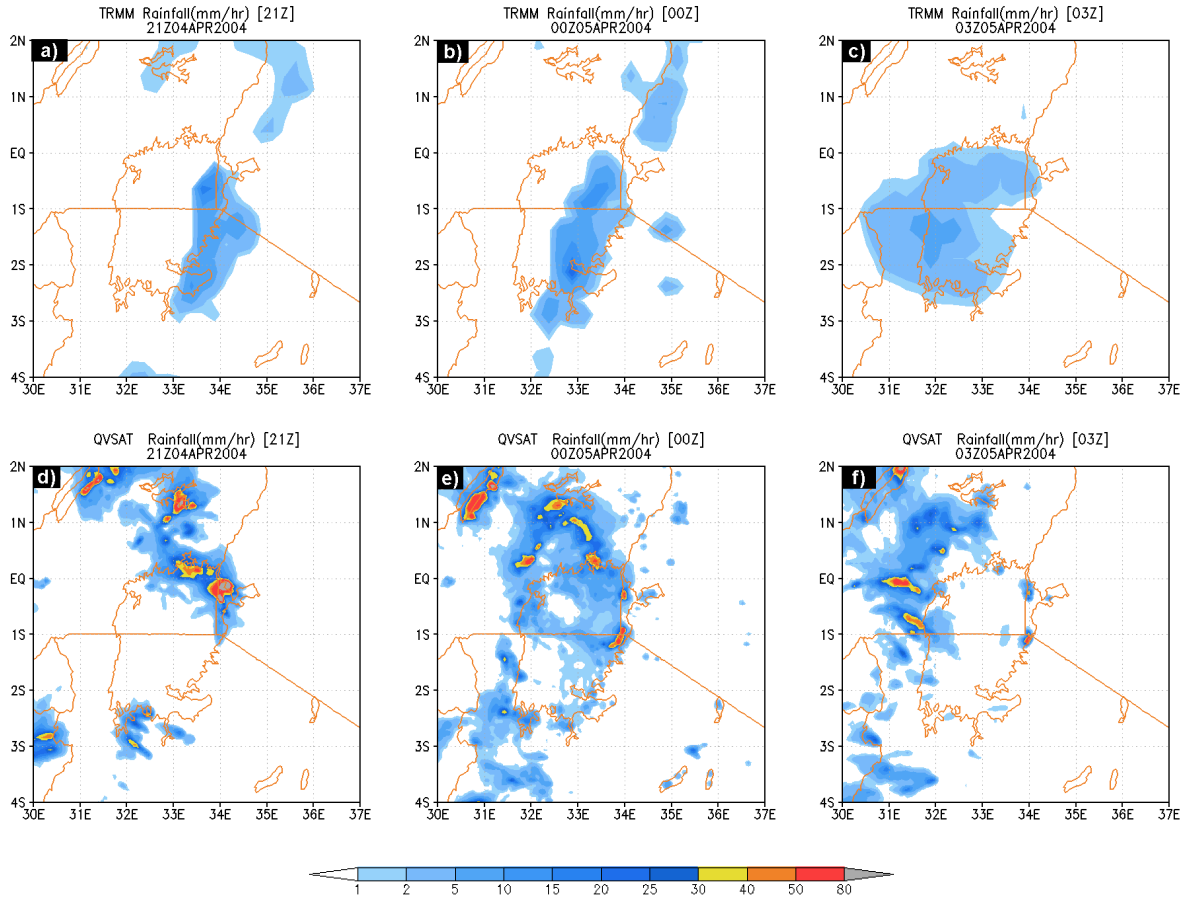

Figure 4.20: Comparison of 3-hourly simulated against observed rainfall (a) 21UTC TRMM, (b) 00UTC TRMM(5^{th} April), (c) 03UTC TRMM, (d) 21UTC QVSAT, (e) 00UTC QVSAT, (f) 03UTC QVSAT

The performance of CALDAS improves considerably with the QVSAT experiment. Rainfall at 00UTC is more homogenous and well spread over the lake. The experiment produces the lined up pattern as observed in TRMM but also characterized by overestimation NW of the domain in a similar pattern to the ARPS experiment (figure 4.17). The experiment is however missing the semi-autonomous event NE of the lake. This implies that there is not much improvement over land. The moisture provided through saturation is able to feed into the clouds leading to the rainfall increase over the lake. However, at 03UTC the simulated rainfall over the lake does not occur and the overestimation present at 00UTC is carried over.

4.4.2 Wind modification on the lower and upper model levels (BOGUS)

The use of "bogus wind" in NWP is not a new concept. The study and prediction of cyclones and hurricanes have benefited widely by the use of wind and pressure modification to estimate the path and intensity (e.g (Xiao et al., 2000; Kleist, 2011; Wang et al., 2011; Barker et al., 2012)). This involves modifying wind pattern and pressure at the eye of the storm based on observed patterns, radius and intensity by use of weather satellites. Since this has been quite successful in many studies, the applicability of a roughly same idea of non-cyclones have not been tested. This experiment sought to test the hypothesis that; by modifying and strengthening weak convergence induced by CMDAS, better rainfall forecasts can be obtained.

The same setup was applied as previous experiments and since the lined up cloud pattern had been identified by TRMM and AMSR-E, modification was done in roughly 1 degree offset. Weak surface convergence had been identified in the CALDAS run and the lower surface level wind was multiplied by a factor of 1.5 as well the upper level. This modification was only done at the assimilation time for one time step and the NWP model left to evolve. This would strengthen the convergence and enhance convective activity.

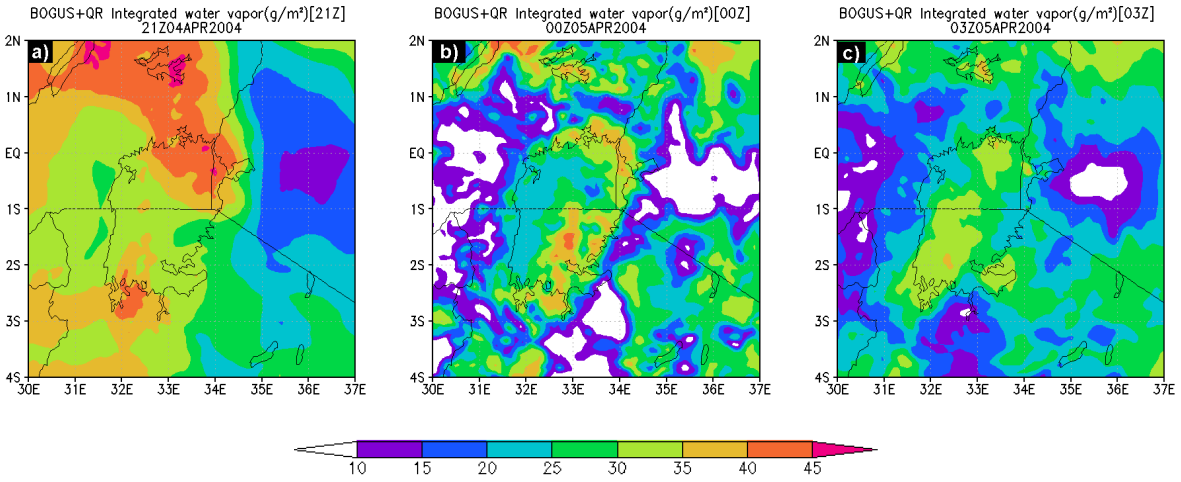

Figure 4.21: Integrated water vapor for BOGUS experiment (a) 21UTC, (b) 00UTC, (c) 03UTC

Figure 4.21 shows the integrated water vapor for the BOGUS experiment. It is clear that modification of surface wind does not solve the problem of water vapor assimilation. In fact, the integrated water vapor reduces greatly as compared to the default CALDAS experiment. This is because accelerating surface convergence and hence the induced convection activity increases the conversion of water vapor to cloud water and rainfall. This is followed by an influx of dry air which soon extinguishes the convective activity. This is confirmed by the almost no rainfall simulation at 03UTC. Nevertheless, the BOGUS experiment produces slightly better results (figure 4.22) compared to the other experiments at 00UTC. The model simulates rainfall over the lake as well as the semi-autonomous event NE of the domain. The regions of maxima over the lake match that of TRMM though with overestimation. A very clear band of rainfall is simulated which closely follows TRMM pattern. In addition, the lake-boundary simulated rainfall is absent in this run. This implies that the strengthening of the induced convective activity through wind enhanced precipitation. However, similar to the CALDAS experiment, the model state could not be kept for long and the model performs poorly at 03UTC and this is caused by the drying up of the water vapor as previously shown in the CALDAS experiment.

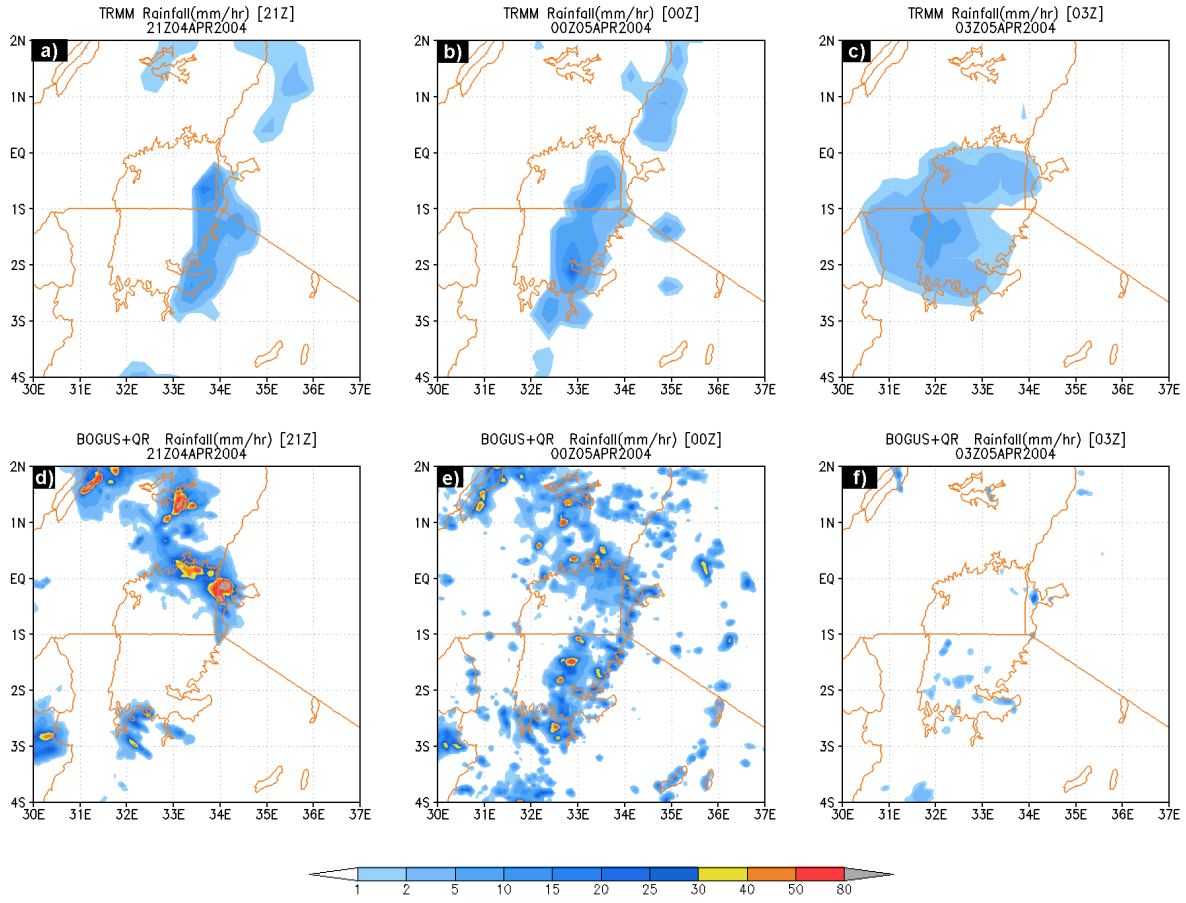

Figure 4.22: Comparison of 3-hourly simulated against observed rainfall (a) 21UTC TRMM, (b) 00UTC TRMM (5^{th} April), (c) 03UTC TRMM, (d) 21UTC BOGUS, (e) 00UTC BOGUS, (f) 03UTC BOGUS

These first set of experiments (Table 4.4) focused on the contribution of water vapor saturation or the strengthening of induced convection by assimilation to a better forecast. Experiments QVSAT and BOGUS demonstrated that, the reason for the water vapor disappearance was not related to surface convergence or saturation, other factors were in play. We hypothesized that; the assimilation of rain water might be the hindrance to cloud generation and sustenance. The assimilation of the raindrop does not involve the change of matter state through conversion from water vapor to cloud water and there is no release of energy. In addition the contribution of rain water in the radiative transfer equation through the emis-

sion or scattering is minimal. So, assimilation of rain water may not be needed. To test this hypothesis, we set up three more experiments without rain water assimilation. This is as given in Table 4.5.

Table 4.5: Set 2 : Without rain water assimilation experiments.

Experiment	**Settings**
QVSAT-QR	Assimilation with saturation of water vapor
BOGUS-QR	Assimilation with introduction of bogus wind modification
NOSAT-QR	Assimilation without saturation of water vapor

4.4.3 Water vapor saturation without rain water (QVSAT-QR)

With a slight improvement in prediction of precipitation by saturation of water vapor, this experiment (QVSAT-QR) sought to investigate the effects of rain water. Rain water assimilation was switched off but saturation of water vapor retained. Limits for cloud water were as set same as the CALDAS experiment using the shuffled evolution complex. Figure 4.23 shows the simulated rainfall for this experiment. There is a remarkable improvement compared to the previous experiments. Rainfall is simulated at 00UTC and the system is maintained till 03UTC when rainfall over the lake is simulated in a pattern that closely resembles TRMM.

This implies that the assimilation rain water in this case is not beneficial. By assimilating rain water we are simply adding rain, which falls down almost immediately. Since there is no conversion of form by condensation, it means that little or no energy is released. The convective system introduced by the cloud water to rainwater conversion is subdued and the system shortly collapses. The risk of adding rainwater is that the vertical velocities initialized at the location where rainwater is added will not support the rainfall; hence the model may create a downdraft (due to the weight of the rainwater) in an area where positive vertical velocity likely exists.

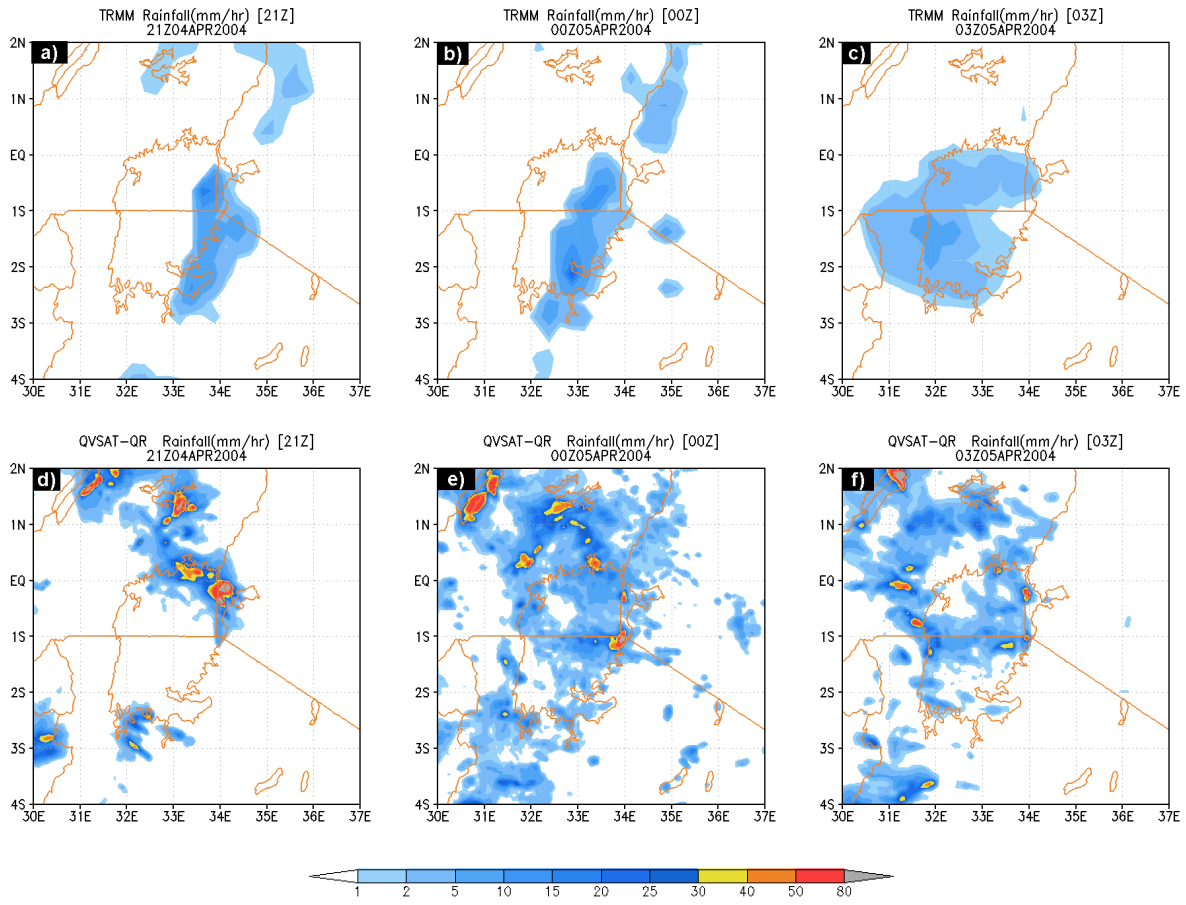

Figure 4.23: Comparison of 3-hourly simulated against observed rainfall (a) 21UTC TRMM,(b) 00UTC TRMM(5^{th} April), (c) 03UTC TRMM, (d) 21UTC QVSAT-QR,(e) 00UTC QVSAT-QR, (f) 03UTC QVSAT-QR

4.4.4 Bogus Wind without water vapor saturation (BOGUS-QR)

The same setup was applied as the previous BOGUS experiment only this time without rain water assimilation.

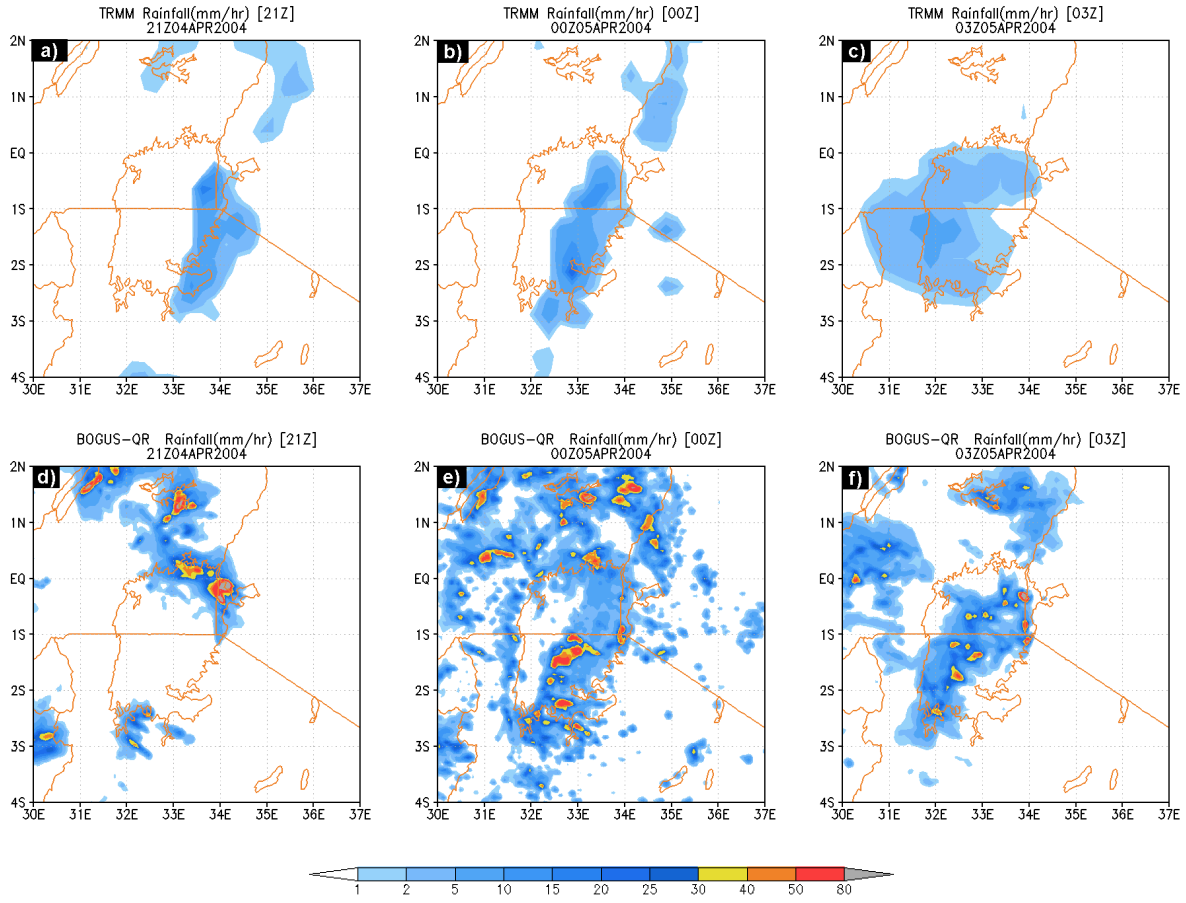

Figure 4.24: Comparison of 3-hourly simulated against observed rainfall (a) 21UTC TRMM, (b) 00UTC TRMM (5^{th} April), (c) 03UTC TRMM, (d) 21UTC BOGUS-QR, (e) 00UTC BOGUS-QR, (f) 03UTC BOGUS-QR

The BOGUS experiment produces slightly better results (figure 4.24) compared to the other experiments. At 00UTC, the model simulates rainfall over the lake as well as the semi-autonomous event NE of the domain. The region of maxima over the lake matches that of TRMM though with overestimation. The prediction improves the forecast for 03UTC with the rainfall system being maintained over that period. The simulated rainfall closely matches TRMM at this time and this presents a major improvement. The strengthening of surface convergence enhances convection over the domain. However, overestimation evidenced in other experiments is still present and this is tied to water vapor assimilation.

4.4.5 Without rain water and water vapor saturation (NOSAT-QR)

Since the BOGUS-QR had produced remarkable results, this experiment checked the significance of using BOGUS wind. In this experiment, both water vapor saturation and rain water assimilation were switched off and there is no modification of wind. Figure 4.25 shows the comparison of TRMM and the simulated rainfall. There is a remarkable improvement in the simulated rainfall for 00UTC and also at 03UTC. The overestimation NW of the domain evident on the other runs has been eliminated. This presents the *"best"* results and was adopted as standard CALDAS run. Statistical and correlation validations are based on this run.

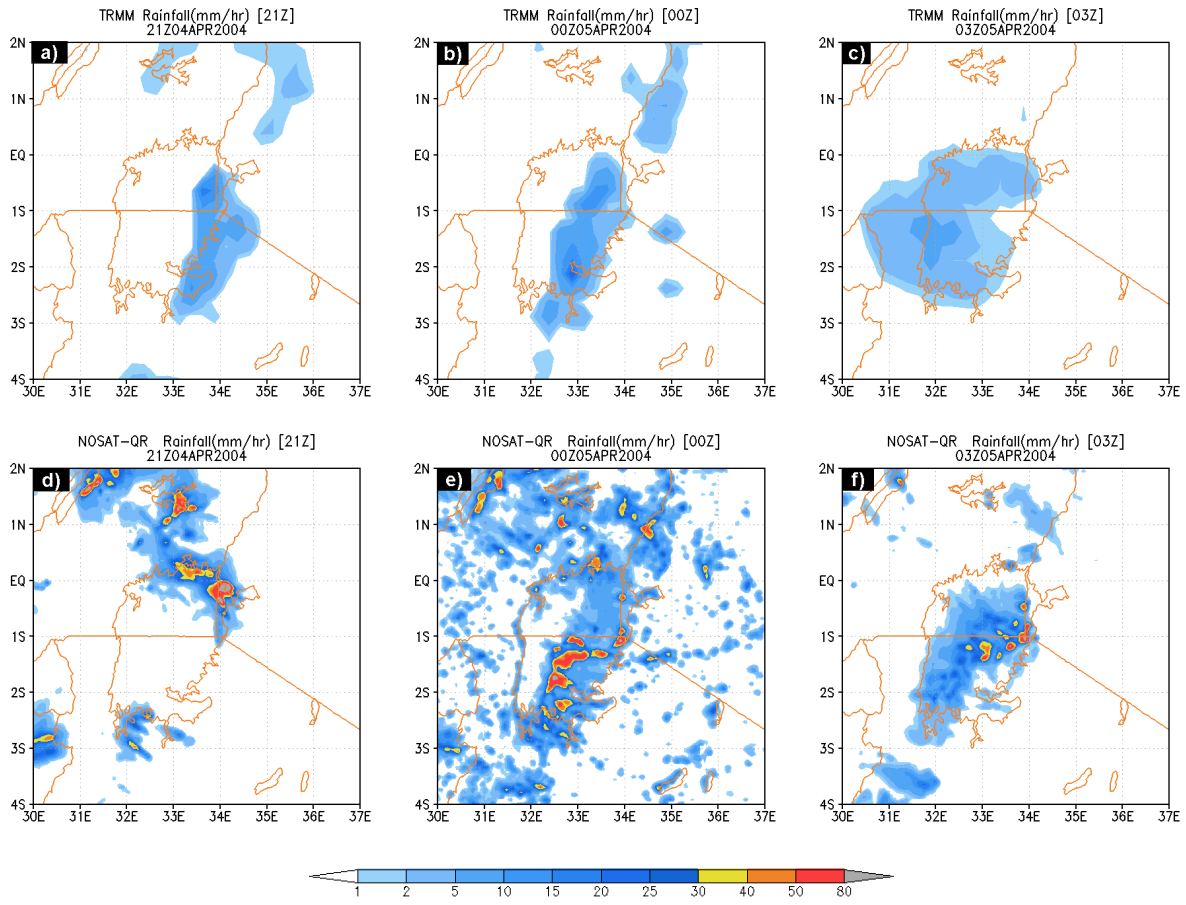

Figure 4.25: Comparison of 3-hourly simulated against observed rainfall (a) 21UTC TRMM,(b) 00UTC TRMM(5^{th} April), (c) 03UTC TRMM, (d) 21UTC NOSAT-QR,(e) 00UTC NOSAT-QR, (f) 03UTC NOSAT-QR

The integrated cloud condensate predicted by the CALDAS assimilation system also showed some good comparisons against the cloud top temperature as a proxy for cloud activity. Figure 4.26 shows that the CALDAS simulation at 03UTC was able to recreate the dense cloud and rainfall over Lake Victoria. However, though the intensity is similar to the observed, the overall pattern over the whole domain was rather different. The spatial correlation of 0.3 was reasonable. Additionally, the intensity of the simulated rainfall was more than 50% compared to TRMM. However, accurate comparisons cannot be made since TRMM is based on satellite observations and 100% coverage is not guaranteed. TRMM's

inadequacies have also been identified (e.g. Tsujimoto and Koike (2011)) and these results were considered reasonable.

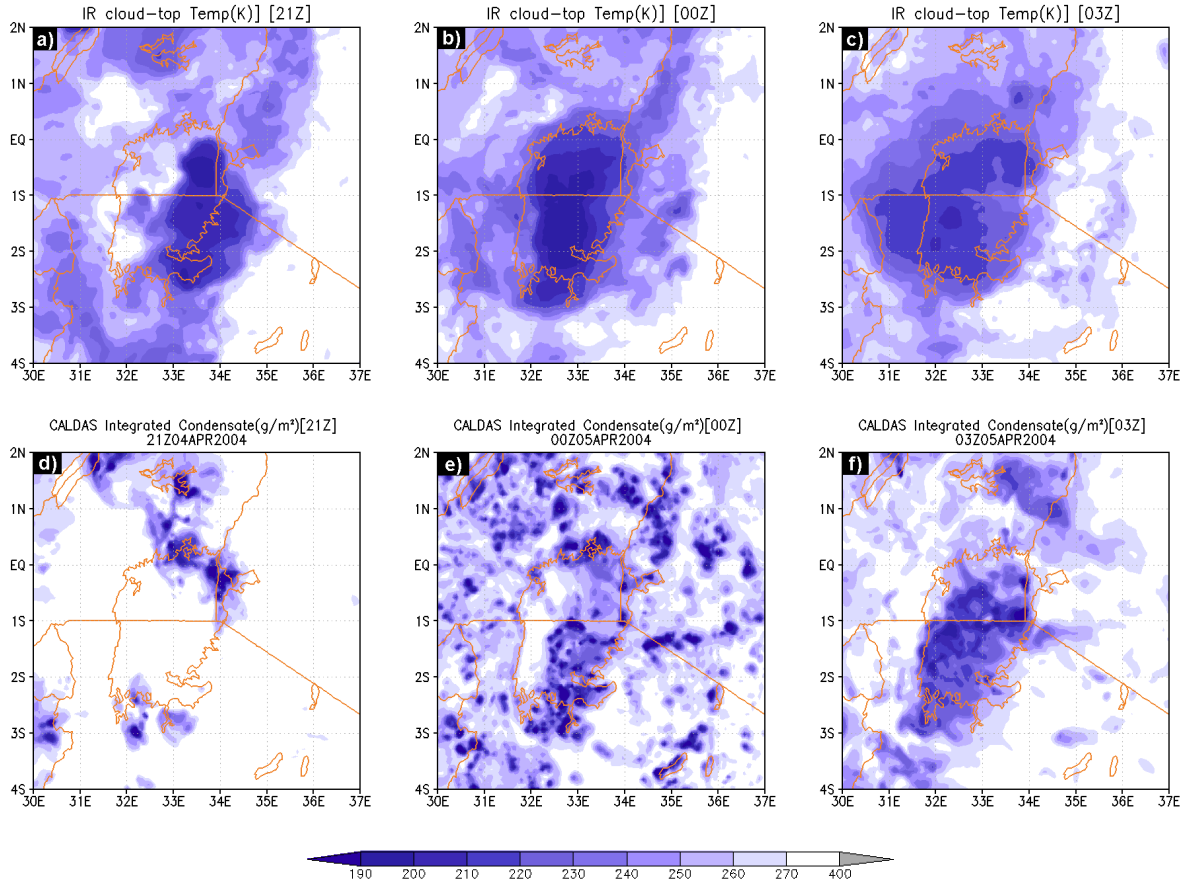

Figure 4.26: Comparison of simulated against observed cloud top temperature(a) 21UTC IR,(b) 00UTC IR(5^{th} April), (c) 03UTC IR, (d) 21UTC CALDAS(*best*),(e) 00UTC CALDAS, (f) 03UTC CALDAS

4.5 Accuracy assessment

Figure 4.27 shows the spatial correlation between TRMM and model simulated 3-hour precipitation starting at 21UTC to midday the following day. This period marks the duration of the extreme event recorded over the LVB. The summary shows that the poorest experiment compared to TRMM is ARPS with a very weak correlation of less than R^2=0. 1 and at times

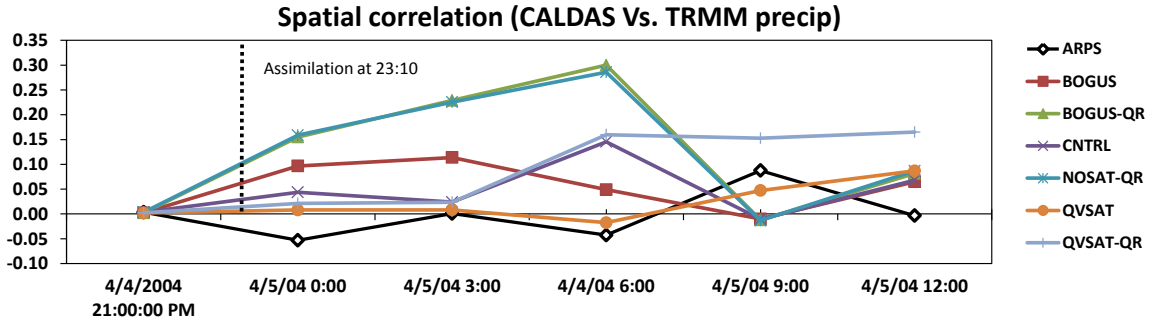

Figure 4.27: Temporal evolution of simulated precipitation Vs. TRMM from 21UTC on 4^{th} April, 2004.

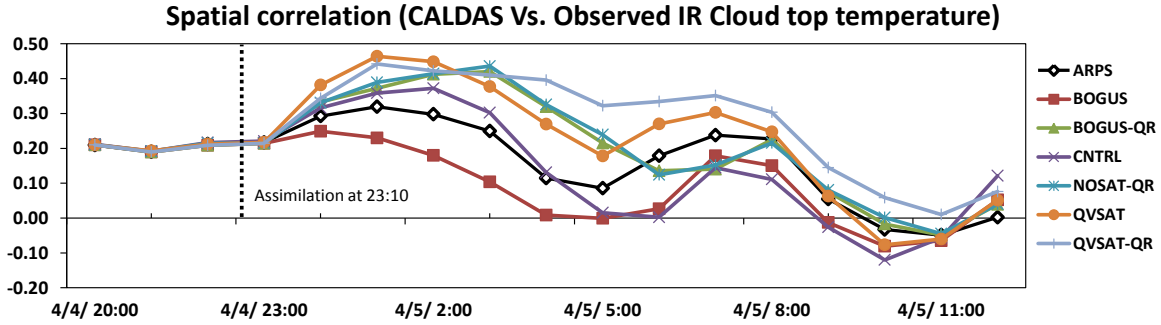

Figure 4.28: Temporal evolution of simulated Vs. observed Cloud-top temperature from 20UTC on 4^{th} April, 2004.

negative correlation. The BOGUS, BOGUS-QR and NOSAT-QR perform better after assimilation. The correlation coefficient for these experiments is greater than R^2=0. 2 especially when QR is not assimilated. This shows that the removal of rainwater assimilation leads to a better forecast. The CALDAS experiment is not any better, the correlation coefficient stays below R^2=0. 2. Inspecting the RMSE for these experiments we see that the BOGUS experiment has the lowest RMSE followed by CALDAS at 03UTC. The experiments with better spatial correlation also tend to have a higher RMSE. This means that even though the pattern is slightly improved, the quantitative forecast is overestimated.

Since precipitation validation in this experiment was limited to TRMM for rainfall, this study also evaluated the simulated cloud pattern against observed cloud top temperature pattern by the globally merged Infra-Red (IR) hourly product. IR cloud top temperature can be used to identify the spatial distribution of clouds with regions of dense clouds having lower cloud top temperatures. We compared the pattern as well as the coefficient of correlation. Figure 4.28 shows the temporal evolution of simulated cloud-top temperature compared to the observed IR for these experiments. The ARPS, CALDAS and BOGUS experiments show the lowest correlation. Since there is no assimilation in the ARPS experiment, the spatial pattern is never close to observation. The case for the BOGUS is slightly different, accelerating convection by strengthening surface convergence and upper level divergence there is consumption of water vapor and cloud-water is quickly converted to rainwater in the convection process. This hinders the cloud development which can only be sustained by a constant supply of water vapor.

The saturation experiments i.e (QVSAT and QVSAT-QR) produce the best of cloud patterns and this is sustained above R^2=0. 3 for more than 12 hours. This means that the saturation of water vapor in the cloud column enhances the cloud activity and this induced system is kept for a longer time compared to other experiments. The NOSAT-QR simulation performs well too but deteriorates after about 6 hours where the pattern correlation falls below R^2=0. 2. Figure 4.29 shows the scatter diagrams for 21UTC, 00UTC and 03UTC for the CALDAS(*"best"*)experiment. Compared to Figure 4.8, the prediction improves though quantitatively overestimated. This is shown by clustering along the prediction axis.

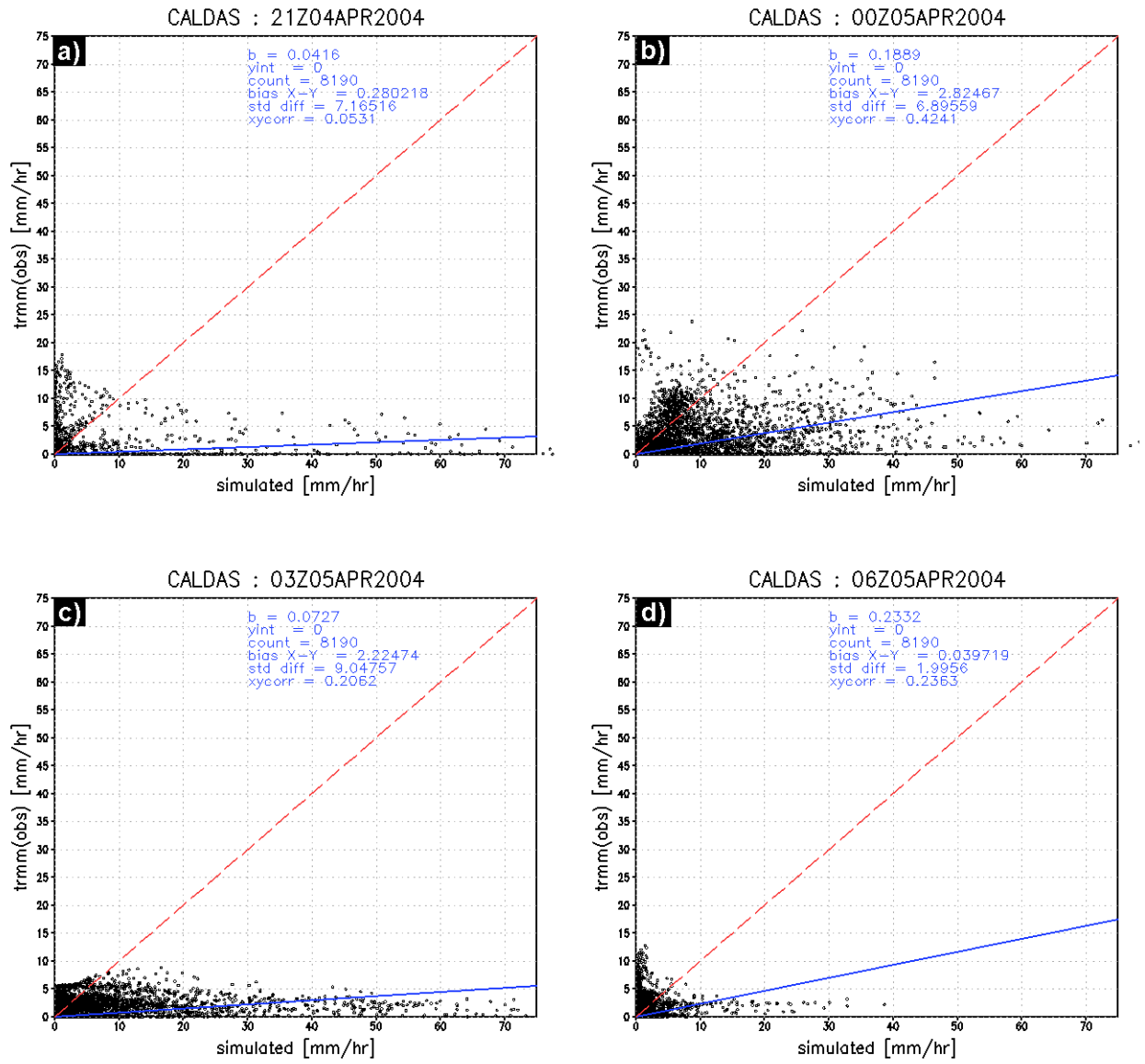

Figure 4.29: Scatter plots for the CALDAS experiment (a) 21UTC, (b) 00UTC, (c) 03UTC (5^{th} April) and (d) 06UTC.

Figure 4.30 shows the probability of detection (POD), false alarm ratio and accuracy of the prediction. The POD increases to about 0.5 after the assimilation and this is far much better than the ARPS experiment where POD stays below 0.2 for the whole of the simulation time. This improvement is noted for all the thresholds meaning prediction improves for all

rainfall amounts. ACC improves for all thresholds to an average of about 0.9 compared to ARPS 0.7. This implies that the rate of all well-predicted locations with respect to the thresholds improves after assimilation.

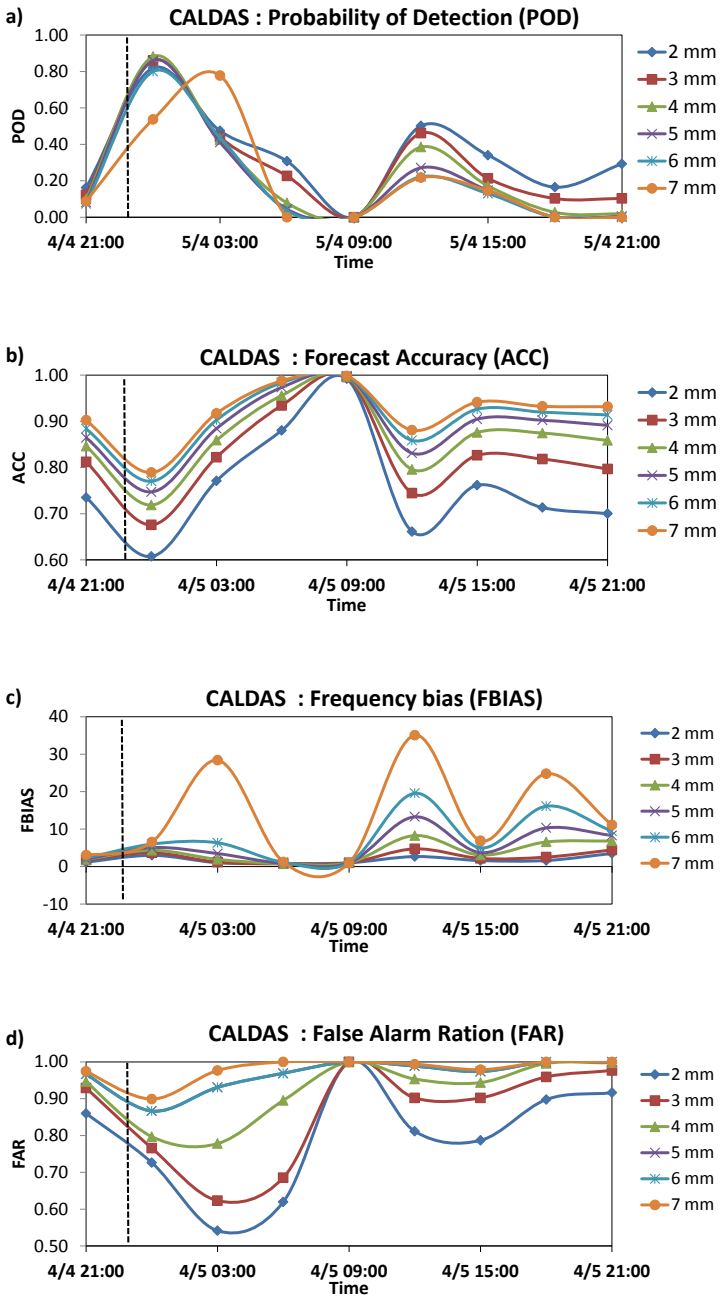

Figure 4.30: Scores computed based on the contingency table for the simulation. Each 3-hour accumulation is presented by one value; a) POD b) ACC, c) FBIAS and c) FAR.

4.6 Radiative transfer model sensitivity experiments

Kuria (2007) performed sensitivity experiments on the radiative transfer model with respect to different soil moisture conditions. They concluded that for the moist case soil moisture, under-prediction gives high brightness temperature (TB) values, while over-prediction lowers TB values. For the moderate moist case, sensitivity reduces with increase in frequency. For low moisture condition, at 36 GHz the difference in vertical polarization shows a large impact of moisture overestimation. We extended the sensitivity experiments not only on soil moisture but also surface temperature which is used in the computation of surface emission. Table (4.6) summarizes these experiments.

Table 4.6: Set 3: Surface temperature/RTM sensitivity experiments.

Experiment	**Settings**
CALDAS-2K	2K subtracted from surface temperature
CALDAS-7K	7K subtracted from surface temperature
CALDAS-10K	10K subtracted from surface temperature

4.6.1 Sensitivity to Surface Temperature

The four stream fast model used in CALDAS computes the contribution of water vapor and cloud-water to emission and scattering. By considering the surface emission as the lower boundary condition and top of the atmosphere brightness temperature the algorithm is able to deduce the amount of water vapor and cloud water in the atmosphere. Since surface emission is a function of surface temperature and soil moisture, these experiments sought to investigate the significance in water vapor assimilation if there are errors in the surface estimation. This was motivated by the recurrent "drying up" witnessed in all previous runs except the "water vapor" experiments.

The CALDAS experiment without saturation and without rainwater produced the best

forecast at least for six hours. However, the initial problem of water vapor drying up was not eliminated completely by switching off rainwater. This was manifested when comparing the assimilated and observed brightness temperature at 23GHZ. It was found out that the RTM has a tendency to assimilate higher brightness temperature for 23GHZ channel which is sensitive to water vapor (figure 4.31). The assimilated brightness temperature NW and SE of the domain was overestimated by about 5-15K. Surface temperature and soil water moisture are the key variables for computation of emissivity which is used by the RTM to obtain surface emission.

Since the results from the first set of experiments showed underestimation of water vapor during the assimilation time and assimilation of higher than observed brightness temperatures; we set up the #set 2 experiments by gradually subtracting 2, 7, and 10k from the surface temperature (only at the assimilation time for one time step) on the domain West of 33^oE. We then investigated the impact on assimilated water vapor and the forecasted precipitation.

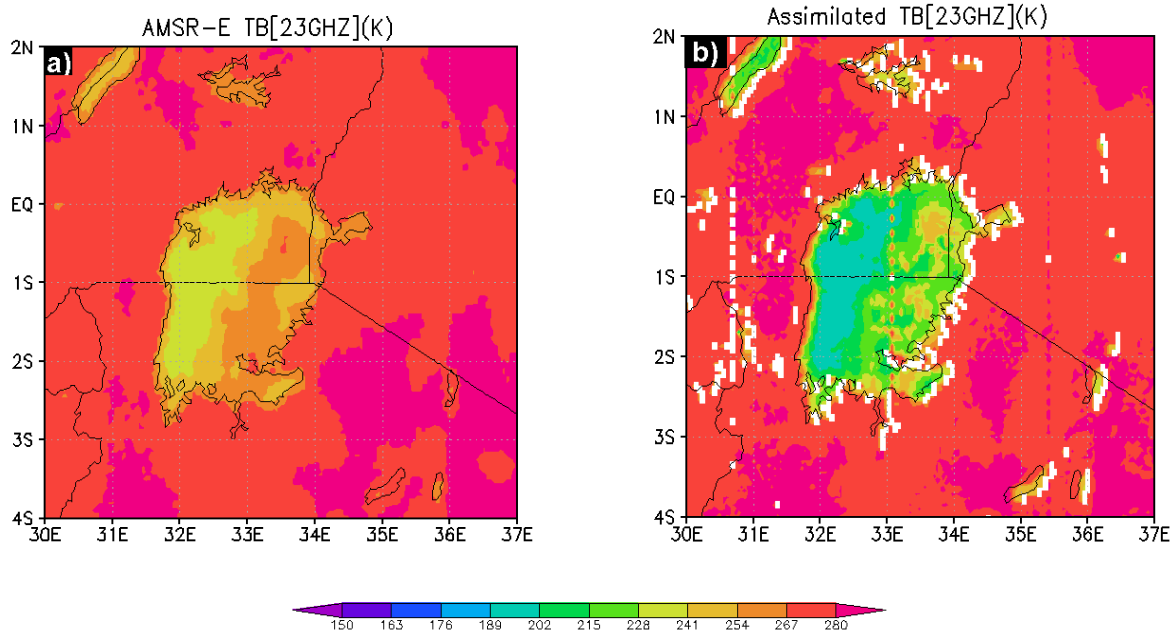

Figure 4.31: 23GHz Brightness temperature (a) Observed (AMSR-E), (b) assimilated.

Figure 4.33 shows the simulated IWV for these experiments as compared to the "best"

run. Specifically, water vapor that dried up in the previous experiments did not occur in the #set 2 experiments. Lower surface temperatures during assimilation meant that lower surface emission was calculated from the surface. Lowering the surface temperature by more than 5K on the western part of the domain led to the assimilation of more water vapor. Higher top of the atmosphere brightness temperature as observed by AMSR-E (TB_{toa}) and lower surface emission (TB_{sfc}) is an indicator that atmospheric emission is dominant and thus associated with abundant water vapor in the atmosphere. As it can be seen from figure 4.33, the parts of the domain that experienced drying up in the previous experiments now have more water vapor coherent with the rest of the domain and this is also reflected in the simulated precipitation (figure 4.32). Subtracting >5K from the surface temperature during assimilation leads to improved precipitation west of the lake.

The microwave RTM used in CALDAS exploits the short window between surface and atmospheric emission. The AMSR-E 23GHz channel is sensitive to water vapor and the difference between atmospheric and the surface emissions is an indicator of water vapor quantity in the atmosphere. This implies that accurate estimation of surface emission is very important. The RTM sensitivity experiments reinforce the fact that for proper assimilation of water vapor, there is a need to estimate surface temperature accurately. On the CALDAS surface forward model, surface temperature at the assimilation time is used to compute surface emission which when compared against satellite observed emissions to give an indication of the amount of water vapor in the atmosphere. CALDAS-2K, CALDAS-7K and CALDAS-10K experiments have demonstrated the need for accurate surface temperature. To be able to get better estimates and ultimately better forecasts, it is important to improve the RTM model to reduce some of the uncertainty associated with model estimation of surface temperature. This study proposes a thorough validation and improvement of the RTM surface emission model through ground-based observations.

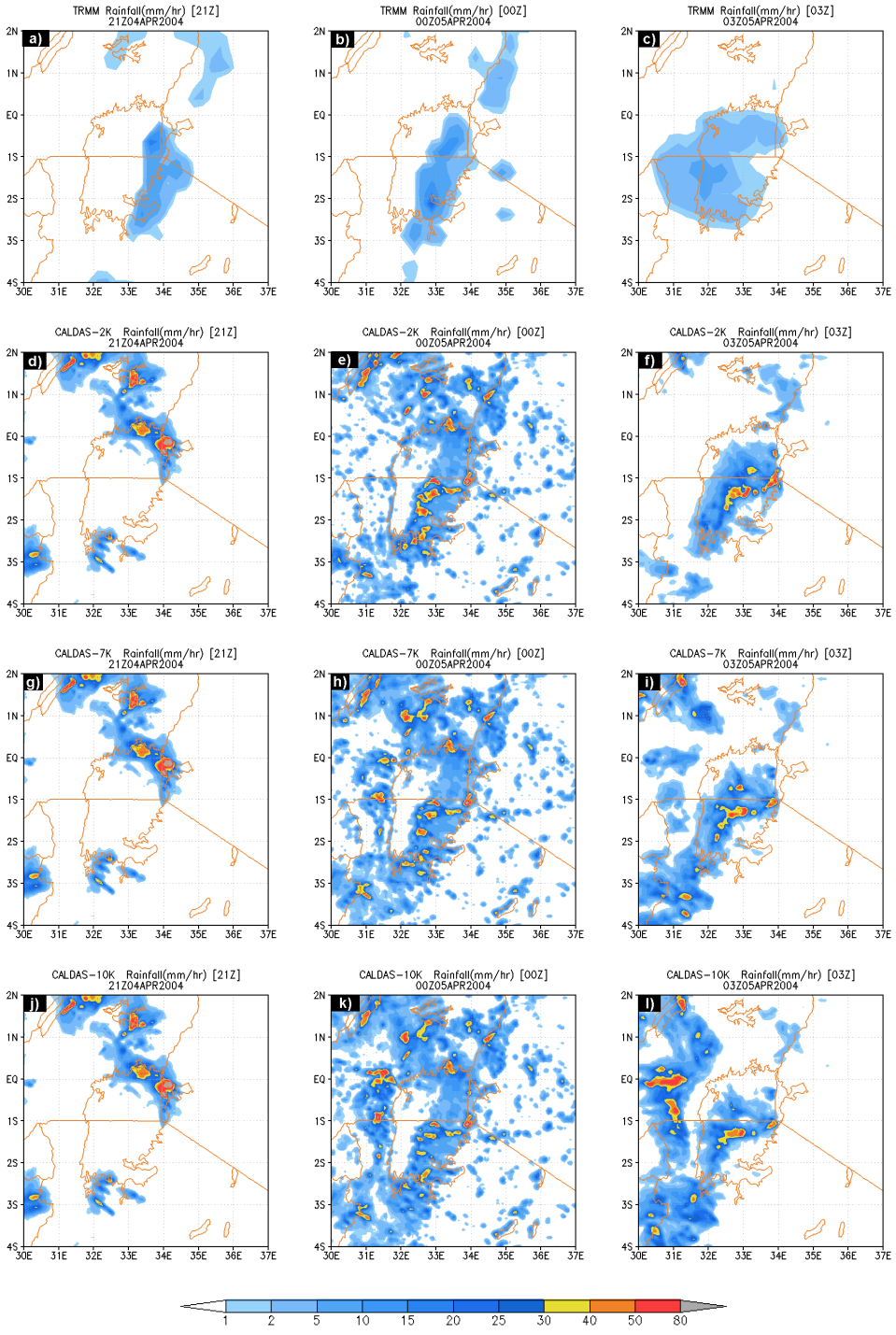

Figure 4.32: Comparison of 3-hourly simulated against observed rainfall (a) 21UTC TRMM,(b) 00UTC TRMM(5^{th} April), (c) 03UTC TRMM, (d) 21UTC -2K, (e) 00UTC -2K, (f) 03UTC -2K, (g) 21UTC -7K, (h) 00UTC -7K, (i) 03UTC -7K, (j) 21UTC -10K, (k) 00UTC -10K, (l) 03UTC -10K,

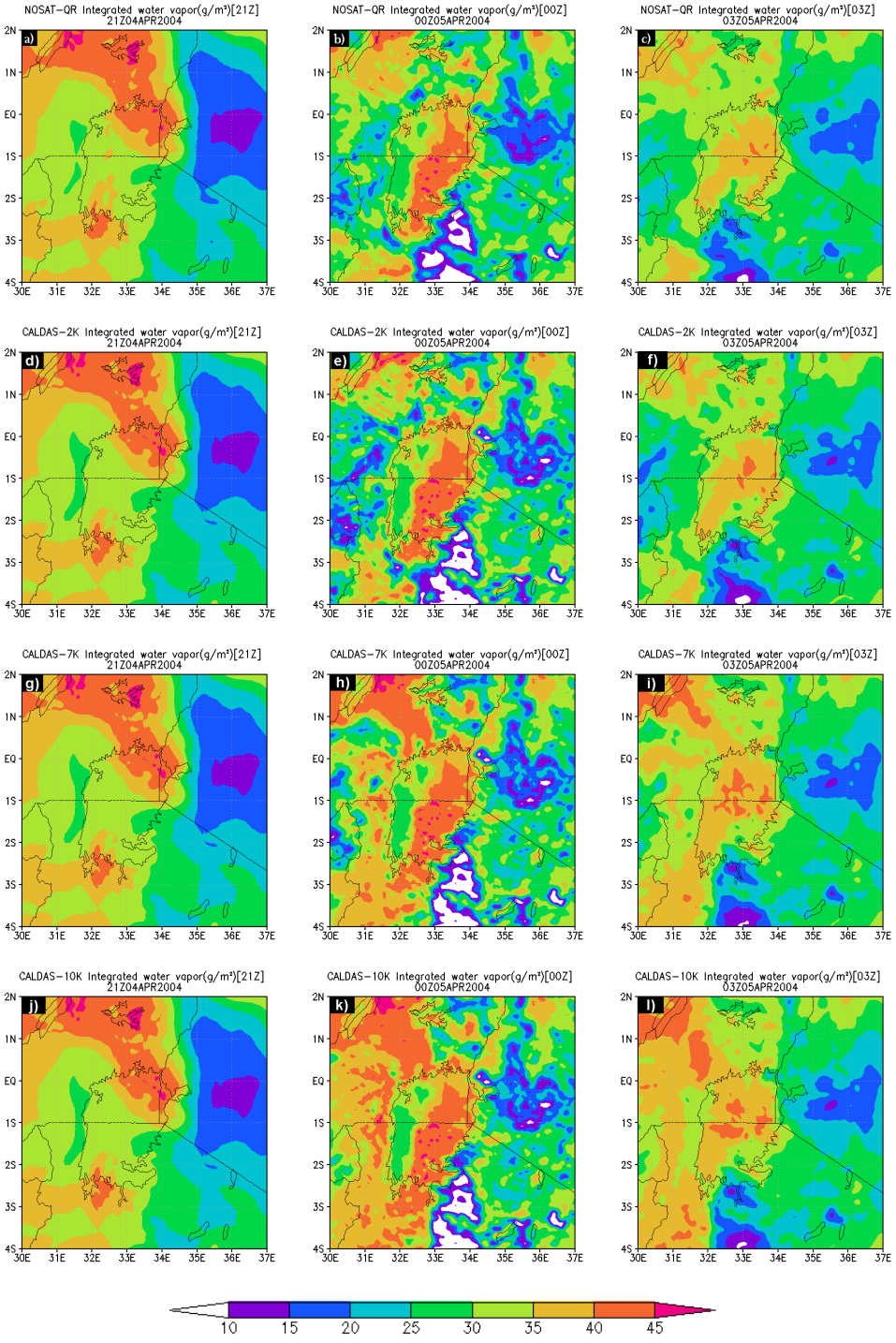

Figure 4.33: Comparison integrated water vapor (a) 21UTC CALDAS(best),(b) 00UTC CALDAS(best)(5^{th} April) CALDAS(best), (c) 03UTC CALDAS(best), (d) 21UTC -2K, (e) 00UTC -2K, (f) 03UTC -2K, (g) 21UTC -7K, (h) 00UTC -7K, (i) 03UTC -7K, (j) 21UTC -10K, (k) 00UTC -10K, (l) 03UTC -10K,

4.6.2 Sensitivity to Soil Moisture

In a similar method to Kuria (2007), we performed six additional water vapor assimilation experiments based on different soil moisture conditions. We introduced additive and subtractive 5%, 10% and 20% to soil moisture and this was only applied at the assimilation time step only. Assimilated water vapor and precipitation at 00UTC and 03UTC was then evaluated for homogeneity and continuity. Evaluation of the assimilated water vapor and predicted precipitation (not shown) showed that regardless of the introduced error to soil moisture, the resulting assimilated water vapor and predicted precipitation was almost the same. There was no remarkable difference in these two variables between the extreme errors in soil moisture. This implies that, unlike Kuria (2007) this experiment shows the insensitivity to soil moisture conditions and the biggest uncertainty / error is associated with estimation of surface emission which is heavily influenced by surface temperature.

4.7 Flood simulation by CALDAS forecasts

One objective of this thesis is to investigate the applicability of downscaled forecasts in an early flood warning system. The study sought to investigate the performance of WEB-DHM in simulating discharge for 4^{th} April, 2004 by using CALDAS meteorological forecasts. Quantitative precipitation forecast and other WEB-DHM forcing were extracted from the LVB domain used in the downscaling experiment and used to drive the model. Due to lack of ground-based rainfall observations and hourly discharge data from the Nyando river basin, only CALDAS results are presented here without any validation. There are five discharge gauges in this basin and the simulated discharge is presented in figure 4.34.

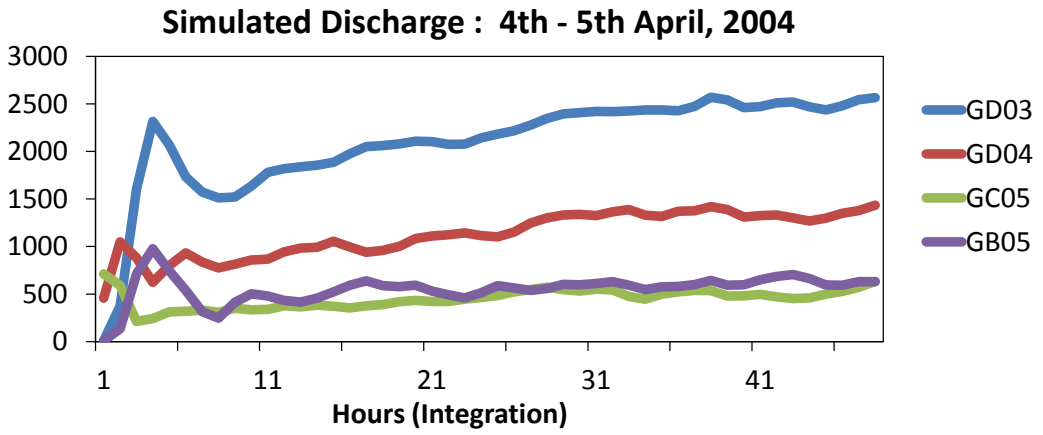

Figure 4.34: Simulated discharge based on CALDAS downscaled meteorological forcing.

Due to the overestimation of rainfall from the NWP the simulated discharge in the Nyando river basin is overestimated compared to daily recorded floods ($30m^3$) at the downstream gauge GD03. However, the flood peaks for 7th-12th exceed ($200m^3$) and this is an indicator that with continuous data assimilation, better flood forecasts can be made. That notwithstanding, this study serves as a major milestone towards forecast-based future flood control interventions.

4.8 Summary

This chapter introduced the concept of NWP and challenges of quantitative precipitation prediction. We sought to improve the prediction of such an event in the LVB. Using TRMM and observed cloud top temperature from geostationary satellites, 4^{th} April, 2004 was selected for further investigation. This event was characterized by a low pressure system over Lake Victoria which started about midday on 4^{th} and ended almost midday the following day. This provided a good opportunity to test predictability, identify deficiencies in the

ARPS/CALDAS prediction system and validate the assimilation system (Section 4.3.2). A nested downscaling approach was used with cumulus parameterization on the outer two grids and switched off for the inner domain.

4.8.1 Downscaling only experiment

The ARPS downscaling numerical experiment performs poorly and though there is some prediction of rainfall in the greater LVB, validating the simulated rainfall against TRMM shows that a low skill was achieved by this experiment and there is a need to improve the prediction. Further, comparison of simulated cloud top temperature against observations showed that there is only some improvement for the first six hours then the skill reduces after ten hours. This was also confirmed by measures of skill based on the binary contingency table statistics.

4.8.2 Downscaling with assimilation experiments

Section 4.3.2 extended the experiments of section 4.2.4 with an aim of improving extreme rainfall predictions through satellite data assimilation. Due to its higher spatial resolution and sensitivity to cloud water and water vapor in the atmosphere, AMSR-E satellite data were used to improve model state. A set of experiments was set up to investigate the 4^{th} April, 2004 event over Lake Victoria and some parts over land. Compared to the ARPS experiment, the CALDAS experiment gave better results with rainfall simulated at 03UTC having a pattern very similar to TRMM. This was reflected by a higher spatial correlation between TRMM and simulated cloud-top temperature. The prediction of the extreme rainfall was consistent with the observation with good results achieved for at least six hours.

4.8.3 Assimilation and RTM sensitivity experiments

These experiments also sought to validate the CALDAS system in a wet humid region. The default CALDAS systems allow for the assimilation of water vapor, rainwater, snow water

and cloud water. Just after assimilation all CALDAS experiments gave better results for about one hour but soon dissipated. Further experiments identified two key issues; 1) the assimilation of rainwater through the shuffled complex evolution was not required. This is because rainwater would not enhance instability but would rather suppress any updrafts introduced by condensation of cloud water. Also, assimilating rainwater does not lead to release of latent heat which initiates convection. 2) Water vapor in all the experiments seemed to dry up even after excluding rainwater assimilation. Further checks revealed that the CALDAS RTM seemed to assimilate higher brightness temperatures compared to AMSR-E observations. This led to assimilation of less water vapor into the NWP model state. While this affected the two channels of AMSR-E; it seemed to affect the 23GHz, sensitive to water vapor.

Experiments were done to check for sensitivity and it was revealed that; changes in surface temperature led to significant changes in assimilated water vapor. Subtracting 2K,7K and 10K from the surface temperature (assimilation time only) led to an increase in the assimilated water vapor. Thus for the best results, the uncertainty in the calculation of surface emission must be solved. Since temperature is key for the RTM, there is a need to improve the treatment of surface temperature during assimilation and get better estimates of surface temperature. This study proposes thorough validation and improvement of the RTM through ground-based observations.

Chapter 5

Conclusions and Recommendations

This thesis sought to demonstrate a comprehensive integrated approach to climate change assessment in the LVB. Identified as one of the most vulnerable(LVBC, 2007, 2011) regions to adverse effects of climate change (IPCC, 2007; Seneviratne et al., 2012), it is essential to have a deeper understanding of projected changes in mean climate as well as extreme weather events. This was achieved through a multi-dimensional approach combining different spatial, numerical and temporal dimensions. Basin scale analysis of climate change and its impacts on flow regimes was done in the Nyando river basin as well regional analysis of the mean climate in the greater LVB and East Africa.

In addition, as a step towards adaptation to extreme weather events, the study sought to improve extreme weather predictability under the current climate through NWP and down-scaling. Additionally, satellite data assimilation was introduced to improve the forecast. Higher resolution output from the NWP model was used to test the applicability in flood prediction by simulating the recorded flood event at the simulation time and comparing against observations. The following sub-sections summarize the key findings and recommendations for future work.

5.1 Climate change: Nyando river basin

Nyando basin is a predominantly flood basin within the greater LVB. Loss of livelihoods, housing and life has been common occurrence almost on a yearly basis. The likelihood of these events recurring in the future under SRESA1B climate change scenario was investigated. Through statistical bias correction and downscaling of GCM projections, the likely changes in basin rainfall and future flood frequency and intensity were determined in the basin. In line with the IPCC AR4 report which suggested that most of East Africa is likely to experience more rainfall, the bias corrected rainfall in this river basin shows the same trend. There is a high probability that the frequency and intensity of extreme events will increase in the future. This is reflected well by the three selected GCMs, showing a positive trend in extreme rainfall. In tandem with rainfall, the likelihood of an increase in floods in the same basin is projected by the three GCMs.

5.2 Regional changes in climate the LVB

Chapter 2 analyzed the projected regional changes in rainfall and associated circulation patterns. It also focused on extreme weather projections by use of extreme weather indices. Under the SRES A1B scenario, the mean of the three selected GCMs project an increase in rainfall in the LVB and East Africa as a whole. Analysis at the seasonal scale shows a similar increasing trend but more pronounced during the October-December season. Over the LVB both seasons are suggested to experience an almost equal increase. The GCM projected anomalies show a pattern very similar to the seasonal migration of the ITCZ with regions that usually experience peak rainfall having more enhanced anomalies. It has been shown that westerly anomalies in the central western Indian Ocean have a strong correlation with East Africa's rainfall. Investigations reveal that, these westerly anomalies are projected to weaken in the future; a scenario associated with a weaker Walker (or even reversal) circulation cell over the central Indian Ocean and anomalously high rainfall in the region.

5.2.1 Projections of extreme events

Extreme weather indices used support Chapter 2's findings; that this region is likely to experience more extreme events. Under the SRESA1B scenario, the number of wet days exceeding the 90% percentile of 1981-2000 is likely to increase by 20-40% in the whole region. An increase of about 5-20% is projected to occur in the LVB and the Congo basin with the highest changes of about more than 30% being projected for the Kenyan-Somali coast. This is also reflected in the number of wet days exceeding the 99% threshold with about 1-8% projected increase. This is accompanied by more than 100% increase on days with rainfall over 40mm east of Lake Victoria and central Kenya and 10% increase in the simple daily intensity index.

5.2.2 Mechanisms of extreme events

We explored the likely mechanisms associated with the projected changes and focused on regional and synoptic systems which have previously been shown to control extreme rainfall in the region like SST anomalies and Walker circulation. Investigations suggest that westerly anomalies are projected to weaken in the future; a scenario associated with a weaker Walker (or even reversal) circulation cell over the central Indian Ocean and anomalously high rainfall in the region.

Investigations of the selected 30 future events in the LVB reveal that moisture flux convergence during the two seasons will likely remain high with the Indian Ocean providing the bulk during the two seasons. Mean sea level pressure anomalies for these events suggest an anomalously low pressure over the region; and this is common during the two months representing the two seasons. Weakening of the Walker circulation and warmer western Indian Ocean SST anomalies are some of the projected synoptic system changes that are likely to be associated with increased precipitation in the EA region.

In general, dynamic and synoptic mechanisms support the projected changes in mean and extreme rainfall in this region. This is clear for the OND season but for MAM the regional

synoptic changes in relating regional / basin scale change in extreme rainfall is not clear and more research and modeling framework especially for this season is suggested.

5.3 Numerical downscaling of weather forecasts

Chapter 4 introduced the concept of NWP and challenges of quantitative precipitation prediction. The chapter sought to improve the prediction of such an event in the LVB. Using TRMM and observed cloud top temperature from geostationary satellites on 4^{th} April, 2004 was selected for further investigation. This event was characterized by a low pressure system over Lake Victoria which started about midday on 4^{th} and ended almost midday the following day. This provided a good opportunity to test predictability, identify deficiencies in the ARPS/CALDAS prediction system and validate the assimilation system (Chapter 4). A nested downscaling approach was used with cumulus parameterization on the outer two grids and switched off for the inner domain.

The "ARPS downscaling only" numerical experiment performs reasonably well and there were some prediction of rainfall in the greater LVB. Validating the simulated rainfall against TRMM shows that a low skill was achieved by this experiment and there is a need to improve the prediction. Further, comparison of simulated cloud top temperature against observations showed that there is some improvement for the first six hours then the skill reduces after ten hours. This was also confirmed by measures of skill based on the binary contingency table statistics.

5.4 Data assimilation and extreme event forecasting

Due to its higher spatial resolution and sensitivity to cloud water and water vapor in the atmosphere, AMSR-E satellite data were used to improve the model state of the NWP model (i.e. ARPS). A set of experiments was set up to investigate the 4^{th} April, 2004 event over Lake Victoria and some parts over land. Compared to the ARPS experiment, the CALDAS

experiment gave better results with rainfall simulated at 03UTC having a pattern weakly similar to TRMM. This was reflected by a higher spatial correlation between TRMM and simulated rainfall as well cloud-top temperature against observed IR.

5.4.1 Assimilation of rain water

The default CALDAS system allows for the assimilation of water vapor, rainwater, snow water and cloud water. Just after assimilation all CALDAS experiments gave better results for about one hour but soon dissipated. Further experiments identified two key issues; 1) the assimilation of rain water through the shuffled complex evolution was not required because rainwater would not enhance instability but would rather suppress any updrafts introduced by condensation of cloud water. Also, assimilating rain water does not lead to release of latent heat which initiates convection. 2) Water vapor in all the experiments seemed to dry up even after excluding rainwater assimilation. Further checks revealed that the CALDAS RTM seemed to assimilate higher brightness temperatures compared to AMSR-E observations. This led to assimilation of less water vapor into the NWP model state. While this affected the two channels of AMSR-E; it seemed to affect the 23GHz which is sensitive to water vapor.

5.4.2 Surface temperature sensitivity

Experiments were done to check for sensitivity and it was revealed that; changes in surface temperature led to significant changes in assimilated water vapor. Subtracting 2K,7K and 10K from the surface temperature (assimilation time only) led to an increase in the assimilated water vapor. Thus for the best results, the uncertainty in the calculation of surface emission must be solved. Since temperature is key for the RTM, there is a need to improve the treatment of surface temperature during assimilation and get better estimates of surface temperature. This study proposes thorough validation and improvement of the RTM through ground-based observations.

5.5 Recommendations

We demonstrated a multi-dimensional approach to integrating climate change assessment and extreme weather forecasting as a step towards extreme weather adaptation. While it is virtually impossible to link a specific event to climate change, knowledge of the likely intensity or frequency is key to adaptation and resilience building. This study has done a preliminary investigation of the likely changes at basin and regional scales of extreme events and the study suggests a likely increase. That notwithstanding, there is a need for an in-depth analysis, more model and analytical integration. To comprehensively address the issue of climate change and extreme events in this region, this study recommends the following:

(a) *GCM projections downscaling approach :* To address some of the documented uncertainties and challenges of statistical downscaling, a dynamic approach is encouraged to provide a clearer picture of the extreme weather projection under climate change in this region

(b) *CMIP5:* CMIP5 will hopefully address some of the challenges and uncertainties especially in the East African region. Consideration should made to investigate the projections of extreme events at a higher spatial and temporal resolutions offered by CMIP5

(c) *Extreme event forecasting :* forecasting was limited to one event only, partly due to data limitations. It is recommended that more similar experiments even at smaller domains be investigated in the future to validate these findings

(d) *Assimilation of rain water :* this study suggests that it may not be necessary to assimilate rain water in CALDAS. There is a need to validate this finding with other events and possibly in other regions

(e) *Sensitivity of surface temperature :* this study identified the need to improve the RTM with respect to assimilation of water vapor. It was suggested that accurate estimation of surface temperature is needed. This study proposes more ground based re-calibration and validation of the RTM

(f) *QPF for flood forecasts :* one of the objectives of the study was to evaluate the performance of the QPF in flood prediction. Despite the improvements in spatial distribution of precipitation, the predicted flood was too high. Nevertheless, data unavailability and daily time scale limited the validation. In addition, though it has been shown that QPF prediction is one of the most challenging tasks of weather prediction, we suggest bias correction of QPFs as an immediate solution to over-prediction.

5.6 Scientific contribution

This research integrated climate change assessment and improved tools and aids to adapt to extreme weather in the LVB and this involved analysis of extreme weather events at both local and regional scales. It was confirmed that in line with the IPCC AR4 report, the projected changes in precipitation; both mean and extremes are likely to increase in the region. Concurrently, the likelihood of increased floods in the Nyando river basin is high. Investigations at the regional scale revealed a similar trend with a likelihood of more extreme days in the region with the eastern parts of LVB being more likely to experience these as projected by CMIP3 GCMs. Analysis of the mechanisms reveal a trend similar to historical extreme events: weaker Walker circulation, anomalous moisture flux and stronger than normal Somali jet.

In order to support adaptation to extreme events even under the current climate, we demonstrated the applicability of a coupled atmosphere and land data assimilation NWP. It is possible to provide better forecasts by assimilating AMSR-E data in this region though there are some specifics of the system that need improvement. Firstly, Kuria et al. (2007) introduced the assimilation of rain water into the CALDAS system. However, investigations revealed that this may not be necessary especially in regions with abundant water vapor in the atmosphere.

Secondly, the current RTM used in the CALDAS system was found to overestimate assimilated brightness temperature. Investigations and sensitivity studies traced the issue to

estimation of surface temperature which ultimately affected the water vapor assimilation through the computation of surface emission. While the performance under the current system can be considered satisfactory, this study identified the need to revise the RTM to provide a better estimation of surface emission. Lastly, an attempt was made to evaluate the performance of the QPF as an input for flood simulation. This was a first step and even though the floods were overestimated, it provided a good starting point for extension of this study

Appendix A

Appendices

Table A.1: Nyando river basin rain gauge stations.

ID	STATION	LATITUDE	LONGITUDE
8935001	Kabagendui Kibet Farm	0.0333	35.3000
8935013	Nandi, Koisagat Tea Estate	0.0833	35.2667
8935033	Nandi Hills, Savani Estate	0.0500	35.1000
8935067	Kaptagat S.F.T. Estate	0.4000	35.4833
8935086	Eldoret Municipal Council	0.5167	35.2667
8935117	Kipkabus Forest Station	0.3167	35.5167
8935148	Kipkurere Forest Station	0.0833	35.4167
8935159	Cerengoni Forest Station	0.1167	35.3667
8935161	Nandi Hills, Kibweri Tea Estate	0.0833	35.1500
8935164	Kaptagat, Sabor Forest Station	0.5000	35.4833
9034009	Miwani Sugar The Hill.	-0.0500	34.9500
9034025	Kisumu Meteorological Station	-0.1000	34.7500
9034086	Ahero Irrig. Research Station	-0.1333	34.9333
9035002	Londiani Forest Station	-0.1500	35.6000
9035020	Kipkelion Railway Station	-0.2000	35.4667
9035042	Equator Barguat Estate	-0.0167	35.4000
9035046	Chemelil Plantation	-0.0667	35.1500
9035068	Kipkelion Morau Company Ltd.	-0.1333	35.4500
9035075	Kaisugu House, Kericho	-0.3167	35.3667
9035102	S. Kalya'S Farm, Kedowa	-0.2667	35.5167
9035148	Koru Bible School	-0.2000	35.2667
9035150	Tinderet Estate	-0.1333	35.3833
9035199	Ainamoi Chiefs Camp, Kericho	-0.3000	35.2667
9035240	Keresoi Forest Station, Londiani	-0.2833	35.5333
9035256	Maragat Forest Station	-0.0500	35.4667
9035279	Hail Research Station, Kericho	-0.3667	35.2667

References

Adler, R. F., Huffman, G. J., Chang, A., Ferraro, R., Xie, P.-P., Janowiak, J., Rudolf, B., Schneider, U., Curtis, S., Bolvin, D., Gruber, A., Susskind, J., Arkin, P., and Nelkin, E. (2003). The version-2 global precipitation climatology project (GPCP) monthly precipitation analysis (1979-present). *Journal of Hydrometeorology*, 4(January 1997):1147–1167.

Andersson, E., Pailleux, J., Thépaut, J.-N., Eyre, J. R., McNally, A. P., Kelly, G. A., and Courtier, P. (1994). Use of cloud-cleared radiances in three/four-dimensional variational data assimilation. *Quarterly Journal of the Royal Meteorological Society*, 120(517):627–653.

Anyah, R., Semazzi, F., and Xie, L. (2006). Simulated physical mechanisms associated with climate variability over Lake Victoria Basin in East Africa. *Monthly weather review*, pages 3588–3609.

Aravéquia, J. A., Szunyogh, I., Fertig, E. J., Kalnay, E., Kuhl, D., and Kostelich, E. J. (2011). Evaluation of a Strategy for the Assimilation of Satellite Radiance Observations with the Local Ensemble Transform Kalman Filter. *Monthly Weather Review*, 139(6):1932–1951.

Arndt, C., Strzepeck, K., Tarp, F., Thurlow, J., Fant, C., and Wright, L. (2010). Adapting to climate change: an integrated biophysical and economic assessment for Mozambique. *Sustainability Science*, 6(1):7–20.

Arnell, N. (1999). Climate change and global water resources. *Global Environmental Change*, 9(June):S31–S49.

Arnell, N. W. (2004). Climate change and global water resources: SRES emissions and socio-economic scenarios. *Global Environmental Change*, 14(1):31–52.

Baede, A., E. Ahlonsou, Y. Ding, D. S., and B. Bolin, S. P. (2001). The climate system: an overview.

Barker, D., Huang, X.-Y., Liu, Z., Auligné, T., Zhang, X., Rugg, S., Ajjaji, R., Bourgeois, A., Bray, J., Chen, Y., Demirtas, M., Guo, Y.-R., Henderson, T., Huang, W., Lin, H.-C., Michalakes, J., Rizvi, S., and Zhang, X. (2012). The Weather Research and Forecasting Model's Community Variational/Ensemble Data Assimilation System: WRFDA. *Bulletin of the American Meteorological Society*, 93(6):831–843.

Bates, B., Kundzewicz, Z. W., Wu, S., and Palutikof, J. (2008). Climate change and water.

Beyene, T., Lettenmaier, D. P., and Kabat, P. (2009). Hydrologic Impacts of Climate Change on the Nile River Basin: Implications of the 2007 IPCC Climate Scenarios. *Climate change*, 100(3):433–461.

Bjerknes, J. (1969). Atmospheric Teleconnections From The Equatorial Pacific 1. *Monthly Weather Review*, 97(3):163–172.

Black, E. (2005). The relationship between Indian Ocean sea-surface temperature and east African rainfall. *hilosophical Transactions of the Royal Society - Series A: Mathematical, Physical and Engineering Sciences*, 363(1826):43–47.

Black, R., Kniveton, D., and Schmidt-Verkerk, K. (2011). Migration and climate change: towards an integrated assessment of sensitivity. *Environment and Planning A*, 43(2):431–450.

Boko M, van Oldenborgh, G. J., Niang, I., Nyong, A., Vogel, C., Githeko, A., Medany, M., Osman-Elasha, B., Tabo, R., and Yanda, P. (2007). Adaptation and Vulnerability. Contribution of Working Group II to the Fourth Assessment Report of the Intergovernmental

Panel on Climate Change. *Parry, ML, OF Canziani, JP Palutikof, PJ van der ...*, pages 433–467.

Bousquet, O., Lin, C. a., and Zawadzki, I. (2006). Analysis of scale dependence of quantitative precipitation forecast verification: A case-study over the Mackenzie river basin. *Quarterly Journal of the Royal Meteorological Society*, 132(620):2107–2125.

Bouttier, F. and Courtier, P. (1999). Data assimilation concepts and methods.

Cane, D. and Milelli, M. (2010). Multimodel SuperEnsemble technique for quantitative precipitation forecasts in Piemonte region. *Nat. Hazards Earth Syst. Sci*, 10(2):265–273.

Castro, C. L. (2005). Dynamical downscaling: Assessment of value retained and added using the Regional Atmospheric Modeling System (RAMS). *Journal of Geophysical Research*, 110(D5):1–21.

Cesaraccio, C., Spano, D., Duce, P., and Snyder, R. L. (2001). An improved model for determining degree-day values from daily temperature data. *International journal of biometeorology*, 45(4):161–9.

Charney, J. G. (1962). Integration of the primitive and balance equations. *Met. Soc. of Japan*, pages 131–152.

Charney, J. G., Fjortfort, R., and Neumann, J. (1950). Numerical Integration of the Barotropic Vorticity Equation. *Tellus*, 2(4):237–254.

Cherubini, T., Ghelli, A., and Lalaurette, F. (2002). Verification of Precipitation Forecasts over the Alpine Region Using a High-Density Observing Network. *Weather and Forecasting*, 17(2):238–249.

Clark, A. J., Kain, J. S., Stensrud, D. J., Xue, M., Kong, F., Coniglio, M. C., Thomas, K. W., Wang, Y., Brewster, K., Gao, J., Wang, X., Weiss, S. J., and Du, J. (2011). Probabilistic Precipitation Forecast Skill as a Function of Ensemble Size and Spatial Scale in a Convection-Allowing Ensemble. *Monthly Weather Review*, 139(5):1410–1418.

Coles, S. and Davison, A. (2008). Statistical Modelling of Extreme Values. Technical report.

Collischonn, W., Haas, R., Andreolli, I., and Tucci, C. E. M. (2005). Forecasting River Uruguay flow using rainfall forecasts from a regional weather-prediction model. *Journal of Hydrology*, 305(1-4):87–98.

Conway, D., Hanson, C. E., Doherty, R., and Persechino, A. (2007). GCM simulations of the Indian Ocean dipole influence on East African rainfall: present and future. *Geophysical Research Letters*, 34(3):L03705.

Coumou, D. and Rahmstorf, S. (2012). A decade of weather extremes. *Nature Climate Change*, (March).

Dee, D. P. and Uppala, S. (2009). Variational bias correction of satellite radiance data in the ERA-Interim reanalysis. *Quarterly Journal of the Royal Meteorological Society*, 135(644):1830–1841.

DeFries, R., Achard, F., and Brown, S. (2006). Reducing Greenhouse Gas Emissions from Deforestation in Developing Countries: Considerations for Monitoring and Measuring, Report of the Global Terrestrial Observing System (GTOS) number 46, GOFC-GOLD report 26, available: www.fao.org/gtos/pubs.html. Technical Report 26.

Delpla, I., Jung, A.-V., Baures, E., Clement, M., and Thomas, O. (2009). Impacts of climate change on surface water quality in relation to drinking water production. *Environment international*, 35(8):1225–33.

Do Hoai, N., Udo, K., and Mano, A. (2011). Downscaling Global Weather Forecast Outputs Using ANN for Flood Prediction. *Journal of Applied Mathematics*, 2011:1–14.

Duan, Q. Y., Gupta, V. K., and Sorooshian, S. (1993). Shuffled complex evolution approach for effective and efficient global minimization. *Journal of Optimization Theory and Applications*, 76(3):501–521.

Easterling, D. and Evans, J. (2000). Observed variability and trends in extreme climate events: a brief review. *Bulletin of the American Meteorological Society*, pages 417–425.

Easterling, D. R., Meehl, G. a., Parmesan, C., Changnon, S. a., Karl, T. R., and Mearns, L. O. (2000). Climate extremes: observations, modeling, and impacts. *Science (New York, N.Y.)*, 289(5487):2068–74.

Elshamy, M. E., Seierstad, I. a., and Sorteberg, a. (2009). Impacts of climate change on Blue Nile flows using bias-corrected GCM scenarios. *Hydrology and Earth System Sciences*, 13(5):551–565.

Evensen, G. (2003). The Ensemble Kalman Filter: theoretical formulation and practical implementation. *Ocean Dynamics*, 53(4):343–367.

Eyre, J. R., Kelly, G. A., McNally, A. P., Andersson, E., and Persson, A. (1993). Assimilation of TOVS radiance information through one-dimensional variational analysis. *Quarterly Journal of the Royal Meteorological Society*, 119(514):1427–1463.

Fankhauser, S. and S.J. Tol, R. (2005). On climate change and economic growth. *Resource and Energy Economics*, 27(1):1–17.

Field, C., Barros, V., and Stocker, T. (2012). Managing the risks of extreme events and disasters to advance climate change adaptation.A Special Report of Working Groups I and II of the Intergovernmental Panel on Climate Change. Technical report.

Fraedrich, K. (1972). A simple climatological model of the dynamics and energetics of the nocturnal circulation at Lake Victoria. *Quarterly Journal of the Royal Meteorological Society*, 98(416):322–335.

Gaiser, T., Printz, a., von Raumer, H. S., Götzinger, J., Dukhovny, V., Barthel, R., Sorokin, a., Tuchin, a., Kiourtsidis, C., Ganoulis, I., and Stahr, K. (2008). Development of a regional model for integrated management of water resources at the basin scale. *Physics and Chemistry of the Earth, Parts A/B/C*, 33(1-2):175–182.

Gao, J., Xue, M., Brewster, K., and KELVIN K. DROEGEMEIER (2004). A Three-Dimensional Variational Data Analysis Method with Recursive Filter for Doppler Radars. (1970):457–469.

Gathenya, M., Mwangi, H., Coe, R., and Sang, J. (2011). Climate- and Land Use-Induced Risks To Watershed Services in the Nyando River Basin, Kenya. *Experimental Agriculture*, 47(02):339–356.

Gilman, S. E., Urban, M. C., Tewksbury, J., Gilchrist, G. W., and Holt, R. D. (2010). A framework for community interactions under climate change. *Trends in ecology & evolution*, 25(6):325–31.

Githui, F. (2008). *Assessing the impacts of environmental change on the hydrology of the Nzoia catchment, in the Lake Victoria Basin*. Ph.d thesis, Vrije Universiteit Brussel.

Githui, F., Gitau, W., Mutua, F., and Bauwens, W. (2009). Climate change impact on SWAT simulated streamflow in western Kenya. *International Journal of Climatology*, 29(12):1823–1834.

Gruber, A. (2008). Assessment of Global Precipitation Products A project of the World Climate Research Programme Global Energy and Water Cycle Experiment (GEWEX) Radiation Panel Lead Authors : May 2008. (1430).

Gu, Y., Liou, K. N., Ou, S. C., and Fovell, R. (2011). Cirrus cloud simulations using WRF with improved radiation parameterization and increased vertical resolution. *Journal of Geophysical Research*, 116(D6):D06119.

GUOSHENG, L. (1998). A fast and accurate model for microwave radiance calculations. *Journal of the Meteorological Society of Japan*, 76(2):335–343.

Handmer, J., Honda, Y., Kundzewicz, Z., N. Arnell, G. B., Hatfield, J., Mohamed, I., P. Peduzzi, S. W., Sherstyukov, B., Takahashi, K., and Yan, Z. (2012). Changes in impacts

of climate extremes: human systems and ecosystems. In: Managing the Risks of Extreme Events and Disasters to Advance Climate Change Adaptation. Technical report.

Hastenrath, S. (2007). Circulation mechanisms of climate anomalies in East Africa and the equatorial Indian Ocean. *Dynamics of Atmospheres and Oceans*, 43(1-2):25–35.

Houze, R. a., Rasmussen, K. L., Medina, S., Brodzik, S. R., and Romatschke, U. (2011). Anomalous Atmospheric Events Leading to the Summer 2010 Floods in Pakistan. *Bulletin of the American Meteorological Society*, 92(3):291–298.

Indeje, M., Semazzi, F. H., and Ogallo, L. J. (2000). ENSO signals in East African rainfall seasons. *International Journal of Climatology*, 20(1):19–46.

Ines, A. V. and Hansen, J. W. (2006). Bias correction of daily GCM rainfall for crop simulation studies. *Agricultural and Forest Meteorology*, 138(1-4):44–53.

IPCC (1990). IPCC First Assessment Report 47. *IPCC*.

IPCC (2007). *Climate Change 2007: The Physical Science Basis. Contribution of Working Group I to the Fourth Assessment Report of the Intergovernmental Panel on Climate Change*, volume 446 of *Climate change 2007*. Cambridge University Press.

Janowiak, J. E., Joyce, R. J., and Yarosh, Y. (2001). A Real-Time Global Half-Hourly Pixel-Resolution Infrared Dataset and Its Applications. *Bulletin of the American Meteorological Society*, 82(2):205–218.

Jaranilla-sanchez, P. A., Wang, L., and Koike, T. (2010). ENSO Influence On The 1982-2000 Hydrological Properties Of The Pantabangan-Carranglan Watershed. 54.

Jarvis, A., Lau, C., Cook, S., Wollenberg, E., Hansen, J., Bonilla, O., and Challinor, A. (2011). an Integrated Adaptation and Mitigation Framework for Developing Agricultural Research: Synergies and Trade-Offs. *Experimental Agriculture*, 47(02):185–203.

Jung, Y., Xue, M., and Tong, M. (2012). Ensemble Kalman Filter Analyses of the 2930 May 2004 Oklahoma Tornadic Thunderstorm Using One- and Two-Moment Bulk Microphysics Schemes, with Verification against Polarimetric Radar Data. *Monthly Weather Review*, 140(5):1457–1475.

Kalnay, E. (2003). *Atmospheric modeling, data assimilation, and predictability*, volume 54. Cambridge Univ Press.

Keefe, W. O. and Kueter, J. (2004). Climate Models: A Primer.

Kinuthia, J. H. (1992). Horizontal and vertical structure of the Lake Turkana jet. *Journal of applied meteorology*.

Kistler, R. (1974). *A study of data assimilation techniques in an autobarotropic primitive equation channel model*. msc, The Pennsylvania State University.

Kleist, D. T. (2011). Assimilation of Tropical Cyclone Advisory Minimum Sea Level Pressure in the NCEP Global Data Assimilation System. *Weather and Forecasting*, 26(6):1085–1091.

Koch, S. E. and Mcqueen, J. T. (1987). A survey of nested grid techniques and their potential for use within the MASS weather prediction model. *NASA Technical Memorandum 87808*.

Krishnamurti, T. N., Molinari, J., and Pan, H. L. (1976). Numerical Simulation of the Somali Jet. *Journal of the Atmospheric Sciences*, 33(12):2350–2362.

Kuligowski, R. J. and Barros, A. P. (1998). Localized Precipitation Forecasts from a Numerical Weather Prediction Model Using Artificial Neural Networks. *Weather and Forecasting*, 13(4):1194–1204.

Kuria, D. (2007). *Improving Precipitation Predictability over Land using Multi-parameter Passive Microwave Remote Sensing and Data Assimilation Strategies* . Ph. d. thesis, The University of Tokyo.

Kuria, D. N., Koike, T., Lu, H. L. H., Tsutsui, H., and Graf, T. (2007). Field-Supported Verification and Improvement of a Passive Microwave Surface Emission Model for Rough, Bare, and Wet Soil Surfaces by Incorporating Shadowing Effects. *IEEE Transactions on Geoscience and Remote Sensing*, 45(5):1207–1216.

Latif, M. and Dommenget, D. (1999). The role of Indian Ocean sea surface temperature in forcing east African rainfall anomalies during December-January 1997/98. *Journal of Climate*, 12(12):3497–3504.

Leutbecher, M. and Palmer, T. (2008). Ensemble forecasting. *Journal of Computational Physics*, 227(7):3515–3539.

Lin, Y.-L., Farley, R. D., and Orville, H. D. (1983). Bulk Parameterization of the Snow Field in a Cloud Model. *Journal of Climate and Applied Meteorology*, 22(6):1065–1092.

Lobell, D. B., Burke, M. B., Tebaldi, C., Mastrandrea, M. D., Falcon, W. P., and Naylor, R. L. (2008). Prioritizing climate change adaptation needs for food security in 2030. *Science (New York, N.Y.)*, 319(5863):607–10.

Lu, C., Yuan, H., Tollerud, E. I., and Wang, N. (2010). Scale-Dependent Uncertainties in Global QPFs and QPEs from NWP Model and Satellite Fields. *Journal of Hydrometeorology*, 11(1):139–155.

Lumb, F. E. (1970). Topographic Influences On Thunderstorm Activity Near Lake Victoria. *Weather*, 25(9):404–410.

LVBC (2007). Strategic Action Plan (SAP) for the Lake Victoria Basin. Technical Report March.

LVBC (2011). Vulnerability Assessment to Climate Change in Lake Victoria Basin, Kenya. *ACTS Press, African Centre for Technology Studies*.

LVBC (2012). Detailed Pre-Investment Analysis/Study on Maritime Communication for Safety on Lake Victoria.

Lynch, P. (2008). The origins of computer weather prediction and climate modeling. *Journal of Computational Physics*, 227(7):3431–3444.

Lyon, B. and DeWitt, D. G. (2012). A recent and abrupt decline in the East African long rains. *Geophysical Research Letters*, 39(2):1–5.

McGuffie, K. and Henderson-Sellers, A. (2005). *A Climate Modelling Primer*, volume 1. John Wiley & Sons, Ltd, Chichester, UK.

McHugh, M. J. (2006). Impact of South Pacific circulation variability on east African rainfall. *International Journal of Climatology*, 26(4):505–521.

Meehl, G. a., Covey, C., Taylor, K. E., Delworth, T., Stouffer, R. J., Latif, M., McAvaney, B., and Mitchell, J. F. B. (2007). THE WCRP CMIP3 Multimodel Dataset: A New Era in Climate Change Research. *Bulletin of the American Meteorological Society*, 88(9):1383–1394.

Mirza, C. R., Koike, T., Kun, Y., and Graf, T. (2006). Retrieval of Integrated Cloud Liquid Water Content and Integrated Water Vapor by Cloud Microphysics Data Assimilation System (CMDAS) Over Ocean by Integrating Satellite Data. *AGU Fall Meeting Abstracts*, -1:1402.

Mirza, C. R., Koike, T., Yang, K., and Graf, T. (2008). Retrieval of Atmospheric Integrated Water Vapor and Cloud Liquid Water Content Over the Ocean From Satellite Data Using the 1-D-Var Ice Cloud Microphysics Data Assimilation System (IMDAS). *IGARSS 2008 - 2008 IEEE International Geoscience and Remote Sensing Symposium*, 46(1):119–129.

Mutai, C. and Ward, M. (2000). East African rainfall and the tropical circulation/convection on intraseasonal to interannual timescales. *Journal of Climate*, pages 3915–3939.

Mutua, F. (2012). A Comparison Of Spatial Rainfall Estimation Techniques: A Case Study Of Nyando River Basin Kenya. *Journal of Agriculture, Science and Technology*, 14(1):95–112.

Mutua, F. and Koike, T. (2013). Adaptation to extreme climate : Improving weather prediction in the Lake Victoria Basin. *Climatic Dynamics*, page (in prep.).

Mutua, F., Mohamed, R., and Koike, T. (2012a). Improving extreme rainfall event prediction using microwave satellite data assimilation and bogus wind modification. *AGU Fall Meeting Abstracts*, 57:1–6.

Mutua, F., Mohamed, R., and Koike, T. (2013a). Improving Extreme Rainfall Event Prediction Using Microwave Satellite Data Assimilation. *Annual Journal of Hydraulic Engineering, JSCE*, 57:1–6.

Mutua, F., Mohamed, R., and Koike, T. (2013b). Projections of extreme weather events in the Lake Victoria basin under climate change. *EGU General Assembly Conference Abstracts*, 15:(submittted).

Mutua, F., Nyunt, C., and Koike, T. (2013c). Multi-scale climate change impact assessment on extreme events in the Lake Victoria Basin (LVB). *WATER RESOURCES RESEARCH*, (in prep.).

Mutua, F., Rasmy, M., Kuria, D., and Koike, T. (2013d). Sensitivity analysis of the CALDAS system : Surface temperature estimation and Significance of rain-water assimilation. *IEEE Transactions on Geoscience and Remote Sensing*, 50(1):(in prep.).

Mutua, F., Wang, L., Yamamoto, A., Nemoto, T., Kitsuregawa, M., and Koike, T. (2012b). Regional Climate Change And Its Impacts On Future Discharges And Flow Characteristics Of The Nyando Basin, Kenya. *Annual Journal of Hydraulic Engineering, JSCE*, 56.

Nash, J. E. and Sutcliffe, J. V. (1970). River flow forecasting through conceptual models part I – A discussion of principles. *Journal of Hydrology*, 10(3):282–290.

Nicholson, S. (1996). A review of climate dynamics and climate variability in eastern Africa. *In The Limnology, Climatology and Paleoclimatology of the East African Lakes*.

Nicholson, S. E. (2009). A revised picture of the structure of the "monsoon" and land ITCZ over West Africa. *Climate Dynamics*, 32(7-8):1155–1171.

Nordhaus, W. D. (2007). Economics of Climate Change. *Journal of Economic Literature*, XLV(September):686–702.

Nyunt, C. T., Koike, T., Sanchez, P. A. J., Yamamoto, A., Nemoto, T., and Kitsuregawa, M. (2013). Bias Correction Method For Climate Change Impact Assessments In The Philippines. *Annual Journal of Hydraulic Engineering, JSCE*, 57:1–6.

Oberthür, S. and Ott, H. E. (1999). *The Kyoto Protocol: International Climate Policy for the 21st Century(Google eBook)*, volume 1999. Springer.

Ogallo, L. J. (1988). Relationships between seasonal rainfall in East Africa and the Southern Oscillation. *Journal of Climatology*, 8(1):31–43.

Okoola, R., Camberlin, P., and Ininda, J. (2008). Wet periods along the East Africa Coast and the extreme wet spell event of October 1997. *Journal of the Kenya meteorological society*, 2(APRIL):65–81.

Onogi, K., Tsutsui, J., Koide, H., Sakamoto, M., Kobayashi, S., Hatsushika, H., Matsumoto, T., Yamazaki, N., Kamahori, H., Takahashi, K., Kadokura, S., Wada, K., Kato, K., Oyama, R., Ose, T., Mannoji, N., and Taira, R. (2007). The JRA-25 reanalysis. *Journal of the Meteorological Society of Japan*, 85(3):369–432.

Overland, J. E., Wang, M., Bond, N. a., Walsh, J. E., Kattsov, V. M., and Chapman, W. L. (2011). Considerations in the Selection of Global Climate Models for Regional Climate Projections: The Arctic as a Case Study*. *Journal of Climate*, 24(6):1583–1597.

Palm, C., Tomich, T., and Noordwijk, M. V. (2004). Mitigating GHG emissions in the humid tropics: case studies from the Alternatives to Slash-and-Burn Program (ASB). *Environment, Development and Sustainability*, pages 145–162.

Patz, J. a., Campbell-Lendrum, D., Holloway, T., and Foley, J. a. (2005). Impact of regional climate change on human health. *Nature*, 438(7066):310–7.

Peterson, T. C. (2002). Recent changes in climate extremes in the Caribbean region. *Journal of Geophysical Research*, 107(D21):1–9.

Phalippou, L. (1996). Variational retrieval of humidity profile, wind speed and cloud liquid-water path with the SSM/I: Potential for numerical weather prediction. *Quarterly Journal of the Royal Meteorological Society*, 122(530):327–355.

Piao, S., Ciais, P., Huang, Y., Shen, Z., Peng, S., Li, J., Zhou, L., Liu, H., Ma, Y., Ding, Y., Friedlingstein, P., Liu, C., Tan, K., Yu, Y., Zhang, T., and Fang, J. (2010). The impacts of climate change on water resources and agriculture in China. *Nature*, 467(7311):43–51.

Rahmstorf, S. and Coumou, D. (2011). Increase of extreme events in a warming world. *Proceedings of the National Academy of Sciences of the United States of America*, 108(44):17905–9.

Randall, D., Wood, R., and Bony, S. (2007). Climate models and their evaluation. *Climate change*.

Rasmy, M., Koike, T., Boussetta, S., Lu, H., and Li, X. (2011). Development of a Satellite Land Data Assimilation System Coupled With a Mesoscale Model in the Tibetan Plateau. *IEEE Transactions on Geoscience and Remote Sensing*, 49(8):2847–2862.

Rasmy, M., Koike, T., Kuria, D., Mirza, C. R., Li, X., and Yang, K. (2012). Development of the Coupled Atmosphere and Land Data Assimilation System (CALDAS) and Its Application Over the Tibetan Plateau. *IEEE Transactions on Geoscience and Remote Sensing*, 50(11):4227–4242.

Reale, O., Lau, K. M., Susskind, J., and Rosenberg, R. (2012). AIRS impact on analysis and forecast of an extreme rainfall event (Indus River Valley, Pakistan, 2010) with a global data assimilation and forecast system. *Journal of Geophysical Research*, 117(D8):1–15.

Reichle, R. H. (2004). Bias reduction in short records of satellite soil moisture. *Geophysical Research Letters*, 31(19):L19501.

Rosenzweig, C., Iglesias, A., Yang, X., Epstein, P. R., and Chivian, E. (2001). Climate change and extreme weather events - implications for food production, plant diseases, and pests. *change human health*, 2(2):90–104.

Rossow, W. B. and Garder, L. C. (1993). Cloud Detection Using Satellite Measurements of Infrared and Visible Radiances for ISCCP. *Journal of Climate*, 6(12):2341–2369.

Saito, K., Ishida, J., Aranami, K., and Hara, T. (2007). Nonhydrostatic atmospheric models and operational development at JMA. *Journal of meteorological society of Japan*, 85.

Saji, N. H., Goswami, B. N., Vinayachandran, P. N., and Yamagata, T. (1999). A dipole mode in the tropical Indian Ocean. *Nature*, 401(6751):360–363.

Sang, J. (2005). *Modeling The Impact Of Changes In Land Use, Climate And Reservoir Storage On Flooding In The Nyando Basin*. Msc. thesis, Jomo Kenyatta University of Agriculture and Technology.

Saunders, R., Matricardi, M., and Brunel, P. (1999). An improved fast radiative transfer model for assimilation of satellite radiance observations. *Quarterly Journal of the Royal Meteorological Society*, 125(556):1407–1425.

Schenkman, A. D., Xue, M., Shapiro, A., Brewster, K., and Gao, J. (2011). The Analysis and Prediction of the 89 May 2007 Oklahoma Tornadic Mesoscale Convective System by Assimilating WSR-88D and CASA Radar Data Using 3DVAR. *Monthly Weather Review*, 139(1):224–246.

Schils, R. L. M., Verhagen, a., Aarts, H. F. M., and Šebek, L. B. J. (2005). A farm level approach to define successful mitigation strategies for GHG emissions from ruminant livestock systems. *Nutrient Cycling in Agroecosystems*, 71(2):163–175.

Sellers, P., Randall, D., Collatz, G., Berry, J., Field, C., Dazlich, D., Zhang, C., Collelo, G., and Bounoua, L. (1996). A Revised Land Surface Parameterization (SiB2) for Atmospheric GCMS. Part I: Model Formulation. *Journal of Climate*, 9(4):676–705.

Semazzi, F. H., Sandra, Y., KiwanukaTondo James, Xie, L., Rose, L., Barakiza, R., Ambenje, P., and Twahirwa, A. (2011). Enhancing Safety of Navigation and Efficient Exploitation of Natural Resources over Lake Victoria and Its Basin by Strengthening Meteorological Services on the Lake. Technical Report October.

Seneviratne, S. I., Nicholls, N., Easterling, D., Goodess, C. M., Kanae, S., Kossin, J., Luo, Y., Marengo, J., McInnes, K., Rahimi, M., Reichstein, M., Sorteberg, A., Vera, C., and Zhang, X. (2012). Changes in climate extremes and their impacts on the natural physical environment: An overview of the IPCC SREX report. *EGU General Assembly Conference Abstracts*, 14:12566.

Shongwe, M. E., van Oldenborgh, G. J., van den Hurk, B., and van Aalst, M. (2011). Projected Changes in Mean and Extreme Precipitation in Africa under Global Warming. Part II: East Africa. *Journal of Climate*, 24(14):3718–3733.

Smith, J. and Lenhart, S. (1996). Climate change adaptation policy options. *Climate Research*, 6(Gleick 1993):193–201.

Solomon, S., D, Q., M, M., Z, C., M, M., K.B, A., Tignor, M., and Miller, H. (2007). Climate change 2007: contribution of working group I to the fourth assessment report of the intergovernmental panel on climate change. *Cambridge University Press*.

Srivastava, K., Gao, J., Brewster, K., Roy Bhowmik, S. K., Xue, M., and Gadi, R. (2010). Assimilation of Indian radar data with ADAS and 3DVAR techniques for simulation of a small-scale tropical cyclone using ARPS model. *Natural Hazards*, 58(1):15–29.

Sun, J. (2005). Initialization and Numerical Forecasting of a Supercell Storm Observed during STEPS. *Monthly Weather Review*, 133(4):793–813.

Suzuki, T. (2010). Seasonal variation of the ITCZ and its characteristics over central Africa. *Theoretical and Applied Climatology*, 103(1-2):39–60.

Swallow, B. M., Sang, J. K., Nyabenge, M., Bundotich, D. K., Duraiappah, A. K., and Yatich, T. B. (2009). Tradeoffs, synergies and traps among ecosystem services in the Lake Victoria basin of East Africa.

Talbot, C., Bou-Zeid, E., and Smith, J. (2012). Nested Mesoscale Large-Eddy Simulations with WRF: Performance in Real Test Cases. *Journal of Hydrometeorology*, 13(5):1421–1441.

Taye, M. T., Ntegeka, V., Ogiramoi, N. P., and Willems, P. (2011). Assessment of climate change impact on hydrological extremes in two source regions of the Nile River Basin. *Hydrology and Earth System Sciences*, 15(1):209–222.

Taylor, K. E. K., Stouffer, R. J. R., and Meehl, G. G. a. (2012). An Overview of CMIP5 and the Experiment Design. *Bulletin of the American Meteorological Society*, 93(4):485–498.

Tebaldi, C., Hayhoe, K., Arblaster, J. M., and Meehl, G. a. (2006). Going to the Extremes. *Climatic Change*, 79(3-4):185–211.

Thieme, M. L., Lehner, B., Abell, R., and Matthews, J. (2010). Exposure of Africa's freshwater biodiversity to a changing climate. *Conservation Letters*, 3(5):324–331.

Tierney, J. E., Lewis, S. C., Cook, B. I., LeGrande, A. N., and Schmidt, G. A. (2011). Model, proxy and isotopic perspectives on the East African Humid Period. *Earth and Planetary Science Letters*, 307(1-2):103–112.

Tierney, J. E., Smerdon, J. E., Anchukaitis, K. J., and Seager, R. (2013). Multidecadal variability in East African hydroclimate controlled by the Indian Ocean. *Nature*, 493(7432):389–392.

Treut, L., Somerville, R., Cubasch, U., Ding, Y., Mauritzen, C., Mokssit, A., Peterson, T., Prather, M., Qin, D., Manning, M., Chen, Z., Marquis, M., Averyt, K. B., Tignor, M., and Kingdom, U. (2007). Historical Overview of Climate Change Science.

Trexler, M. C. and Kosloff, L. H. (1998). The 1997 Kyoto protocol: what does it mean for project-based climate change mitigation? *MITIGATION AND ADAPTATION STRATEGIES FOR GLOBAL CHANGE*, (May):1–58.

Tsujimoto, K. and Koike, T. (2011). The post-monsoon rainfall in the western Cambodia its mechanism and occurrence factors. *WCRP-OSC in Denver, Session C1: Climate Variability and Change in the Australian-Asian Region*, page 2011.

Vaidya, S. S., Mukhopadhyay, P., Trivedi, D. K., Sanjay, J., and Singh, S. S. (2004). Prediction of tropical systems over Indian region using mesoscale model. *Meteorology and Atmospheric Physics*, 86(1-2):63–72.

Vecchi, G. A., Soden, B. J., Wittenberg, A. T., Held, I. M., Leetmaa, A., and Harrison, M. J. (2006). Weakening of tropical Pacific atmospheric circulation due to anthropogenic forcing. *Nature*, 441(7089):73–6.

Vuuren, D. P., Lowe, J., Stehfest, E., Gohar, L., Hof, A. F., Hope, C., Warren, R., Meinshausen, M., and Plattner, G.-K. (2009). How well do integrated assessment models simulate climate change? *Climatic Change*, 104(2):255–285.

Waako, T., Thuo, S., and Ndayizeye, A. (2009). Impact of climate change on the Nile river basin. *Rural 21*, 43(4):19–21.

Wang, L., Koike, T., Yang, K., Jackson, T. J., Bindlish, R., and Yang, D. (2009). Development of a distributed biosphere hydrological model and its evaluation with the Southern Great Plains Experiments (SGP97 and SGP99). *Journal of Geophysical Research*, 114(D8):D08107.

Wang, S., Liu, J., and Wang, B. (2011). A new typhoon bogus data assimilation and its sampling method: A case study. *Atmos. Oceanic Sci. Lett*, 4(5):276–280.

Weart, S. R. (2003). *The Discovery of Global Warming*, volume 98. Harvard University Press.

Whitehead, p. g., Wilby, r. l., Battarbee, r. w., Kernan, M., and Wade, a. j. (2009). A review of the potential impacts of climate change on surface water quality. *Hydrological Sciences Journal*, 54(1):101–123.

Williams, a. P. and Funk, C. (2011). A westward extension of the warm pool leads to a westward extension of the Walker circulation, drying eastern Africa. *Climate Dynamics*, 37(11-12):2417–2435.

Xiao, Q., Zou, X., and Wang, B. (2000). Initialization and simulation of a landfalling hurricane using a variational bogus data assimilation scheme. *Monthly weather review*, 1995:2252–2269.

Xue, M., Droegemeier, K. K., and Wong, V. (2000). The Advanced Regional Prediction System (ARPS) A multi-scale nonhydrostatic atmospheric simulation and prediction model . Part I : Model dynamics and veri cation. *Meteorology and Atmospheric Physics*, 193(3-4):161–193.

Xue, M., Droegemeier, K. K., Wong, V., Shapiro, A., Brewster, K., Carr, F., and Weber, D. (2001). The Advanced Regional Prediction System (ARPS) A multi-scale nonhydrostatic atmospheric simulation and prediction tool . Part II : Model physics and applications. 165:143–165.

Xue, M., Wang, D., Gao, J., Brewster, K., and Droegemeier, K. K. (2003). The Advanced Regional Prediction System (ARPS), storm-scale numerical weather prediction and data assimilation. *Meteorology and Atmospheric Physics*, 82(1-4):139–170.

Yan, B. and Weng, F. (2011). Assimilation of F16 Special Sensor Microwave Imager/Sounder Data in the NCEP Global Forecast System. *Weather and Forecasting*, page 111227101347009.

Yang, D., Herath, S., and Musiake, K. (1998). Development of a geomorphology-based hydrological model for large catchments. *Annual Journal of Hydraulic Engineering, JSCE*, 42.

Yates, E., Anquetin, S., Ducrocq, V., Creutin, J.-D., Ricard, D., and Chancibault, K. (2006). Point and areal validation of forecast precipitation fields. *Meteorological Applications*, 13(01):1.